NUMERICAL MODELLING OF NEUTRON FLUX IN NUCLEAR REACTORS

Bachelor's Thesis

submitted by

Milan Hanuš

completed at

Department of Mathematics
Faculty of Applied Sciences
University of West Bohemia

under supervision of

Ing. Marek Brandner, Ph.D.

Pilsen, June 2007

Declaration

I hereby declare that this Bachelor's Thesis is the result of my own work and that all external sources of information have been duly acknowledged.

.....

Milan Hanuš

Abstract in English

The aim of this thesis is to develop an efficient method that describes neutron distribution within a reactor. The method is based on neutron transport equation which can be derived from physical foundations presented at the beginning of the thesis. By using a general balance principle, an accurate albeit overly complex neutron transport equation is obtained from the derivation. Simplifications are discussed next and lead to a two-group system of steady state diffusion equations. An eigenvalue problem is then formulated for the established boundary value problem whose dominant eigenpair is the critical number of the reactor and a corresponding neutron flux distribution. Application of reactor criticality calculations in the area of fuel reloading optimization is explained. The eigenvalue problem is solved by the power method in which the dominant eigenvector is determined by solving a set of algebraic equations arising from finite-volume discretization scheme. To obtain a sufficiently accurate solution on a coarse hexagonal assembly mesh, the standard finite-volume method is refined by a nodal method based on a special transverse integration procedure. For solving the one-dimensional diffusion problems arising from the procedure, semi-analytic method is employed. The resulting numerical scheme is then benchmarked on a model VVER-1000 type reactor configuration. Improvement directions are discussed at the end.

Keywords:

nuclear reactor, reactor physics, neutron transport equation, neutron balance, neutron diffusion equation, two-group approximation, reactor criticality, eigenvalue problem, power method, finite volume method, CMFD system, neutron flux, neutron current, nodal method, transverse integration, semi-analytic method, hexagonal assembly, fuel reloading optimization.

Abstrakt v češtině

V práci je navržena efektivní metoda pro popis rozložení neutronů v jaderném reaktoru, vycházející z transportní rovnice neutronů. Teoretický přehled reaktorové fyziky v druhé kapitole slouží k popsání veličin potřebných pro odvození této rovnice. Pro praktické výpočty je však obecný transportní model příliš složitý, a tak práce pokračuje jeho difuzní dvougrupovou aproximací ve stacionárním režimu. Pro vzniklou okrajovou úlohu difuze neutronů je dále formulována úloha na vlastní čísla, jejíž dominantní řešení popisuje tzv. kritické číslo reaktoru a příslušné rozložení neutronových toků. V práci je blíže rozebrána aplikace tohoto výsledku na problém optimalizace palivových vsázek. Dominantní vlastní číslo je hledáno iterativní mocninnou metodou, přičemž příslušný vlastní vektor je v každém kroku získán řešením soustavy rovnic sestavené na základě diskretizace dané okrajové úlohy. Tu je možné provést např. metodou konečných objemů, avšak pro potřeby co nejvěrnějšího popisu neutronových toků v reaktoru s šestiúhelníkovými kazetami je nutno klasický konečně-objemový přístup zpřesnit. K tomu je v práci použita tzv. nodální metoda sestávající ze speciální příčné integrace difuzních rovnic a následného semi-analytického řešení vzniklých jednorozměrných problémů. Výsledkem je efektivní a přesná numerická metoda, jež je v závěru práce otestována na modelové palivové konfiguraci reaktoru typu VVER-1000. Práce je zakončena přehledem možností jejího vylepšení.

Klíčová slova:

jaderný reaktor, reaktorová fyzika, transportní rovnice neutronů, neutronová bilance, difuzní rovnice neutronů, dvougrupová aproximace, kritické číslo reaktoru, úloha na vlastní čísla, mocninná metoda, metoda konečných objemů, CMFD soustava, neutronové toky, neutronové proudy, nodální metoda, příčná integrace, semi-analytická metoda, šestiúhelníková palivová kazeta, optimalizace palivové vsázky.

Acknowledgements

I would like to thank my supervisor Ing. Marek Brandner, Ph.D., for his constant support and guidance throughout the course of thesis preparation. Without his insight, my understanding of the subject would never reach present levels. I would also like to thank Ing. Roman Kužel, Ph.D., for his invaluable advises on implementation of the methods in MATLAB. Finally, I am gratefull to all who had patience with me in times when progress became slow and time-consuming.

Contents

List of Symbols

Usage guideline

The list of letters used throughout the text is divided into two categories: those written in Roman script and those in Greek script. The entries are sorted alphabetically in each category, and the page where they first appear in the text is displayed after each item. If some letter is used with different meanings in different chapters, a remark is made just after its statement. Letters not used beyond first few lines after their definition are normally not listed. If the letter denotes some quantity for which there is a numbered definition relation in the text, the equation number is referenced after the description of the quantity.

Dependency of functions is written in terms of variables used in the place of their first appearance. Transport theory functions are in the text first presented in a general time-dependent form and this dependence is later removed by the assumption of steady state (section 3.1.2). Basic meaning of both forms of the function is preserved, however, so the list includes only the general time-dependent functions for the sake of brevity. If for any other reason two different symbols share the same meaning (e.g. due to omission of some indices that became redundant under additional assumptions), they are separated by semicolon but make one entry in the list.

The table of general non-letter symbols follows. For greater clarity, auxiliary letters are used together with symbols of universal meaning (e.g. of an operation applicable to any arbitrary function). The letters are:

- $\mathbf{a}$, $\mathbf{b}$ any arbitrary vectors
- q an arbitrary function
- W an arbitrary domain

In addition to explanations of indexed letters in the above mentioned lists, commonly used indices are also enumerated separately in the next two tables (for subscripts, resp. superscripts). Listing of acronyms concludes the summary.

ROMAN LETTERS

N_j	number of nodes in row j of the nodal mesh 43
$\mathbb{N}$	a set of natural numbers 43
n	number of neutrons in a unit volume of a sample 9
$\mathbf{n}(\mathbf{r})$; $\mathbf{n}$	vector field of outward-pointing unit normal vectors to a given hyperplane (surface in Chap. 3, edge in Chap. 4) 19
$\mathbf{n}_{i,x\pm}$, $\mathbf{n}_{i,u\pm}$, $\mathbf{n}_{i,v\pm}$; $\mathbf{n}_{i,\xi\pm}$	unit outward normal vectors to the respective faces of node $\mathcal{V}_i$ 45
$\mathbf{n}_{i,\sigma}$	unit outward normal to boundary edge σ of node $\mathcal{V}_i$ 47
$\bar{\bar{P}}_i$	average power produced by assembly (node) $\mathcal{V}_i$ 81
$p_k(x)$	k-th basis function of the space of orthogonal polynomials used in the semi-analytic method 69
$\mathbf{P}$	2×2 matrix representing neutron addition into the respective groups 69
$\mathbb{R}^n$	n-dimensional Euclidean space 20
r_*	reaction rate for an arbitrary reaction *(eq. 2.3)* 9
$r_*(\mathbf{r}, E, \mathbf{\Omega}, t)$	transport theory expression for reaction rate *(eq. 3.3)* 19
$r_{is}(\mathbf{r}, E, \mathbf{\Omega}, t)$	transport theory expression for the in-scatter reaction rate 22
$\mathbf{R}$	2×2 matrix representing neutron removal from the respective groups 69
$\mathbf{r}$	position of a neutron ($\mathbf{r} = (x, y, z)$ in Chap. 3, $\mathbf{r} = (x, y)$ in Chap. 4) 17
s_0, s_1, s_2	coefficients of the transverse leakage shape function $f(x)$ 67
$s_{ex}(\mathbf{r}, E, \mathbf{\Omega}, t)$	density function of external neutron sources 22
$s_f(\mathbf{r}, E, \mathbf{\Omega}, t)$	density function of fission sources of neutrons *(eq. 3.7)* 21
$s(\mathbf{r}, E)$	density function of isotropic fission sources of neutrons *(eq. 3.25)* .. 29
$s_i^g(x, y)$	neutron sources density in group g for the two-dimensional problem *(eq. 4.64)* 62
$\tilde{S}_i^g(x)$	inexact version of $\tilde{s}_i^g(x)$ 64
$\tilde{s}_i^g(x)$	transverse averaged neutron sources density in group g 64

$s^g_{t,i}(x)$ transverse integrated neutron sources density in group g 63

$\tilde{\tilde{S}}^g_i$ approximate group sources density, integrally averaged over all transverse cross sections of the node along the x-axis ($\tilde{S}^g_i(x)$ averaged over the width of the node) 66

$\mathbf{S}_\mathrm{f}$ $2N \times 2N$ fission sources matrix 57

$\mathcal{T}$ a mesh of hexagonal nodes 42

t time variable 17

u local spatial variable (direction) associated to a node

V neutron balance domain 20

v local spatial variable (direction) associated to a node

v speed of a neutron (a scalar) 9

$\mathbf{v}(E)$ velocity of a neutron (a vector) 17

$\mathcal{V}_i$ an arbitrary reference node 44

$\mathbf{w}$ power method weighting factor *(eq. 4.49)* 58

x local spatial variable (direction) associated to a node (identified with the Cartesian x-direction)

x_{ij} point with Cartesian coordinates $[x_i, y_j]$ 43

$y_{t,ij}(x)$; $y_{t,i}(x)$; $y_t(x)$
a function representing the top boundary of node $\mathcal{V}_i$ (centered at point x_{ij}) *(eq. 4.2)* 43

Z atomic number 5

Greek letters

α albedo constant (a ratio of the number of neutrons escaping the core and the number entering it through the same point) *(eq. 3.20)* 27

$\chi_p(E)$ energy spectrum of prompt fission neutrons 12

$\chi_p(\mathbf{r}, E' \to E, \mathbf{\Omega}' \to \mathbf{\Omega})$; $\chi(\mathbf{r}, E' \to E, \mathbf{\Omega}' \to \mathbf{\Omega})$ transport theory expression for the energetic spectrum of prompt fission neutrons 21

$\frac{1}{4\pi}\chi(E' \to E)$ diffusion theory expression for the energy spectrum of fission neutrons (*normalized isotropic fission spectrum*) 28

χ^g group-discretized fission spectrum *(eq. 3.43)* 34

$\chi_d(E)$ energy spectrum of delayed fission neutrons 12

ε convergence criterion for the eigenvalue updating method 58

ϕ neutron flux *(eq. 2.2)* 9

$\phi(\mathbf{r}, E, \mathbf{\Omega}, t)$ transport theory expression for neutron flux (*angular neutron flux*) *(eq. 3.2)* 19

$\phi^g(\mathbf{r})$; ϕ^g group discretized neutron flux *(eq. 3.44)* 34

$\phi(\mathbf{r}, E)$ diffusion theory expression for neutron flux (angularly independent *total flux density*) *(eq. 3.23)* 28

$[\phi^1(\mathbf{r}), \phi^2(\mathbf{r})]_i$ i-th eigenvector of the two-group criticality problem 37

$\bar{\bar{\Phi}}_i^g$ numerical approximation of the integral average of flux over node $\mathcal{V}_i$ *(eq.* (4.23)*)* 50

$\bar{\bar{\phi}}_i^g$ integral average of flux over node $\mathcal{V}_i$ *(eq. 4.6)* 46

$\bar{\Phi}_{i,x+}^g$ numerical approximation of the integral average of flux over face $\Gamma_{i,x+}$ 52

$\phi_{t,i}^g(x)$ transverse integrated neutron flux *(eq. 4.66)* 63

$\tilde{\Phi}_i^g(x)$ inexact version of $\tilde{\phi}_i^g(x)$ 64

$\tilde{\phi}_i^g(x)$ transverse averaged neutron flux *(eq. 4.69)* 64

$\tilde{\bar{\Phi}}_i^g$ approximate flux, integrally averaged over all transverse cross sections of the node along the x-axis ($\tilde{\Phi}_i^g(x)$ averaged over the width of the node) 66

$\bar{\bar{\mathbf{\Phi}}}_i$ 2×1 column vector of flux averages for node $\mathcal{V}_i$ and both groups .. 70

$\bar{\bar{\mathbf{\Phi}}}^g$ $N \times 1$ column vector of flux averages for all nodes and group g 57

$\hat{\mathbf{\Phi}}_{x\pm}$; $\hat{\mathbf{\Phi}}_{i,x\pm}$ 2×2 auxiliary matrix for the relationship between flux and current at the same interface *(*(4.101a) *or* (4.101b)*)* 72

$\tilde{\mathbf{\Phi}}(x)$; $\tilde{\mathbf{\Phi}}_i(x)$ 2×1 vector of transverse averaged fluxes in respective groups (the complete solutions to the transverse integrated ODE) 69

$\tilde{\mathbf{\Phi}}_h(x)$ 2×1 vector of the homogeneous solutions (for each group) of the transverse integrated ODE 69

$\tilde{\mathbf{\Phi}}_p(x)$ 2×1 vector of the particular solutions (for each group) of the transverse integrated ODE 69

$\tilde{\bar{\mathbf{\Phi}}}_{x\pm}$; $\tilde{\bar{\mathbf{\Phi}}}_{i,x\pm}$ 2×1 vectors of transverse averaged fluxes (for each group) at sides $\Gamma_{i,x\pm}$ *(eq. 4.97)* 71

γ boundary condition coefficient *(eq. 3.40)* 33

$\Gamma_{i,x\pm}$, $\Gamma_{i,u\pm}$, $\Gamma_{i,v\pm}$; $\Gamma_{i,\xi\pm}$ faces of node $\mathcal{V}_i$ 44

λ criticality parameter (eigenvalue of the associated eigenvalue problem (4.1)) *(eq. 3.21)* 27

λ_i i-th eigenvalue of the two-group criticality problem 37

λ_1 smallest eigenvalue of the two-group criticality problem (*principal eigenvalue*) 38

ν average number of neutrons released by fission 12

ν_p (resp. ν_d) average number of prompt (resp. delayed) neutrons released by fission 12

$\nu_p(\mathbf{r}, E')$; $\nu(\mathbf{r}, E')$ transport theory expression for prompt fission neutrons yield 20

Ω the whole core domain 42

$\mathbf{\Omega}$ unit direction vector of neutron movement 17

$\mathbf{\Omega}'$ direction vector of neutrons not belonging to the balance set 19

Σ macroscopic cross section 8

σ *(in Chap. 4)* any arbitrary face of a given node 45

σ *(in Chap. 2)* microscopic cross section 8

Σ_* macroscopic cross section for an arbitrary reaction 9

$\Sigma_*(\mathbf{r}, E, t)$ transport theory expression for a general macroscopic cross section. 19

$\mathbf{\Sigma}_*^g$ $N \times N$ matrix of cross sections substituted by $*$ 57

σ_a (resp. Σ_a) microscopic (resp. macroscopic) cross section for neutron absorption 10

$\Sigma_a(\mathbf{r}, E, t)$ transport theory expression for the macroscopic absorption cross section 23

$\Sigma_a^g(\mathbf{r})$; Σ_a^g group-discretized absorption cross section *(eq. 3.45)* 35

σ_f (resp. Σ_f) microscopic (resp. macroscopic) cross section for fission 8

$\Sigma_f(\mathbf{r}, E', t)$ transport theory expression for the fission cross section 21

$\Sigma_{i,f}^g$ discrete value of the fission cross section for node $\mathcal{V}_i$ *(eq. 4.14)* 49

$\Sigma_f^{g'}(\mathbf{r})$; $\Sigma_f^{g'}$ group-discretized fission cross section *(eq. 3.45)* 35

$\Sigma_r^g(\mathbf{r})$; Σ_r^g total neutron removal cross section *(eq. 3.47)* 36

$\Sigma_{i,r}^g$ discrete value of the neutron removal cross section for node $\mathcal{V}_i$ *(eq. 4.12)* 49

σ_s (resp. Σ_s) microscopic (resp. macroscopic) cross section for scattering 9

$\Sigma_s(\mathbf{r}, E' \to E, \mathbf{\Omega}' \to \mathbf{\Omega}, t)$ transport theory expression for the macroscopic scattering cross section (*differential scattering cross section*) *(eq. 3.1)* 19

$\Sigma_s(\mathbf{r}, E, t)$ transport theory expression for the macroscopic scatter-out cross section *(eq. 3.12)* 23

$\Sigma_{i,s}^{1\to 2}$ discrete value of the neutron in-scatter cross section for node $\mathcal{V}_i$ *(eq. 4.13)* 49

$\Sigma_s^{g'\to g}(\mathbf{r})$; $\Sigma_s^{g'\to g}$ cross section for neutron scattering from group g' into group g (group-discretized in-scatter cross section) *(eq. 3.45)* 35

$\Sigma_s^g(\mathbf{r})$; Σ_s^g cross section for neutron scattering from group g into any energy group (group-discretized out-scatter cross section) *(eq. 3.45)* 35

Symbols

$\mathbf{a} \cdot \mathbf{b}$	dot product of vectors $\mathbf{a}$, $\mathbf{b}$ 19
∇	operator *nabla*: formally $\nabla = (\frac{\partial}{\partial x}, \frac{\partial}{\partial y}, \frac{\partial}{\partial z})$ in Chap. 3, $\nabla = (\frac{\partial}{\partial x}, \frac{\partial}{\partial y})$ in Chap. 4 24
$\mathbf{0}$	$N \times N$ zero matrix 57
$\times$	a separator between the integration symbols and the $\mathrm{d}E\,\mathrm{d}\mathbf{\Omega}$ symbol specifying the balance neutrons 20
$\mathrm{d}E$	elementary (differential) energy range 18
$\mathrm{d}E\,\mathrm{d}\mathbf{\Omega}$	differential subset of neutron phase space describing neutrons involved in the balance relation (*balance neutrons*) 20
$\mathrm{d}\mathbf{\Omega}$	elementary (differential) solid angle 18
$\mathrm{d}\mathbf{r}$	elementary (differential) spatial volume 18
$\mathrm{d}\sigma$	integration symbol for line integrals over a face 45
$\mathrm{d}S$	differential surface element (a scalar value) 19
$\mathrm{d}\mathbf{S}$	oriented differential surface element (a vector) 19
$\mathrm{d}t$	elementary (differential) time interval 18
$\langle q_k(x), q_l(x) \rangle$	inner product def. by eq. (4.90) 69
U-235	isotope
${}^{\mathrm{A}}_{\mathrm{Z}}\mathrm{X}$	nuclide
∂W	boundary of some domain W
Q	numerical approximation of quantity q
$q(\mathbf{r}, \ldots)\big\|_{\partial W\pm}$, $q(\partial W\pm)$	limit of function q as $\mathbf{r}$ approaches ∂W from inside, resp. outside of W)
$\bar{\bar{q}}$	integral average of quantity q over a node
$\tilde{\tilde{q}}$	integral average of quantity q over all transverse cross sections of a node along the x-axis

$\tilde{q}(x)$	integral average of quantity q over a transverse cross section of a node at point x
$\bar{q}$	integral average of quantity q over a face
$\frac{\partial q}{\partial t}$	time partial derivative of function q
$\frac{\partial q}{\partial x}$, $\frac{\partial q}{\partial y}$, $\frac{\partial q}{\partial z}$	spatial partial derivatives of q

Subscripts

$*$	placeholder for an arbitrary reaction type (fission, absorption, scattering)
a	absorption
$x\pm$, $u\pm$, $v\pm$; $\xi\pm$	indices of nodal faces, perpendicular to the x, u and v (coll. ξ) directions (respectively), with positive (plus sign), resp. negative (minus sign) orientation with respect to that direction
f	fission
h	homogeneous solution of ODE
i, k	linear index of a node
$i-1/2$, $i+1/2$	index of point lying on the left, resp. right face of node $\mathcal{V}_i$
$i+1$	index of node adjacent to $\mathcal{V}_i$ in a positive x-direction
$i\pm x$, $i\pm u$, $i\pm v$; $i\pm\xi$	indices of neighbouring nodes of $\mathcal{V}_i$
j	row index of nodal mesh
n	index representing relation to normal vector $\mathbf{n}$
p *(in Chap. 4)*	particular solution of ODE
p *(in Chap. 2, 3)*	related to prompt fission neutrons
s	scattering
t	for denoting transverse integrated quantities, also used in the symbol for transverse profile function
x, u, v	denote quantities oriented in x, u, resp. v directions
ξ	a placeholder for either of the indices x, u, v
∞	denotes the matrix infinity norm

Superscripts

$*$	excited state of a nuclide
C	prescript to symbolize quantities approximated by the nodal-corrected scheme
g	index of actual energy group
1	related to fast energy group
2	related to thermal energy group
g'	index of some group different from the actual group g (also summation index over energy groups)
$(\bullet)$	iteration index

Acronyms

ANC-HM	**A**dvanced **N**odal **C**ode for **H**exagonal Geometry using Conformal **M**apping ... 82
ANM	**A**nalytic **N**odal **M**ethod ... 41
CMFD	**C**oarse **M**esh **F**inite **D**ifference ... 61
FDM	**F**inite **D**ifference **M**ethod ... 39
FV	**F**inite **V**olume ... 39
GET	**G**eneralized **E**quivalence **T**heory ... 40
NEM	**N**odal **E**xpansion **M**ethod ... 41
ODE	ordinary differential equation ... 40
PDE	**P**artial **D**ifferential **E**quation ... 33
PWR	**P**ressurized Light-**W**ater-Moderated and Cooled **R**eactor ... 1
VVER	**V**oda-**V**odyanoi **E**nergetichesky **R**eaktor (Russian term for the pressurized water reactor) ... 2

List of Figures

Chapter 1

Introduction

1.1 Motivation

The field of nuclear power plant engineering is a good example of usefulness of mathematical modelling. Reactors find their use not only in power plants but also in naval and space transportation, medical industry or materials testing, therefore a thorough understanding of processes occuring in them is of great concern. Mathematical models play an important role in effective nuclear reactor design, control of its smooth operation or assessment of various malfunctions and accidents. Specifically, this thesis chooses as a model problem the optimal *fuel reloading* strategy, which requires many long-term test runs of the reactor for different fuel loading patterns – a task clearly needing computer simulations to accomplish.

The most important part of the reactor is its core. It consists of a set of assemblies loaded with fuel, control mechanisms and cooling material. There, during an event called *fission*, a great amount of energy is released. To produce more energy, each fission event can under suitable conditions trigger another in a process called *chain reaction*. Since the essential ingredients in fission chain reaction are the *neutrons*, the exact knowledge of their distribution and movement throughout the reactor core is sought. The mathematical model that provides this information is based on the *neutron transport equation*.

1.2 Problem description

The fuel reloading problem will be studied for pressurized water reactors (PWR). Fuel assemblies powering these reactors consist mainly of rods loaded with slightly enriched uranium. During a run of the reactor, fissions continually occur in the assemblies and result in conversion of uranium into products that can't be fissioned anymore – the assemblies are *burning up*. The process of fuel depletion doesn't occur spatially uniformly within the core and is directly dependent on neutron distribution in each assembly. After a period of a so called *fuel cycle*, the core will contain assemblies with various levels of depletion – some will have to be replaced completely by fresh fuel while the others will have to be

moved to places where they would contribute to power production more effectively[1].

This operation changes the overall reactivity of the reactor and adjustment of the distribution of neutron absorbers becomes necessary as well. The new core configuration must preserve the best possible performance and meet various operational and safety regulations for the course of next fuel cycle. Fuel reloading has thus form of a constrained discrete optimization problem.

To evaluate reactor effectivity for a particular assembly arrangement, a tunable parameter is introduced to the transport equation. As we wish to know a long-term behaviour of a reactor configured according to the selected strategy, a steady-state solution is sought. It turns out that there exists only one value of the parameter for which a physically plausible, non-trivial solution exists. This value specifies how the quantity varied by the parameter has to be changed in order to ensure steady state operation. The associated solution describes the neutron distribution (referred to as *flux*) within the steady core and may then be further used to calculate power production of each assembly. The uniformity of power distribution is a crucial safety issue since high power levels may result in temperature increases beyond the cooling ability of the surrounding coolant.

Mathematically, previous paragraph describes an eigenvalue problem for the steady-state neutron transport equation. It must be solved for each loading pattern found by the optimization method. Since there is a huge number of arrangement possibilities[2], the solving eigenpair must be found rapidly. Development of a method that satisfies this requirement is subject of this thesis.

1.3 Overview of solution methods

The problem as described in previous section features a solution of neutron transport equation. In its full generality, it is a complicated integrodifferential equation which is extremely difficult to solve. Hence for practical computations some simplifications must be made. Often used is the *diffusion approximation* in which the accurate transport theory is replaced by approximate diffusion theory. Diffusion formulation consists of a parabolic partial differential equation describing the neutron balance at each point in the core and a constitutive relation called Fick's law. In general, the energetic dependence of neutron distribution is discretized into so called *groups* and a system of *multigroup diffusion equations* arises as a result. In this work, a two group model is considered and a steady state, time-independent solution is sought, hence two coupled elliptic differential equations will be solved.

Analytical solution to these equations may be found only in some special cases. For real situations, numerical methods have to be employed. Apart from statistical Monte-Carlo approach based on simulating collision probabilities for individual neutrons and atoms,

[1] for instance, fuel cycle for the Temelin power plant spans one year; 1/4th of assemblies are replaced during a refuelling process ([ČEZ])

[2] e.g. the PWR reactor of type VVER-1000 used in Temelin contains 163 assemblies ([ČEZ])

deterministic methods are also popular for reactor analyses. Their representatives are e.g. the finite-difference method, the finite-elements method or the *nodal method*.

Monte-Carlo methods are still too computationally expensive for the given problem. Methods utilizing standard finite differences pose strict conditions on discretization granularity in order to preserve sufficient accuracy. The final choice of the nodal approach over that based on finite elements was driven by the ease of implementation. In a nodal method, the multigroup diffusion equations are solved on a coarse grid of *nodes* (with each node corresponding to a single assembly), using the *finite-volume method*. To solve the equations arising from such discretization, quantities defined for nodal surfaces must be related to those defined within the nodes. A set of local two-node coupling problems in one dimension, obtained by the *transverse integration* method, is solved for this purpose since it allows a higher order representation of surface quantities than the traditional finite-volume technique. To achieve reasonable accuracy and efficiency alike, the non-linear iterative scheme ties the transverse integration procedure with the whole-core finite-volume method.

1.4 Organization of the thesis

The following chapter serves as an overview of the most important concepts of reactor physics. Quantities defined in this chapter are then used in chapter 3 to derive the mathematical model based on transport theory. That chapter further outlines transition to multigroup diffusion equations. In chapter 4, the finite-volume method is described and provides a basis for development of the nodal method. Transverse integration procedure is needed for this second step and is described next, together with an effective method for solving the associated equations. Implementation of this method in MATLAB is briefly discussed in chapter 5 and compared with verified test results. The final chapter summarizes the whole work and concludes with possible future improvements and research directions.

Chapter 2

Physical background

2.1 Notation

Atomic nuclei consist of *nucleons* – the protons and the neutrons. Their total number is called *atomic mass* and is denoted by A, the number of protons only is called *atomic number* and is denoted by Z (thus the number of neutrons only can be obtained as the difference $A - Z$). When I want to write about a particular nucleus with specific number of protons and neutrons, I will call that nucleus a *nuclide*. Nuclides will be denoted by symbol ${}^{\mathrm{A}}_{\mathrm{Z}}\mathrm{X}$ (neutrons similarly by ${}^{1}_{0}\mathrm{n}$). Nuclides of the same element, differing only in the number of neutrons (i.e. with same Z but different A), are called *isotopes*. Usually, I denote already mentioned nuclides and their isotopes only by their atomic mass and omit their atomic number (for instance, U-235 and U-238, respectively, will refer to ${}^{235}_{92}\mathrm{U}$ and ${}^{238}_{92}\mathrm{U}$, respectively).

2.2 Basic concepts

Nucleus structure. Within a stable nucleus, nucleons are kept together by attractive strong nuclear forces they exert on each other. They reside in a well of negative potential energy, as schematically depicted in figure 2.2. Further away from the center of the nucleus, neutrons are not held by any force and thus their potential energy approaches zero (assuming that they are not moving). Protons receding from the nucleus first obtain some positive kinetic energy due to repulsive electrostatic forces which take over the short-range strong nuclear force. They repell the protons from the nucleus, but infinitely far away from its center, also these electrostatic forces vanish.

Binding energy *of some nucleon to the nucleus* is defined as difference between the energy of the nucleon infinitely far away from the nucleus and its energy inside that nucleus. It is released when the nucleon joins other nucleons in the event of nucleus creation, i.e. when it descends into the potential well. Equivalently, the same amount of energy must be supplied in order to free it from the nucleus. Nucleons always fill the lowest unoccupied

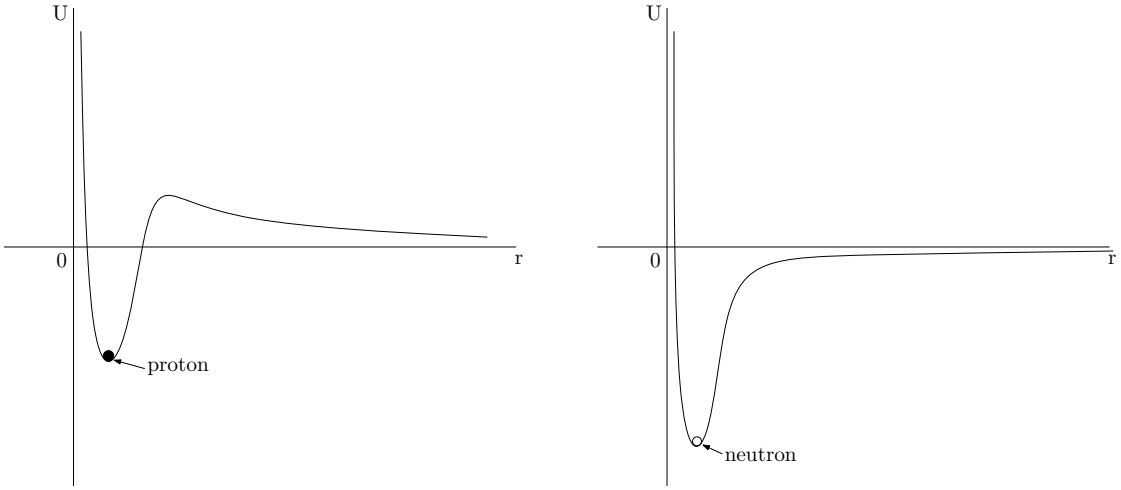

(a) Proton potential (b) Neutron potential

Figure 2.1: Nucleons inside a stable nucleus and their potential energy U with increasing distance r from the centre of the nucleus at $r = 0$

energy levels – the lower they can descend when creating the nucleus, the higher is their binding energy.

The average quantity used when describing actual nuclides from energetic point of view is the *binding energy of nucleus per nucleon* which is defined as the sum of binding energies of all the nucleons comprising the nuclide divided by their number (that is, by atomic mass). It is the binding energy of an average nucleon to the nucleus.

Energy release from nuclear reactions. According to discussion above, in order to gain energy we need to convert nuclides with lower binding energy per nucleon (imagine a shallower potential well for nucleons to fall into) to those with higher (deeper potential well). Looking at figure 2.2, one easily spots that most tightly bound are the nuclides with atomic mass around 60. Both lighter and heavier nuclides have lower binding energies per nucleon. Therefore a nucleus heavier than $A \approx 60$ will release energy when it splits apart (in a reaction called *fission*), while two nuclei lighter than $A \approx 60$ will release energy when they fuse together (*fusion*). Actual energy yield from either fission or fusion corresponds to the difference of binding energies per nucleon of the original nucleus and the reaction products multiplied by their respective atomic masses.

By comparing the steepness of the fusion part of the graph in figure 2.2 with that of the fission part, one can deduce that much more energy is released by fusion – however, the actual construction of a commercially suitable fusion device is accompanied by lots of technical difficulties and to this day only fission-employing power generators are economically effective.

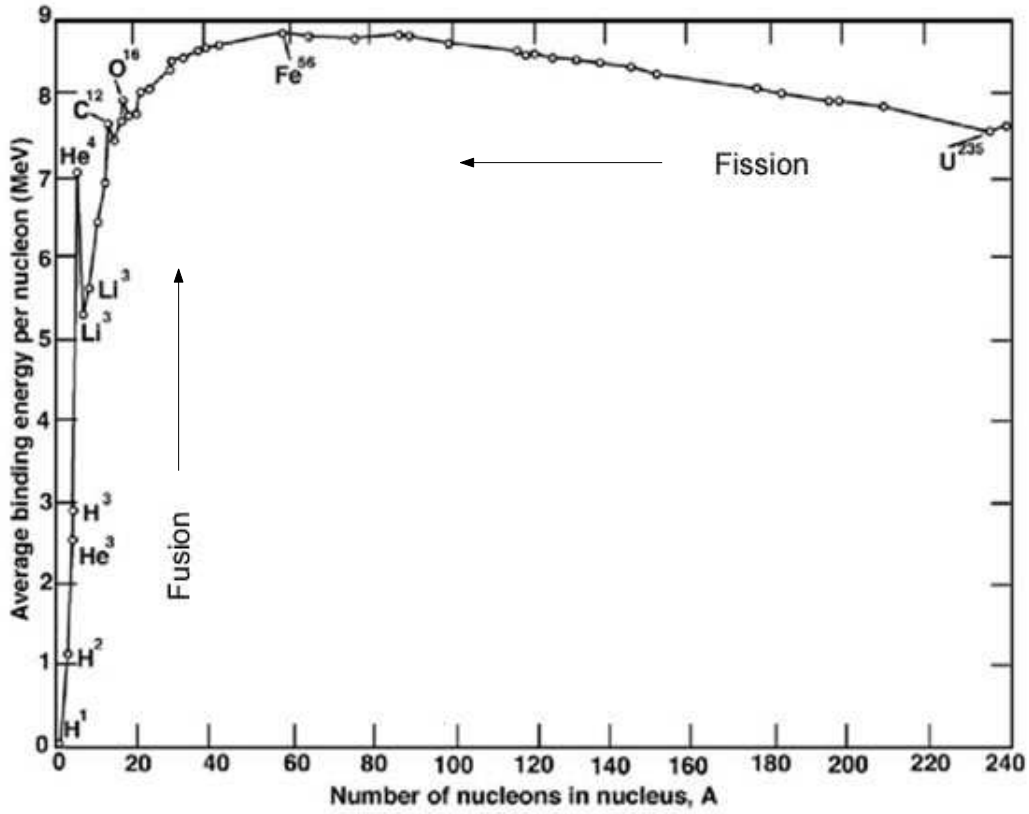

Figure 2.2: Binding energy per nucleon (adapted from `http://en.wikipedia.org/wiki/Image:Binding_energy_curve_-_common_isotopes.svg` , courtesy of "Wikimedia Commons")

2.3 Neutron-nuclei interactions

2.3.1 Neutron properties

Neutron is a subatomic particle that does not carry any electric charge and has a slightly higher mass than proton. When free, neutrons are unstable and decay into proton, electron and antineutrino. Their mean lifetime of about 15 minutes ([Y+06]) is much longer than the mean lifetime of neutrons freed during reactions in a reactor and therefore neutron decay does not influence these reactions.

Concerning energy, neutrons may be divided roughly into three classes:

- fast, with energies $E > 1\,\mathrm{MeV}$,
- intermediate, with energies in the range $1\,\mathrm{keV} < E < 1\,\mathrm{MeV}$,
- slow, with energies under $1\,\mathrm{keV}$.

Neutrons moving at the slowest possible speed in a given environment are put into a special category and are called *thermal neutrons*. They are in thermal equilibrium with surrounding atoms and have energies of the order of $\sim 10^{-1}$ eV. Energy of the interacting neutron strongly influences behaviour of the interaction, as described in next section.

2.3.2 Interactions quantification

Microscopic cross section. Probability of a specific nuclear reaction is commonly measured by cross sections. Microscopic cross section, σ, is the probability that a neutron coming perpendicularly to a unit area interacts with a nucleus on that area. Units of cross section are areal, most often of the order of 1 *barn*: $10^{-24}\,\mathrm{cm}^2$. This is the reason why we usually percieve cross section as the area presented to an incoming neutron by the nucleus, for a particular reaction process. It deserevs mentioning, however, that the reaction probability generally does not have any relation to the geometry of the nuclei ([Sch97]).

Macroscopic cross section. If microscopic cross section is imagined as the area for a specific interaction presented by one nucleus, the macroscopic cross section would be the interaction area made up by all the nuclei in a unit volume of material. More precisely, it is the probability that a specific interaction occurs when the neutron travels a unit distance through a homogeneous sample of material. Using the microscopic cross section of each of the nuclei in the sample, it can be expressed as

$$\Sigma = N\sigma, \tag{2.1}$$

where N is the number of nuclei per cm^3 of the sample (*atomic density*). It's units are cm^{-1}.

Properties of cross sections. Besides their dependence on nucleus structure, cross sections also exhibit a very complex dependence on energy of the reacting neutron. Furthermore, they are related to a particular reaction. The reaction is commonly specified in a subscript, e.g. σ_f (resp. Σ_f) denotes the cross section for fission.

It is also worth noting that the probability of neutron-neutron interactions is negligible comparing to probabilities of their interaction with atomic nuclei since the density of neutrons per unit volume is negligible when compared to atomic density. This has an important implication on linearity of the governing equation, as will be shown in chapter 3.

Although the microscopic cross section is the basic material property actually measured by experiments, only the macroscopic cross sections will be important for constructing the equations. Eq. (2.1) explains how they can be obtained from microscopic cross sections for a given material.

Reaction rate. Let's consider a beam of neutrons with density n neutrons per cm^3, all moving at speed v through a unit volume[1]. The number of interactions per unit time they will have with nuclei in that volume can be expressed as

$$r_* = \Sigma_* n v$$

and represents the *reaction rate*. The asterisks in the equation replace any specific kind of reaction. Furthermore, it is expedient for the purposes of derivation of the transport equation in chapter 3 to define the *neutron flux* as

$$\phi = nv \tag{2.2}$$

and thus the reaction rate as

$$r_* = \Sigma_* \phi. \tag{2.3}$$

Note that in such a definition, the flux is a scalar quantity, since it is the product of the scalar neutron density and the scalar magnitude of neutron velocity vector. The term flux originates again from its units ($\mathrm{cm}^{-2}\mathrm{s}^{-1}$) which correspond to units of (vector) fluxes in many other disciplines (e.g. heat transfer or electromagnetic theory).

2.3.3 Types of reactions

There are two classes of possible interactions between neutrons and nuclei: *scattering* and *absorption*.

Scattering. When the neutron is subject to a scattering collision, the direction of its movement is changed and its energy (or, equivalently, speed) lowered. Scattering reactions come in two fashions – *elastic* and *inelastic*. The former can be imagined as a classic collision of two perfectly elastic balls[2]. The energy of the neutron-nucleus system is conserved, all energy that the neutron loses in the moment of collision is transferred to the target nucleus. The latter, on the other hand, is not conservative – some of the transferred energy escapes in the form of gamma photons. It happens only with neutrons of MeV-range energies and thus affects the neutrons only during the first few moments of their life in the reactor. Therefore mainly elastic scattering is interesting for reactor modelling purposes. Scattering probability is measured by the scattering cross section, σ_s (resp. Σ_s).

Absorption. In an absorption event, a freely flying neutron hits a nucleus and is captured. Such a neutron is lost for further interactions but (via fission, a special case of absorption) can liberate new neutrons. When the neutron is absorbed, the nucleus (A, Z) turns into an unstable compound nucleus ($A+1$, Z). The compound nucleus obtains the kinetic and the binding energy of the neutron and this additional energy allows nucleons

[1] if each neutron had different speed (a typical case in real situations), the following equations had to be integrated over v

[2] however, the exact course of that reaction is naturally determined by quantum mechanical laws

to get to higher energy levels – the nucleus is said to attain an *excited* state. In order to get back to its stable *ground state* (with nucleons in positions of lowest energy), it has to *deexcite*. Deexcitation has the form of particle emission where the actual particle emitted is determined by the type of the absorption reaction. The two absorption reactions that mostly affect neutron distribution in a reactor – *fission* (cross section σ_f) and *radiative capture* (cross section σ_γ) – are described in next two sections in more detail. However, there are more types of absorption events leading to an excited state of the nucleus (interested reader is referred to publications devoted to nuclear physics, such as [Sta01]). The overall probability that a neutron will be captured in any way is expressed by the total absorption cross section, σ_a (thus $\sigma_a = \sigma_f + \sigma_\gamma + \ldots$ where the ellipsis represents any unmentioned capture events). Macroscopic absorption cross section Σ_a is defined accordingly.

2.3.4 Fission

Fission is the reaction that makes power production in nuclear energy stations possible. For fission to start, the neutron and proton potential barriers must be surpassed in order to separate the nucleons from each other and let them reorganize into different nuclides with higher binding energies per nucleon (recall paragraph about nucleus structure on page 5). There are several possibilities how to overcome the barrier, though only two are viable in a nuclear reactor:

1. *Quantum tunneling* allows penetration of the barrier without much effort, but happens extremely rarely. Its probability becomes measurable only at high atomic masses. Nevertheless, certain of those heavy nuclides like ${}^{252}_{98}\mathrm{Cf}$ exhibit this so called *spontaneous fission* quite often and are even used as additional neutron sources in nuclear reactors.

2. *Neutron induced fission*, on the other hand, is common in the reactor and serves as the principal source of neutrons.

Neutron induced fission. As noted in section 2.3.1, neutron is uncharged which means that it is not repelled by protons inside the nucleus. As a consequence it can easily come close enough to other nucleons inside the nucleus to be bound by strong nuclear forces. The compound nucleus in an excited state is formed in the process. If there is sufficient excitation (above a threshold called *activation energy of the nucleus*), fissioning may start.

There are nuclides, called *fissile*, whose activation energy is not much higher than the binding energy of an additional neutron to that nuclide. The neutron doesn't need to have much kinetic energy in order to initiate fission on these nuclides. They are represented e.g. by ${}^{235}_{92}\mathrm{U}$ or ${}^{239}_{94}\mathrm{Pu}$ – generally heavy nuclides with odd atomic mass number ([Sta01, p. 6]). Fission of fissile nuclides is utilized in *thermal reactors*, so called because fission-inducing neutrons can be slow, even thermal (section 2.4 explains why having thermal neutrons initiate fission is so effective).

The other kind of nuclides must also utilize high kinetic energies of impacting neutrons in order to split apart. These are called *fissionable* (e.g. ${}^{238}_{92}\mathrm{U}$ or ${}^{240}_{94}\mathrm{Pu}$, heavy nuclides

with even masses) [3]. *Fast reactors* utilizing fast moving neutrons ($E_k \gtrsim 1\,\mathrm{MeV}$) to fission fissionable material will not be considered since the PWR reactors studied in this work fall into the former category.

Scheme of the reaction. A fission of ${}^{235}_{92}\mathrm{U}$ (U-235) has the following general form (the asterisk denotes the excited state of the nuclide):

$$\begin{aligned} {}^{235}_{92}\mathrm{U} + {}^{1}_{0}\mathrm{n} &\longrightarrow ({}^{236}_{92}\mathrm{U})^{*} \\ &\longrightarrow 2 \text{ fission fragments } + \text{ recoil energy} \\ &\longrightarrow 2 \text{ fission products } + \nu\, {}^{1}_{0}\mathrm{n} + (\beta^{-} + \gamma) + \Delta\mathrm{E}. \end{aligned} \tag{2.4}$$

The heavy uranium nucleus splits into two medium sized nuclei called *fission fragments*. When split, nucleons of the fragments are in the range of dominating electrostatic repulsion and thus the fragments recoil at very high speed. However, due to their limited movement possibility in solid fuel (only a few centimeters), all their kinetic energy (about 170 MeV) gets quickly converted to heat. This comprises about 85% of the total energy produced by fission, the rest being released during subsequent decays of the fragments (ΔE).

Fission fragments are highly unstable and begin stabilizing almost instantly ($\sim 10^{-12}\,\mathrm{s}$) by emission of the so called *prompt neutrons* and rays of *prompt gamma* photons. This process is governed by statistical rules, usually two or three prompt neutrons are freed per fission. The result of this initial decay is a conversion of fission fragments into more stable *fission products*. Again, the precise pair of fission products cannot be determined, but usually nuclides with atomic masses around 95, respectively 139, come out of a U-235 fission event (e.g. Ba+Kr or Xe+Sr, see e.g. [Heř81, p. 23]).

Delayed neutrons. Although more stable than fission fragments, the initial fission products are typically still radioactive and undergo a series of electron emissions (β^{-}–decay) followed by gamma radiation to finally end up as stable isotopes. Some nuclides in this sequence may also decay by emitting neutrons instead of electrons. Such neutrons are called *delayed* because they may be released as late as $\sim 10^{1}\,\mathrm{s}$ after fission. Nuclides exposing this behaviour are called *delayed neutron precursors* and are typically divided into six groups according to their half-lives.

Emission of a delayed neutron is a rare event – only about 1% of neutrons liberated by fission are delayed and the rest are prompt. However, even such a small fraction increases the average time of neutron presence in the reactor from about $10^{-4}\,\mathrm{s}$ (considering only prompt neutrons) to about $10^{-1}\,\mathrm{s}$ (taking into account also the delayed neutrons), depending on the half-life of the precursor. By increasing the neutron lifetime, delayed neutrons make it possible to control the rate of power generation by adjusting the neutron production rate – without them, a small change in neutron production rate would result in an unmanageably fast change in power production rate.

[3] note that from the point of view of additional neutron energy needed to trigger the fission process, every fissile nuclide is also fissionable

The effect of delayed neutrons becomes important in reactor dynamics calculations. As this thesis deals with a steady state problem, it is not necessary to be concerned with them in much detail. A more thorough treatment of dynamical topics can be found e.g. in [Sta01, Chap. 5] or [Heř81, Chap. 6].

Properties of neutrons released by fission. I will denote the average number of prompt and delayed neutrons, respectively, by ν_p and ν_d. These counts depend on energy of the neutron responsible for the reaction and on the nucleus being fissioned. The average number of both prompt and delayed neutrons obtained is then denoted by ν, $\nu = \nu_p + \nu_d$. For U-235 fissioned by thermal neutrons, its value is $\nu = 2.5$ neutrons.

The energy with which are the neutrons emitted is of the order of $\sim$1 MeV for prompt neutrons and ~ 0.1 MeV for delayed neutrons. The probability of prompt (respectively delayed) neutron being released with energy E is measured by the *fission spectrum*, $\chi_p(E)$, resp. $\chi_{d,i}(E)$, where index i represents the particular precursor group from which the delayed neutron originated. Empirical behaviours of these functions of energy are known, figure 2.3 shows an example of prompt neutrons spectrum of an U-235 fission event. After

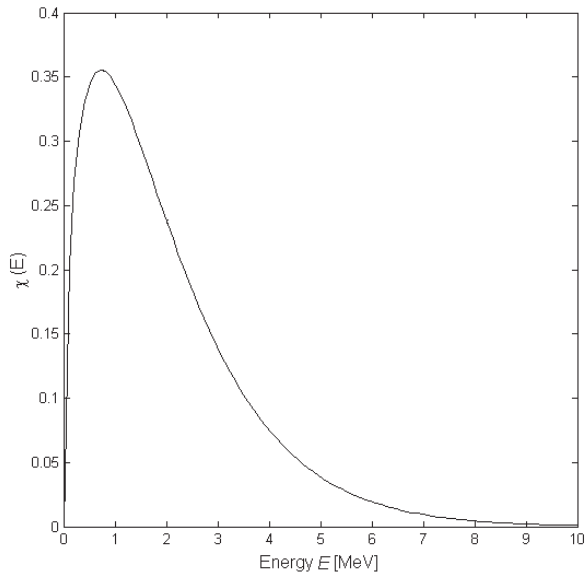

Figure 2.3: Fission spectrum of prompt neutrons for U-235 (from [Sta01, p. 12])

setting free, neutrons diffuse through the surrounding environment and lose their energy by scattering, until they are captured by some nucleus, escape the core or even up their energy with the nuclei around.

Fission cross section. The probability that a neutron causes fission is expressed by the *fission cross section*, σ_f. As pointed out in section 2.3.2, the cross section is a very complicated function of neutron energy. For instance, microscopic fission cross sections of

two main isotopes contained in natural uranium are plotted in fig. 2.4 against the energy of the neutron inducing that reaction. The fission neutron is born in the rightmost part of the graph (MeV energy range) and slows down during its life to the leftmost part. The difference between fissile U-235 and fissionable U-238 can be clearly spotted from the graphs. Apart from resonances in the intermediate energy range, the probability that U-238 will be fissioned by a neutron with energy below 1 MeV is negligible. On the other hand, note that the less energetic a neutron is, the greater chance it has to fission a U-235 nucleus.

2.3.5 Radiative capture

The most common type of interaction that can happen when a neutron hits a nucleus of virtually any element is the radiative capture. The excited compound nucleus achieves its ground state by emission of a photon of gamma radiation. This kind of absorption is parasitic since the absorbed neutron can no longer cause any other reaction and no new neutron is freed as a compensation. For some kind of nuclei (called *fertile*, e.g. U-238), this form of decay may result in conversion of the nucleus to a fissile one. Reactors utilizing this process to breed new fuel on the course of their run are called *breeder reactors* (see e.g. [Sta01, chap. 7]).

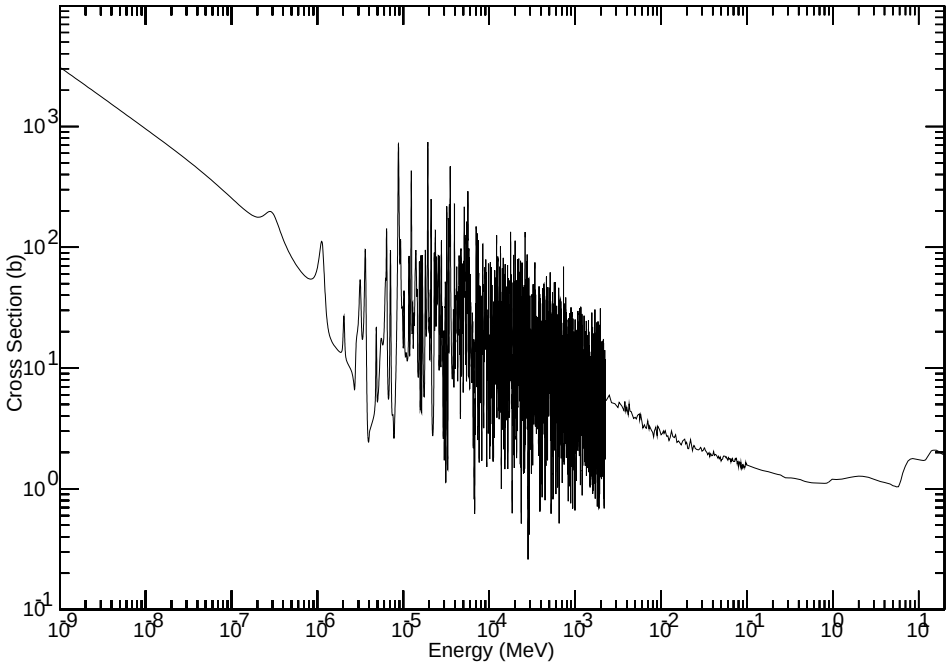

(a) Microscopic cross section of U-235 fission

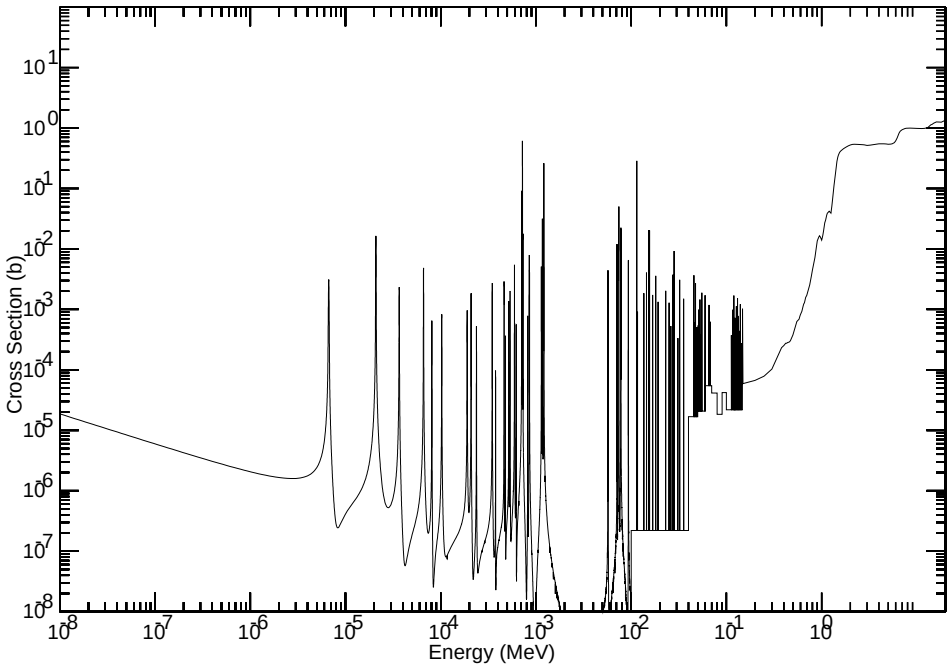

(b) Microscopic cross section of U-238 fission

Figure 2.4: Energetic dependence of fission cross section (from reference [Kor] (`http://atom.kaeri.re.kr/cgi-bin/endfplot.pl`))

2.4 Chain Reaction

Every fission reaction consumes one free-moving neutron, but releases a few more in exchange. Each of these liberated neutrons might induce new fission reactions if they hit a fuel element. However, not all manage to hit that fuel nucleus in a way that makes it split. To sustain fission in the reactor, at least one of the liberated neutrons must, on average, survive to induce new fission. This process of sustaining fission is called *chain reaction*.

Neutron lifecycle. Chain reaction takes place in the reactor core, sometimes also called *active zone*. The active zone contains fuel assemblies, coolant, moderating and absorbing material and some structural material like cladding and spacers.

The fuel has typically a form of uranium-filled rods plugged into the assemblies. Natural uranium, however, contains more than 99% of fissionable isotope U-238 and only about 0.7% of fissile U-235[4]. Only neutrons with high energy (on MeV levels) can induce the fission of U-238 (see figure 2.4(b)). Such neutrons are present only near the origin of their liberation since with increasing time they gradually lose their energy due to collisions with other nuclei.

Isotope U-235, on the other hand, may be fissioned by neutrons of any energy but the probability is much higher for thermal neutrons (see figure 2.4(a)). In thermal reactors, most fission events are caused by thermal neutrons hitting U-235 nuclides. Since there is so little of U-235 in natural uranium, the effort is to slow down the neutrons as much as possible to facilitate the reaction. This is the job for the *moderator* nuclei. However, as neutron energy sinks to the keV range, the probability of non-productive radiative capture (see section 2.3.5) on U-238 becomes quite high. Therefore, a good moderator should slow down the neutrons as quickly as possible in order to avoid these unwanted captures. Naturally, it should also capture the neutrons by itself as little as possible. Efficient moderators having both these properties are e.g. heavy water or graphite; PWR reactors with slight fuel enrichment can also use ordinary water to moderate fast fission neutrons (in addition to its use as a coolant).

Freely moving neutron can also be non-productively absorbed by other nuclides inside the active zone, e.g. by coolant, moderator and structural atoms or even by U-235 (though more often this capture event ends by productive fission). Except being absorbed, the neutron can also leak entirely out of the core through its boundary[5]. This may be remedied by placing a special material around the active zone that reflects a portion of the neutrons back (hence the commonly used term *reflector*).

[4] PWR designs utilize slightly enriched natural uranium with concentration of fissile material raised to about 3% ([ČEZ], [Heř81, p. 210]).

[5] this is possible since neutrons do not interact with the electron clouds of atoms comprising the boundary walls; only the minuscule nuclei stand in the way of the escaping neutron

Effective multiplication constant. The conclusion of the previous paragraph is that only a small fraction of neutrons initially created by fission events in fuel assemblies will have the opportunity to induce further fissions of U-235. Such neutrons give birth to a new generation of neutrons. If their number is n_{g-1} and the number of neutrons in this new generation is denoted by n_g then the ratio

$$k_{\text{eff}} = \frac{n_{g-1}}{n_g} \tag{2.5}$$

is called *effective multiplication constant*. Depending on its value, the reactor can be running in three different states:

- $k_{\text{eff}} < 1$, *subcritical state.* The population of neutrons in the active zone decreases; chain reaction is dying out.
- $k_{\text{eff}} = 1$, *critical state.* The population of neutrons in the active zone remains constant; chain reaction is self-sustained.
- $k_{\text{eff}} > 1$, *supercritical state.* The population of neutrons increases; chain reaction grows.

Critical state corresponds to steady operation of the reactor – number of neutrons within the core doesn't change and power production is constant. The aim is to always be as close to this state as possible. The condition for criticality depends on the size and geometry of the reactor (affecting leakage) and on the material composition (affecting number of absorptions and fissions). Usually, geometrical properties are given and can't be changed, so in order to maintain neutron equilibrium, material properties must be adjusted.

During reactor operation, changes in multiplication coefficent are handled by manipulating absorption devices. In PWR reactors, absorption is controlled by two principal mechanisms. In the first, absorbing rods made of boron steel are moved into fuel assemblies to control the momentary fluctuations in neutron population density (usually during startup and shutdown operations). To compensate for the slow changes in long-term chain reaction, absorbing boric acid is dissolved in the cooling water and its concentration is varied appropriately.

In the fuel management area, the multiplication coefficient is interesting as a measure of long-term stability of chain reaction for a proposed fuel charge pattern. The primary objective of fuel loading optimization is to find such a configuration that supports a self-sustained chain reaction of the core for a required time. The multiplication coefficient serves thus as an optimality indicator. Since various mathematical models with various reactivity profiles can be obtained by adjusting a parameter in the governing equations (as mentioned earlier in section 1.2), this parameter seems to be directly related to the multiplication factor. The connection will be revealed in more detail in section 3.1.4.

Chapter 3

Mathematical model

Neutron distribution inside the reactor core is mathematically best described by transport theory, originally developed by Boltzmann to explain distribution of particles in gas. However, it has been observed that the complicated equations constituting the theory can be simplified to well-examined diffusion equations which still retain sufficient amount of accuracy.

3.1 Neutron transport theory

3.1.1 Neutron transport equation

The transport equation governs neutron balance within the active zone of a reactor. In order to formulate it in its full generality, one must take into account all the dependencies of quantities mentioned in chapter 2. As an important assumption, this chapter will study the three dimensional reactor core on a macroscopic scale, i.e. as a continuous environment, and also all involved time-dependent quantities will be assumed continuous in time. Moreover, all external forces (like gravity) that may act on the particles and nuclei will be neglected.

3.1.1.1 Basic quantities

Description of neutrons' state. Let's think of a neutron moving throughout the core in the direction of unit vector $\mathbf{\Omega}$. If $v = v(E)$ is the speed of its movement, then its velocity vector, $\mathbf{v} = \mathbf{v}(E)$, is given by

$$\mathbf{v} = v\mathbf{\Omega}.$$

Denoting m the mass of the neutron, its energy[1] is

$$E = \frac{1}{2}mv^2.$$

The state of the neutron at any time t is completely described by its position $\mathbf{r}$ ($\mathbf{r} = (x, y, z)$), energy E, and direction $\mathbf{\Omega}$ in which it is moving. These are the fundamental quantities

[1] in the form of kinetic energy, since no other force affects the free neutral particle

uniquely characterizing each neutron and various others may be expressed in their terms[2]. The ranges of all the possible values they can take form the *neutron phase space*.

Fundamental quantities of reactor modelling. The most important physical quantity used to quantify processes caused by neutrons is the *angular neutron density*, denoted[3] by N:

$$N = N(\mathbf{r}, E, \mathbf{\Omega}, t).$$

It is defined in a statistical sense, such that $N(\mathbf{r}, E, \mathbf{\Omega}, t)\,\mathrm{d}\mathbf{r}\,\mathrm{d}E\,\mathrm{d}\mathbf{\Omega}\,\mathrm{d}t$ expresses the expected number of neutrons located in time interval $[t, t+\mathrm{d}t\,]$ in volume element $\mathrm{d}\mathbf{r}$ around $\mathbf{r}$, having energy in interval $[E, E+dE]$ and moving within a cone formed by a solid angle $\mathrm{d}\mathbf{\Omega}$ around the unit direction vector $\mathbf{\Omega}$ ([Wil71, p. 12]). The velocity vector within solid angle $\mathrm{d}\mathbf{\Omega}$ of one of the neutrons from within $\mathrm{d}\mathbf{r}$ is depicted in figure 3.1.

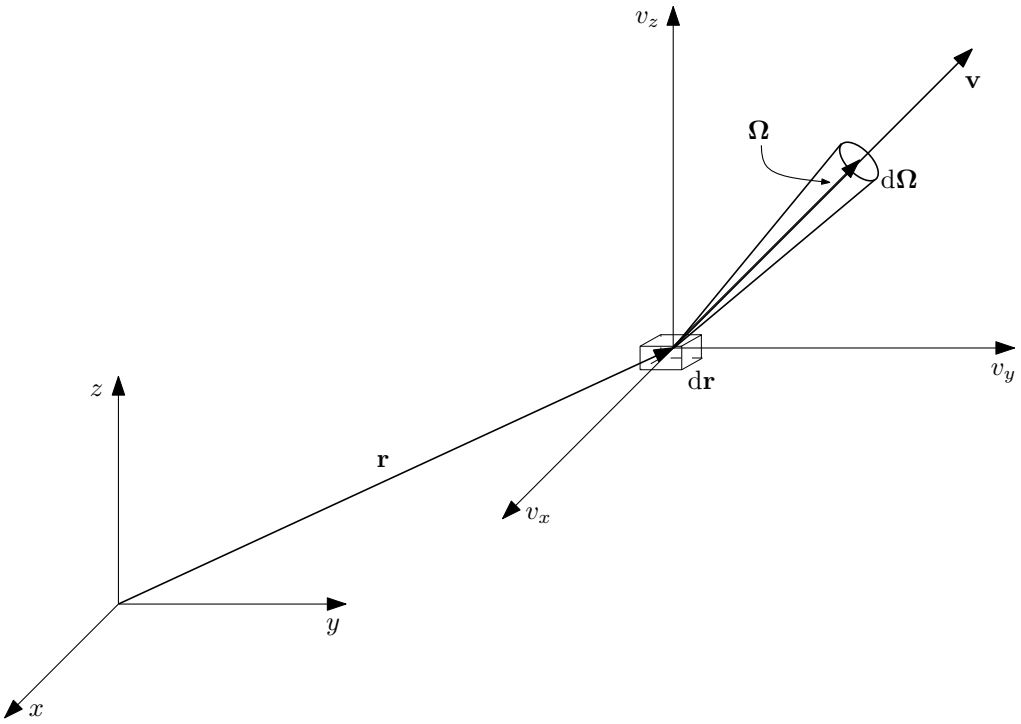

Figure 3.1: Position and movement direction of neutrons (adapted from [Wil71])

To describe the reactions occuring within the reactor, their cross sections need to be determined. Because of the macroscopic nature of the model, only macroscopic cross sections have to be considered. Writing explicitly their dependence on energy (as mentioned in section 2.3.2) and time (since cross section is a material property and material attributes

[2]note that this choice of quantities is not unique, e.g. the set $\mathbf{r}$, v and $\mathbf{\Omega}$ could have been used instead to describe the neutrons

[3]the atomic density for which the same letter was used in chapter 2 will not be needed anymore

change during the run of a reactor):

$$\Sigma_* = \Sigma_*(\mathbf{r}, E, t),$$

we get the general probability of neutron with energy E interacting with a nucleus at point $\mathbf{r}$. Reactions that may be substituted for the asterisk were discussed in section 2.3.3.

In the case of scattering, the *differential scattering cross section* is usually introduced ([Wil71, p. 13], [Sch97, p. 10]) to emphasize the fact that scattering changes energy and direction of the inciding neutron:

$$\Sigma_s(\mathbf{r}, E' \to E, \mathbf{\Omega}' \to \mathbf{\Omega}, t) = \Sigma_s(\mathbf{r}, E', t) P(\mathbf{r}, E' \to E, \mathbf{\Omega}' \to \mathbf{\Omega}), \tag{3.1}$$

where $P(\mathbf{r}, E' \to E, \mathbf{\Omega}' \to \mathbf{\Omega})\,\mathrm{d}E\,\mathrm{d}\mathbf{\Omega}$ is the probability that collision at point $\mathbf{r}$ will change neutron's energy and direction from $\mathrm{d}E'\,\mathrm{d}\mathbf{\Omega}'$ to $\mathrm{d}E\,\mathrm{d}\mathbf{\Omega}$.

The *angular neutron flux* is defined by using equation (2.2):

$$\phi(\mathbf{r}, E, \mathbf{\Omega}, t) = v(E) N(\mathbf{r}, E, \mathbf{\Omega}, t). \tag{3.2}$$

As already noted in section 2.3.2, the angular neutron flux is a *scalar* quantity. Instead of representing a *flow* of neutrons through some surface, it rather characterizes the *rate* at which the neutrons are passing through that surface regardless of its orientation[4].

Neutron flux is the unknown quantity which is actually solved for in the neutron transport equation, since it allows to quantify reaction rates. Using the definition of angular neutron flux, the *reaction rate density* is given as in (2.3) by the product:

$$r_*(\mathbf{r}, E, \mathbf{\Omega}, t)\mathrm{d}E\,\mathrm{d}\mathbf{\Omega} = \Sigma_*(\mathbf{r}, E, t)\phi(\mathbf{r}, E, \mathbf{\Omega}, t)\mathrm{d}E\,\mathrm{d}\mathbf{\Omega}\,. \tag{3.3}$$

It represents the expected rate per unit time about t at which neutrons characterized by energies and directions within $\mathrm{d}E\,\mathrm{d}\mathbf{\Omega}$ are interacting with nuclei in a unit volume around point $\mathbf{r}$.

In deriving the transport equation, a *vector* quantity corresponding to neutron flux is needed to specify the directional flow of neutrons. *Angular neutron current* obtained by

$$\mathbf{j}(\mathbf{r}, E, \mathbf{\Omega}, t) = \mathbf{\Omega}\phi(\mathbf{r}, E, \mathbf{\Omega}, t) = \mathbf{v}(E) N(\mathbf{r}, E, \mathbf{\Omega}, t) \tag{3.4}$$

provides such a tool. Indeed, let's take an arbitrary volume V enclosed by oriented surface S. Let $\mathrm{d}S$ be the element of that surface located at point $\mathbf{r}$ with a unit outward normal $\mathbf{n}$ and let $\mathrm{d}\mathbf{S} = \mathbf{n}\,\mathrm{d}S$. Then[5]

$$\mathbf{j}(\mathbf{r}, E, \mathbf{\Omega}, t)\mathrm{d}\mathbf{S}\,\mathrm{d}E\,\mathrm{d}\mathbf{\Omega} \equiv \phi(\mathbf{r}, E, \mathbf{\Omega}, t)(\mathbf{\Omega} \cdot \mathbf{n})\mathrm{d}S\,\mathrm{d}E\,\mathrm{d}\mathbf{\Omega} \tag{3.5}$$

stands for the expected number of neutrons energetically distributed within $\mathrm{d}E$ around E, flowing per unit time through surface element $\mathrm{d}\mathbf{S}$ in a direction within $\mathrm{d}\mathbf{\Omega}$ around $\mathbf{\Omega}$ and with orientation given by $\mathbf{n}$: in the case of $\mathbf{\Omega} \cdot \mathbf{n} > 0$, neutrons leak out of V, in the case of $\mathbf{\Omega} \cdot \mathbf{n} < 0$, neutrons flow in.

[4] perhaps *flow rate* would be a more appropriate name but *flux* has already become well-established in reactor physics field

[5] the *dot* $(\cdot)$ between vector quantities signifies a dot product

3.1.1.2 Neutron balance

Let $V \subset \mathbb{R}^3$ be an arbitrary balance domain within the reactor core and $[t_1, t_2] \subset [0, +\infty)$ an arbitrary time interval. According to the general balance principle, the change in neutron population in V between times t_1 and t_2 must be equal to the amount of neutrons produced by sources inside the domain less the amount of them lost due to sinks in the domain and their net outflow (leakage) across the domain boundary, during the interval $[t_1, t_2]$.

In addition to position, energy and movement direction must be determined in order to fully characterize each neutron at any given time instant. To complete the conservation statement, I will treat the remaining two independent variables locally in the sense that balance in volume V will be affected only by neutrons having energy within some differential element $\mathrm{d}E$ and moving in the direction of some vector from a differential solid angle $\mathrm{d}\mathbf{\Omega}$. Both these elements may be chosen arbitrarily and the differential area defined by them in the neutron phase space will be denoted by $\mathrm{d}E\,\mathrm{d}\mathbf{\Omega}$. I will ocassionally refer to these neutrons as to *balance neutrons*, i.e. neutrons with direct influence on the balance. Integration over the appropriate energy and direction ranges would yield balance for a general set of neutrons.

Changes in neutron population

The expression for change in the amount of neutrons with energies and directions from balance range $\mathrm{d}E\,\mathrm{d}\mathbf{\Omega}$, in volume V and between times t_1 and t_2, has the following form:

$$\int_V \left[N(\mathbf{r}, E, \mathbf{\Omega}, t_2) - N(\mathbf{r}, E, \mathbf{\Omega}, t_1)\right] \mathrm{d}\mathbf{r} \times \mathrm{d}E\,\mathrm{d}\mathbf{\Omega} \tag{3.6}$$

(the "times sign", $\times$, has been included to separate the integration symbol $\mathrm{d}\mathbf{r}$ and the symbol $\mathrm{d}E\,\mathrm{d}\mathbf{\Omega}$ originating from statistical foundations of the variables and specifying the energetic and directional range of balance neutrons).

Sources

Primary sources of new neutrons with given energy and direction distribution are the fission reactions and particular forms of decay. Secondary means of increasing the population of such neutrons is scattering of existing neutrons originally having different energies and moving in different directions into the balance range.

Fission. In the average fission reaction, ν_p neutrons are emitted promptly in the process and ν_d neutrons are released during the subsequent decay of fission products (see section 2.3.4).

- *Prompt fission neutrons.* Let us consider only the prompt neutrons for the moment. Number of liberated neutrons, ν_p, is a function of energy of the fission-initiating neutron and, to be exact, depends also on what nuclide is being fissioned. This translates to dependency on $\mathbf{r}$ as each point in the considered domain represents some atomic species. Thus $\nu_p = \nu_p(\mathbf{r}, E')$.

Consistently with the discussion on neutron properties on p. 12, distribution of promptly released neutrons in energy will be measured by their fission spectrum χ_p. As in the case of differential scattering, rigorous treatment of fission requires one to take into account not only the energy of the outgoing neutron, but also in which direction it is emitted. Moreover, the energy and incoming direction of neutron that actually caused the reaction have an influence on fission neutrons distribution. Fission spectrum is usually used in place of the probability function P that appeared in definition (3.1) of scattering cross section ([Wil71, p. 16]). So $\chi_p = \chi_p(\mathbf{r}, E' \to E, \mathbf{\Omega}' \to \mathbf{\Omega})$ is the probability that a prompt neutron is released with energy E and direction $\mathbf{\Omega}$ as a result of fission caused by a neutron with energy E' coming from $\mathbf{\Omega}'$.

Number of fissions caused by neutrons of energy E' is characterized by the *fission cross section*, $\Sigma_f = \Sigma_f(\mathbf{r}, E', t)$.

In thermal reactors, it is reasonable to expect the same fissile material distributed throughout the core (within fuel bundles). Therefore, the number of neutrons coming from fission and their energetic and directional distribution will be the same (within statistical margins) for all these reactions regardless of the point at which they occur. Dependency on $\mathbf{r}$ can thus be omitted from variables characterizing fission neutrons.

Applying definition (3.3) to fission and integrating over all initial energies and directions[6], the overall expected fission rate in a unit volume around point $\mathbf{r}$ per unit time at t is given by

$$\int_0^{4\pi} \int_0^{\infty} \Sigma_f(\mathbf{r}, E', t)\phi(\mathbf{r}, E', \mathbf{\Omega}', t)\,\mathrm{d}E'\,\mathrm{d}\mathbf{\Omega}'\,.$$

As each fission triggered by a neutron with energy E' (incoming from $\mathbf{\Omega}'$) follows by the release of $\nu_p(E')\chi_p(E' \to E, \mathbf{\Omega}' \to \mathbf{\Omega})$ prompt neutrons with energy E and moving in the direction of unit vector $\mathbf{\Omega}$,

$$s_f(\mathbf{r}, E, \mathbf{\Omega}, t) = \int_0^{4\pi} \int_0^{\infty} \chi_p(E' \to E, \mathbf{\Omega}' \to \mathbf{\Omega})\nu_p(E')\Sigma_f(\mathbf{r}, E', t)\phi(\mathbf{r}, E', \mathbf{\Omega}', t)\,\mathrm{d}E'\,\mathrm{d}\mathbf{\Omega}' \qquad (3.7)$$

specifies the total expected yield of prompt fission neutrons with energy E and direction $\mathbf{\Omega}$ in a unit volume around $\mathbf{r}$ at t.

• *Delayed fission neutrons.* The yield of delayed neutrons is proportional to the concentration of their precursors. In general case, the concentration of precursor nuclei from each of the six precursor groups would at any point in the core change in time and depend on neutron flux. In order to include the effects of delayed neutrons, the balance equation must be modified to account for them and must be solved simultaneously with six additional partial differential equations governing the concentration changes. However, in the case of a two-group model of the reactor and steady state calculations, the terms concerning delayed neutrons essentially disappear from the balance equation and there will

[6] using the fact that solid angle spans from 0 to 4π and letting energy span interval $[0, +\infty)$

be no contribution of delayed neutrons to the total fission neutron production ([Gar05]). Therefore, for the purposes of derivation of the final set of equations (steady state, two-group, diffusion equations) which will be further discussed in this thesis, taking delayed neutrons into account is not necessary. Hence I also omit the redundant indexing, namely $\chi \equiv \chi_p$ and $\nu \equiv \nu_p$.

• *External sources.* There may be other mechanisms of neutron production besides fission (for instance, neutrons are spontaneously released from Cf-252, as described in section 2.3.4), though their yield is usually negligible comparing to fission. It is sufficient to treat all those additional sources by a general term $s_{ex}(\mathbf{r}, E, \mathbf{\Omega}, t)$.

So the total source of new neutrons is the sum $s_f + s_{ex}$ and the sources density

$$[s_f(\mathbf{r}, E, \mathbf{\Omega}, t) + s_{ex}(\mathbf{r}, E, \mathbf{\Omega}, t)] \, \mathrm{d}E \, \mathrm{d}\mathbf{\Omega} \tag{3.8}$$

describes the amount of new balance neutrons introduced per unit time at t to a unit volume element around $\mathbf{r}$.

In-scatter. The rate at which collisions between neutrons and nuclei result in changing the colliding neutron's energy and travelling direction from $\mathrm{d}E' \, \mathrm{d}\mathbf{\Omega}'$ to the balance range $\mathrm{d}E \, \mathrm{d}\mathbf{\Omega}$ may be characterized by differential scattering cross section from (3.1) as follows:

$$\Sigma_s(\mathbf{r}, E' \to E, \mathbf{\Omega}' \to \mathbf{\Omega}, t) \phi(\mathbf{r}, E', \mathbf{\Omega}', t) \, \mathrm{d}E \, \mathrm{d}\mathbf{\Omega} \, .$$

The total amount of neutrons scattered from all possible initial states to $\mathrm{d}E \, \mathrm{d}\mathbf{\Omega}$ per unit volume at $\mathbf{r}$ and unit time interval at t is then obtained by integrating the rate over the whole solid angle and full energy range of the incoming neutrons:

$$r_{is}(\mathbf{r}, E, \mathbf{\Omega}, t) \times \mathrm{d}E \, \mathrm{d}\mathbf{\Omega} = \int_0^{4\pi} \int_0^{\infty} \Sigma_s(\mathbf{r}, E' \to E, \mathbf{\Omega}' \to \mathbf{\Omega}, t) \phi(\mathbf{r}, E', \mathbf{\Omega}', t) \, \mathrm{d}E' \, \mathrm{d}\mathbf{\Omega}' \times \mathrm{d}E \, \mathrm{d}\mathbf{\Omega} \, . \tag{3.9}$$

Note that this definition includes also neutrons that are scattered to $\mathrm{d}E \, \mathrm{d}\mathbf{\Omega}$ from within the same element, i.e. neutrons initially with energies and directions already in $\mathrm{d}E \, \mathrm{d}\mathbf{\Omega}$. This will not cause balance problems, however, as these neutrons are effectively removed from the equations by analogously defined out-scattering.

The total increase of the number of balance neutrons in V between times t_1 and t_2 can be summarized by collecting (3.8) and (3.9):

$$\int_{t_1}^{t_2} \int_V \big[r_{\mathrm{is}}(\mathbf{r}, E, \mathbf{\Omega}, t) + s_f(\mathbf{r}, E, \mathbf{\Omega}, t) + s_{ex}(\mathbf{r}, E, \mathbf{\Omega}, t) \big] \mathrm{d}\mathbf{r} \, \mathrm{d}t \times \mathrm{d}E \, \mathrm{d}\mathbf{\Omega} \, . \tag{3.10}$$

Sinks

The obvious way of losing neutrons within some elementary volume is due to their absorptions in nuclei, as described in section 2.3.3. Since only neutrons having specific

energies and moving in specific directions are contributing to the balance, their leaving of that state due to scattering is also important.

Absorption. Absorption rate of balance neutrons per unit time at t in the unit volume around $\mathrm{d}\mathbf{r}$ is given by

$$\Sigma_a(\mathbf{r}, E, t)\phi(\mathbf{r}, E, \mathbf{\Omega}, t)\,\mathrm{d}E\,\mathrm{d}\mathbf{\Omega}\,. \tag{3.11}$$

Out-scatter. Analogous approach to that taken to define in-scattering of neutrons from $\mathrm{d}E'\,\mathrm{d}\mathbf{\Omega}'$ to $\mathrm{d}E\,\mathrm{d}\mathbf{\Omega}$ can be adopted to obtain the expression for out-scatter from $\mathrm{d}E\,\mathrm{d}\mathbf{\Omega}$ to $\mathrm{d}E'\,\mathrm{d}\mathbf{\Omega}'$. The rate of this reaction per unit time and volume is thus given by

$$\int_0^{4\pi}\int_0^{\infty} \Sigma_s(\mathbf{r}, E\to E', \mathbf{\Omega}\to\mathbf{\Omega}', t)\phi(\mathbf{r}, E, \mathbf{\Omega}, t)\,\mathrm{d}E'\,\mathrm{d}\mathbf{\Omega}'\times\mathrm{d}E\,\mathrm{d}\mathbf{\Omega} = \Sigma_s(\mathbf{r}, E, t)\phi(\mathbf{r}, E, \mathbf{\Omega}, t)\,\mathrm{d}E\,\mathrm{d}\mathbf{\Omega}\,, \tag{3.12}$$

where

$$\Sigma_s(\mathbf{r}, E, t) := \int_0^{4\pi}\int_0^{\infty} \Sigma_s(\mathbf{r}, E\to E', \mathbf{\Omega}\to\mathbf{\Omega}', t)\,\mathrm{d}E'\,\mathrm{d}\mathbf{\Omega}'$$

is the macroscopic cross section for out-scattering of neutrons with energy E and direction $\mathbf{\Omega}$ into any energy and direction range. It should be remarked again that definition (3.12) removes neutrons that actually do not leave $\mathrm{d}E\,\mathrm{d}\mathbf{\Omega}$ because scattering will not change their energies and directions past the balance domain. These are taken to compensate for those erroneously added by defining in-scattering with (3.9).

Collecting the individual terms (3.11) and (3.12), one arrives at the expression for total decrease in population of balance neutrons inside V between times t_1 and t_2 due to sinks:

$$\int_{t_1}^{t_2}\int_V \big[\Sigma_s(\mathbf{r}, E, t) + \Sigma_a(\mathbf{r}, E, t)\big]\phi(\mathbf{r}, E, \mathbf{\Omega}, t)\,\mathrm{d}\mathbf{r}\,\mathrm{d}t\;\times\mathrm{d}E\,\mathrm{d}\mathbf{\Omega}\,. \tag{3.13}$$

Flow across boundary

Let us assume that V is compact with piecewise smooth boundary ∂V that is oriented by outwards-pointing normal field $\mathbf{n} = \mathbf{n}(\mathbf{r})$. The net outflow of balance neutrons (*leakage*) through the boundary during $[t_1, t_2]$ is given by

$$\int_{t_1}^{t_2}\int_{\partial V} \mathbf{j}(\mathbf{r}, E, \mathbf{\Omega}, t)\cdot\mathbf{n}(\mathbf{r})\,\mathrm{d}S\,\mathrm{d}t\;\times\mathrm{d}E\,\mathrm{d}\mathbf{\Omega}\,.$$

Let's assume further that the angular current $\mathbf{j}$ represents a continuously differentiable vector field in V which is continuous on ∂V. Then the divergence theorem of Gauss states

that

$$\int_{\partial V} \mathbf{j} \cdot \mathbf{n} \, \mathrm{d}S = \int_V \nabla \cdot \mathbf{j} \, \mathrm{d}\mathbf{r} \,,$$

where the standard mathematical operator $\nabla = (\frac{\partial}{\partial x}, \frac{\partial}{\partial y}, \frac{\partial}{\partial z})$ is formally used to express the divergence of the vector field. Net leakage of balance neutrons from time t_1 to t_2 out of volume V through ∂V can now be written as

$$\int_{t_1}^{t_2} \int_V \nabla \cdot \mathbf{j}(\mathbf{r}, E, \mathbf{\Omega}, t) \, \mathrm{d}\mathbf{r} \, \mathrm{d}t \times \mathrm{d}E \, \mathrm{d}\mathbf{\Omega} \,. \tag{3.14}$$

With all terms of neutron balance relation now being properly established, the relation can be expressed by the following scheme:

$$(3.6) = (3.10) - (3.13) - (3.14)$$

and mathematically formulated by the following integral equality for balance neutrons:

$$\begin{aligned}
&\int_V \left[N(\mathbf{r}, E, \mathbf{\Omega}, t_2) - N(\mathbf{r}, E, \mathbf{\Omega}, t_1) \right] \mathrm{d}\mathbf{r} \times \mathrm{d}E \, \mathrm{d}\mathbf{\Omega} \\
&\quad = \int_{t_1}^{t_2} \int_V \left[r_{\mathrm{is}}(\mathbf{r}, E, \mathbf{\Omega}, t) + s_f(\mathbf{r}, E, \mathbf{\Omega}, t) + s_{ex}(\mathbf{r}, E, \mathbf{\Omega}, t) \right] \mathrm{d}\mathbf{r} \, \mathrm{d}t \times \mathrm{d}E \, \mathrm{d}\mathbf{\Omega} \\
&\quad - \int_{t_1}^{t_2} \int_V \left[\Sigma_s(\mathbf{r}, E, t) + \Sigma_a(\mathbf{r}, E, t) \right] \phi(\mathbf{r}, E, \mathbf{\Omega}, t) \, \mathrm{d}\mathbf{r} \, \mathrm{d}t \times \mathrm{d}E \, \mathrm{d}\mathbf{\Omega} \\
&\quad - \int_{t_1}^{t_2} \int_V \nabla \cdot \mathbf{j}(\mathbf{r}, E, \mathbf{\Omega}, t) \, \mathrm{d}\mathbf{r} \, \mathrm{d}t \times \mathrm{d}E \, \mathrm{d}\mathbf{\Omega} \,.
\end{aligned} \tag{3.15}$$

Because the derivation was carried out for an arbitrarily chosen set of balance energies and directions, the $\mathrm{d}E \, \mathrm{d}\mathbf{\Omega}$ term may be removed.

Under the assumption of continuous time dependence of angular neutron density N, left-hand side can be rewritten as

$$\int_V \int_{t_1}^{t_2} \frac{\partial}{\partial t} N(\mathbf{r}, E, \mathbf{\Omega}, t) \, \mathrm{d}t \, \mathrm{d}\mathbf{r} \,.$$

Further, let also $\frac{\partial N}{\partial t}$ be continuous so that the order of integration may be reversed. Then the change of neutron population may be described by:

$$\int_{t_1}^{t_2} \int_V \frac{\partial}{\partial t} N(\mathbf{r}, E, \mathbf{\Omega}, t) \, \mathrm{d}\mathbf{r} \, \mathrm{d}t = \frac{1}{v(E)} \int_{t_1}^{t_2} \int_V \frac{\partial}{\partial t} \phi(\mathbf{r}, E, \mathbf{\Omega}, t) \, \mathrm{d}\mathbf{r} \, \mathrm{d}t \,,$$

where also the definition of flux (3.2) has been used. Since the time interval $[t_1, t_2]$ was chosen arbitrarily, the global balance equation (3.15) may be written in the equivalent time-local form:

$$\begin{aligned}\frac{1}{v(E)}\int\limits_V \frac{\partial}{\partial t}\phi(\mathbf{r},E,\mathbf{\Omega},t)\,\mathrm{d}\mathbf{r} &= \int\limits_V r_{\mathrm{is}}(\mathbf{r},E,\mathbf{\Omega},t)+s_f(\mathbf{r},E,\mathbf{\Omega},t)+s_{ex}(\mathbf{r},E,\mathbf{\Omega},t)\,\mathrm{d}\mathbf{r}\\ &\quad-\int\limits_V \big[\Sigma_s(\mathbf{r},E,t)+\Sigma_a(\mathbf{r},E,t)\big]\phi(\mathbf{r},E,\mathbf{\Omega},t)\,\mathrm{d}\mathbf{r}\\ &\quad-\int\limits_V \nabla\cdot\mathbf{j}(\mathbf{r},E,\mathbf{\Omega},t)\,\mathrm{d}\mathbf{r}\,.\end{aligned} \tag{3.16}$$

The balance domain V was also chosen arbitrarily, so a version of the equation local in both time and space may be written immediatly. Before doing that, note that $\mathbf{r}$ and $\mathbf{\Omega}$ are independent variables and hence the spatial operator ∇ doesn't act on $\mathbf{\Omega}$. This allows us to write

$$\nabla\cdot\mathbf{j}(\mathbf{r},E,\mathbf{\Omega},t)=\nabla\cdot\big[\mathbf{\Omega}\phi(\mathbf{r},E,\mathbf{\Omega},t)\big]=\mathbf{\Omega}\cdot\nabla\phi(\mathbf{r},E,\mathbf{\Omega},t). \tag{3.17}$$

Now the local version of neutron balance may be formulated in terms of only one unknown quantity ϕ. Grouping the non-source terms on the left-hand side and explicitly writing the in-scattering and fission source terms, the local equation for neutron balance reads

$$\begin{aligned}&\left[\frac{1}{v(E)}\frac{\partial}{\partial t}+\mathbf{\Omega}\cdot\nabla+\Sigma_s(\mathbf{r},E,t)+\Sigma_a(\mathbf{r},E,t)\right]\phi(\mathbf{r},E,\mathbf{\Omega},t)\\ &\qquad=\int_0^{4\pi}\int_0^{\infty}\Sigma_s(\mathbf{r},E'\to E,\mathbf{\Omega}'\to\mathbf{\Omega},t)\phi(\mathbf{r},E',\mathbf{\Omega}',t)\mathrm{d}E'\,\mathrm{d}\mathbf{\Omega}'\\ &\qquad+\int_0^{4\pi}\int_0^{\infty}\big[\chi(E'\to E,\mathbf{\Omega}'\to\mathbf{\Omega})\nu(E')\Sigma_f(\mathbf{r},E',t)\big]\phi(\mathbf{r},E',\mathbf{\Omega}',t)\mathrm{d}E'\,\mathrm{d}\mathbf{\Omega}'\\ &\qquad+s_{ex}(\mathbf{r},E,\mathbf{\Omega},t).\end{aligned} \tag{3.18}$$

This is the general integro-differential form of neutron transport equation whose derivation may also be found e.g. in [Wil71] or [Sch97]. Unlike the similar Boltzmann transport equation for gases, it is *linear* in ϕ due to the fact that neutrons do not interact with each other (see section 2.3.2). This makes its solution much easier, but due to its overall complexity it still quite intractable.

3.1.2 Steady state formulation

If a fuel configuration should be optimal, it should guarantee a long-term self-sustained operation of the reactor. This indicates a state in which the neutron population doesn't change anymore, or equivalently the neutron flux has a stable constant value. It is therefore

necessary that the time derivative of flux – the first term in equation (3.18) – be zero. Together with flux, also the material properties are assumed to be settled down. Hence the equation that governs such an equilibrium regime is not dependent on time at all. It is known as a *steady state transport equation*:

$$\begin{aligned}\Big[\boldsymbol{\Omega}\cdot\nabla+\Sigma_s(\mathbf{r},E)+\Sigma_a(\mathbf{r},E)\Big]\phi(\mathbf{r},E,\boldsymbol{\Omega})&\\ =\int_0^{4\pi}\int_0^{\infty}\Sigma_s(\mathbf{r},E'\to E,\boldsymbol{\Omega}'\to\boldsymbol{\Omega})\phi(\mathbf{r},E',\boldsymbol{\Omega}')\mathrm{d}E'\,\mathrm{d}\boldsymbol{\Omega}'&\\ +\int_0^{4\pi}\int_0^{\infty}\big[\chi(E'\to E,\boldsymbol{\Omega}'\to\boldsymbol{\Omega})\nu(E')\Sigma_f(\mathbf{r},E')\big]\phi(\mathbf{r},E',\boldsymbol{\Omega}')\mathrm{d}E'\,\mathrm{d}\boldsymbol{\Omega}'&\\ +s_{ex}(\mathbf{r},E,\boldsymbol{\Omega})&\end{aligned}\tag{3.19}$$

and will be the subject of further investigation.

3.1.3 Conditions on angular flux

In order to have a reasonable physical meaning, the angular flux must be a real, bounded, non-negative function of position:

$$0\le\phi(\mathbf{r},E,\boldsymbol{\Omega})<\infty,\quad\forall\mathbf{r},\,E,\,\boldsymbol{\Omega}.$$

Interface conditions. To complete the mathematical model of steady state neutron transport, angular neutron flux must be specified on boundaries of the balance region[7]. If the boundary forms an interface between two regions inside the reactor core (maybe of different material composition), the number of neutrons passing accross that interface from one region to another should be conserved, thus imposing a continuity condition on the flux:

$$\phi(\mathbf{r},E,\boldsymbol{\Omega})\big|_{\partial V-}=\phi(\mathbf{r},E,\boldsymbol{\Omega})\big|_{\partial V+},\quad\forall E,\,\boldsymbol{\Omega},$$

where $\partial V-$ and $\partial V+$ stand for the limits from "left" and "right" ("inside" and "outside"), respectively, of the flux function at the interface ∂V.

Boundary conditions. On the boundary of the reactor, angular neutron flux is determined by physical properties of reactor surroundings. The angular flux is prescribed at the surface for all incoming angles:

$$\phi(\mathbf{r},E,\boldsymbol{\Omega})\big|_{\partial V}=f(\mathbf{r},E,\boldsymbol{\Omega}),\quad\forall\boldsymbol{\Omega}:\boldsymbol{\Omega}\cdot\mathbf{n}<0,\,E,$$

[7]The general transient case requires also an initial condition, which is usually given by the solution to the steady state problem ([Sch97]); this work does not deal with this case, however, and only boundary conditions will suffice to close the problem.

where $\mathbf{n}$ is the unit outward normal to ∂V and f is defined on ∂V. The most obvious is the case of *vacuum* surrounding the reactor, where no neutrons can come from outside across the boundary:

$$\phi(\mathbf{r}, E, \mathbf{\Omega})\big|_{\partial V} = 0, \quad \forall \mathbf{\Omega} : \mathbf{\Omega} \cdot \mathbf{n} < 0,\ E.$$

However, this work examines the effects of more general *albedo boundary conditions*, which allow a certain amount of neutrons escaping the core across boundary ∂V to be reflected back. This is described by the relation

$$\phi(\mathbf{r}, E, \mathbf{\Omega})\big|_{\partial V} = \alpha\phi(\mathbf{r}, E, \mathbf{\Omega}_r)\big|_{\partial V}, \quad \forall \mathbf{\Omega} : \mathbf{\Omega} \cdot \mathbf{n} < 0,\ E, \tag{3.20}$$

where $\mathbf{\Omega}_r$ is the angle of reflection defined by conditions $\mathbf{\Omega}\cdot\mathbf{n} = \mathbf{\Omega}_r\cdot\mathbf{n}$ (the angle of incidence equals the angle of reflection) and $(\mathbf{\Omega} \times \mathbf{n}) \cdot \mathbf{n} = 0$ (neutrons re-enter the volume in the same plane in which they have left it). Term α is assumed to be constant and defines the fraction of neutrons to be reflected ($\alpha \in [0, 1]$). If $\alpha = 0$, the vacuum boundary condition is obtained, $\alpha = 1$ means that all escaped neutrons are reflected back (*reflecting boundary conditions*).

Remark 3.1 (Re-entrant cores)
In complex reactor designs, the boundary of the balance domain may be re-entrant, in the sense that neutrons leaving the domain may enter it through the same surface at different place. Such a case is described in more detail in [Wil71, chap. 3], but the model developed in this thesis will not take this case into account.

3.1.4 Criticality calculations

Neutron flux in a critical reactor is given by a real, finite and non-negative solution to equation (3.19). However, the solution exists only for certain sets of coefficients appearing in the equation, given by the material properties of the actual core composition. To determine how it must be modified in order to yield the coefficients ensuring a physically possible solution and thus a critical reactor, a freely adjustable parameter is added to the equation. Since we are optimizing the arrangement of fuel assemblies, we are allowed to vary the intensity of fissions in order to achieve criticality. Hence it is reasonable to bestow the additional degree of freedom on the fission source term in (3.19):

$$\big[\mathbf{\Omega} \cdot \nabla + \Sigma_s(\mathbf{r}, E) + \Sigma_a(\mathbf{r}, E)\big]\phi(\mathbf{r}, E, \mathbf{\Omega}) = r_{is}(\mathbf{r}, E, \mathbf{\Omega}) + \lambda s_f(\mathbf{r}, E, \mathbf{\Omega}) \tag{3.21}$$

(balance sources were written compactly like in eq. (3.16)). As is usual when searching for criticality, the contribution of external neutron sources will be neglected, $s_{ex}(\mathbf{r}, E, \mathbf{\Omega}) \equiv 0$, and this absence of non-fission sources of new neutrons will be assumed also for the rest of this thesis. If now equation (3.21) has non-trivial solution for $\lambda > 1$, the steady state transport equation (3.19) requires a bigger fission term, i.e. the given fuel charge is insufficient to support the steady operation of the reactor. It corresponds to a subcritical reactor with $k_{\text{eff}} < 1$. Similarly, $\lambda < 1$ indicates that steady state operation will be achieved by reducing the fission term, thus the arrangement of fissile material is supercritical. Finally

the optimal value of $\lambda = 1$ signifies that criticality will be achieved with the current material distribution.

The relation between mathematical parameter λ and physical quantity k_{eff} is thus intuitively found to be

$$\lambda = \frac{1}{k_{\text{eff}}}, \tag{3.22}$$

which may be more rigorously proven by rearranging (3.21) and realizing physical meaning of its terms. I refer the reader to [Sta01, p. 124] where this procedure is accomplished for a bare reactor[8] and equation (3.21) with already removed angular and energetic dependencies.

To produce a numerically solvable version of eq. (3.21), I will first remove its angular dependency in the following section. This process does not require explicit consideration of the criticality parameter, so I proceed from eq. (3.19) rather than from eq. (3.21). I will return to the criticality problem in section 3.3.1.1 after treating the energetic dependence.

3.2 Neutron diffusion theory

3.2.1 Basic angularly-independent quantities

In order to reduce the steady-state transport equation (3.19) to a form that does not depend on neutrons' directions, let us first define the appropriate fundamental quantities. The (time-independent) *total flux density* (or simply *flux*) is obtained by taking an integral of angular flux over the whole solid angle:

$$\phi(\mathbf{r}, E) = \int_0^{4\pi} \phi(\mathbf{r}, E, \mathbf{\Omega}) \, \mathrm{d}\mathbf{\Omega} \, . \tag{3.23}$$

Analogously, the angularly independent *net current density* (or just *current*) is given by the relation

$$\mathbf{j}(\mathbf{r}, E) = \int_0^{4\pi} \mathbf{j}(\mathbf{r}, E, \mathbf{\Omega}) \, \mathrm{d}\mathbf{\Omega} \, = \int_0^{4\pi} \mathbf{\Omega} \phi(\mathbf{r}, E, \mathbf{\Omega}) \, \mathrm{d}\mathbf{\Omega} \, . \tag{3.24}$$

3.2.2 Basic physical assumptions

Isotropic source. I will assume that directions in which neutrons leave the fissioned nuclei are distributed evenly within the full solid angle 4π and independently on the direction of the reaction-inducing neutron ([Wil71, p. 16]). Hence

$$\chi(E' \to E, \mathbf{\Omega}' \to \mathbf{\Omega}) = \frac{1}{4\pi} \chi(E' \to E)$$

[8] reactor without a reflector zone

and fission source from (3.7) becomes (in the time-independent case):

$$\begin{aligned} s(\mathbf{r}, E) &= \int_0^\infty \frac{1}{4\pi}\chi(E' \to E)\nu(E')\Sigma_f(\mathbf{r}, E') \int_0^{4\pi} \phi(\mathbf{r}, E', \mathbf{\Omega}')\,\mathrm{d}\mathbf{\Omega}'\,\mathrm{d}E' \\ &= \int_0^\infty \frac{1}{4\pi}\chi(E' \to E)\nu(E')\Sigma_f(\mathbf{r}, E')\phi(\mathbf{r}, E')\,\mathrm{d}E'\,. \end{aligned} \tag{3.25}$$

Term $1/4\pi$ is used to normalize the isotropic fission spectrum with respect to $\mathbf{\Omega}$ and its use will be justified later when (3.25) will be integrated over the full solid angle.

Isotropic scattering. Angular dependency of in-scattering will be removed next. The simplest way of doing so is to make the same argument as with fission and assume scattering to be isotropic:

$$\Sigma_s(\mathbf{r}, E' \to E, \mathbf{\Omega}' \to \mathbf{\Omega}) = \frac{1}{4\pi}\Sigma_s(\mathbf{r}, E' \to E).$$

The influence of incident direction could be neglected due to the averaging effects of random orientation of nuclei which the neutrons bounce off ([Mou96, p. 11]).

Integral (3.9) defining total scattering rate turns in the isotropic time-independent case into

$$\int_0^\infty \frac{1}{4\pi}\Sigma_s(\mathbf{r}, E' \to E) \int_0^{4\pi} \phi(\mathbf{r}, E', \mathbf{\Omega}')\,\mathrm{d}E'\,\mathrm{d}\mathbf{\Omega}' = \int_0^\infty \frac{1}{4\pi}\Sigma_s(\mathbf{r}, E' \to E)\phi(\mathbf{r}, E')\,\mathrm{d}E'\,. \tag{3.26}$$

3.2.3 Neutron diffusion equation

Isotropic source (3.25) and scattering (3.26) may now be used in eq. (3.19) to replace their angularly dependent counterparts:

$$\begin{aligned} \Big[\mathbf{\Omega}\cdot\nabla + \Sigma_s(\mathbf{r}, E) + \Sigma_a(\mathbf{r}, E)\Big]\phi(\mathbf{r}, E, \mathbf{\Omega}) &= \int_0^\infty \frac{1}{4\pi}\Sigma_s(\mathbf{r}, E' \to E)\phi(\mathbf{r}, E')\,\mathrm{d}E' \\ &\quad + \int_0^\infty \frac{1}{4\pi}\chi(E' \to E)\nu(E')\Sigma_f(\mathbf{r}, E')\phi(\mathbf{r}, E')\,\mathrm{d}E'\,. \end{aligned} \tag{3.27}$$

The only appearance of variable $\mathbf{\Omega}$ is now on the left-hand side of the balance equation. It may be removed by integrating the equation with respect to $\mathbf{\Omega}$ over the solid angle 4π

and using definitions (3.23) and (3.24):

$$\nabla \cdot \mathbf{j}(\mathbf{r}, E) + \big[\Sigma_s(\mathbf{r}, E) + \Sigma_a(\mathbf{r}, E)\big]\phi(\mathbf{r}, E) = \int_0^\infty \Sigma_s(\mathbf{r}, E' \to E)\phi(\mathbf{r}, E')\mathrm{d}E' + \int_0^\infty \chi(E' \to E)\nu(E')\Sigma_f(\mathbf{r}, E')\phi(\mathbf{r}, E')\mathrm{d}E' . \quad (3.28)$$

This equation is known as the *neutron diffusion equation* and describes neutron conservation without the effects arising from neutrons' directional distribution. However, it contains two unknown quantites – the current and flux densities – whose relationship must be worked out.

Fick's law. To develop the required relation I shall outline the approach that utilizes partial currents, presented in more detail e.g. in [Sta01, chap. 3]. In the reference, the derivation initially supposed uniform material distribution within the core (so that spatial dependence of cross sections may be neglected) and monoenergetic neutrons (so that the energetic dependence of relevant quantities may be omitted as well). As will be shown later in section 3.3, the diffusion approximation with Fick's law will be in actual computation employed in a set of monoenergetic equations obtained by the energy-spectrum discretization. Hence the second assumption poses no real problem in practice. However, uniformity of material distribution is a serious assumption that should be treated carefully. A brief discussion on the issues connected with it will be given in section 4.2.2.2; for now, I will take both assumptions for granted.

Derivation begins with choosing a local coordinate system and considering a differential area in the x-y plane at the origin. Then a differential current of neutrons crossing this area in a downward z-direction is determined under the assumption of isotropic scattering. If further flux varies sufficiently slowly about the origin, it can be linearized by first-order Taylor series and used with another assumption – that scattering dominates the absorption (so that $\Sigma_s + \Sigma_a \sim \Sigma_s$) – to obtain the total downward current:

$$j_z^-(\mathbf{0}) \approx \frac{1}{4}\phi(\mathbf{0}) + \frac{1}{6\Sigma_s}\frac{\partial\phi(\mathbf{0})}{\partial z}. \quad (3.29)$$

Similarly, the upward current is given by

$$j_z^+(\mathbf{0}) \approx \frac{1}{4}\phi(\mathbf{0}) - \frac{1}{6\Sigma_s}\frac{\partial\phi(\mathbf{0})}{\partial z}. \quad (3.30)$$

The net current density at the origin is then defined as the surplus current in the positive z-direction:

$$j_z(\mathbf{0}) = j_z^+(\mathbf{0}) - j_z^-(\mathbf{0}) \approx -\frac{1}{3\Sigma_s}\frac{\partial\phi(\mathbf{0})}{\partial z}. \quad (3.31)$$

Using the same procedure for elementary surfaces placed at the center of the y-z and x-z planes reveals the connection between the flux and the three-dimensional current densities:

$$\mathbf{j}(\mathbf{0}) = [j_x(\mathbf{0}), j_y(\mathbf{0}), j_z(\mathbf{0})] \approx -\frac{1}{3\Sigma_s}\nabla\phi(\mathbf{0}). \tag{3.32}$$

Since the local coordinate system may be chosen at any point in space, the final constitutive relation between flux and current at any point is found (for neutrons with arbitrary energy E):

$$\mathbf{j}(\mathbf{r}, E) \approx -D(\mathbf{r}, E)\nabla\phi(\mathbf{r}, E), \tag{3.33}$$

where

$$D(\mathbf{r}, E) = \frac{1}{3\Sigma_s(\mathbf{r}, E)} \tag{3.34}$$

represents the *diffusion coefficient*. The last relation is known as *Fick's law* and describes the net flow in the direction of least density, a behaviour commonly exhibited by many other diffunding particles than just neutrons.

Equations (3.28) and (3.33) form a standard system of second-order diffusion equation and a constitutive relation. The diffusion theory based formulation of neutron conservation with only one unknown variable is obtained by inserting eq. (3.33) into eq. (3.28):

$$\begin{aligned} -\nabla \cdot D(\mathbf{r}, E)\nabla\phi(\mathbf{r}, E) + \big[\Sigma_s(\mathbf{r}, E) + \Sigma_a(\mathbf{r}, E)\big]\phi(\mathbf{r}, E) \\ = \int_0^\infty \Sigma_s(\mathbf{r}, E' \to E)\phi(\mathbf{r}, E')\mathrm{d}E' + \int_0^\infty \chi(E' \to E)\nu(E')\Sigma_f(\mathbf{r}, E')\phi(\mathbf{r}, E')\mathrm{d}E' . \end{aligned} \tag{3.35}$$

However, it should be held in memory that the balance equation (3.28) is mathematically considered an exact expression, while Fick's law is an approximate relation ([Mou96, p. 17], [Sta01, p. 346]).

3.2.4 Diffusion conditions on flux and current

Since the approximated flux ϕ is an integral quantity, it may be required only to satisfy the weak form of transport boundary conditions specified in section 3.1.3.

At the interface between two regions within the core, both flux and current must be continuous:

$$\phi(\mathbf{r}, E)\big|_{\partial V-} = \phi(\mathbf{r}, E)\big|_{\partial V+} \quad \text{and} \quad \mathbf{j}(\mathbf{r}, E) \cdot \mathbf{n}\big|_{\partial V-} = \mathbf{j}(\mathbf{r}, E) \cdot \mathbf{n}\big|_{\partial V+}, \tag{3.36}$$

where $\partial V-$ and $\partial V+$ represent the limits from "left" and "right" ("inside" and "outside") at the interface ∂V, as in section 3.1.3, and $\mathbf{n}$ is the unit normal to the interface, oriented e.g. into the interior of the "right" region (and hence out of the "left" region). Using Fick's law (3.33), the current continuity requirement can be written in terms of flux as

$$-D(\mathbf{r}, E)\frac{\partial\phi(\mathbf{r}, E)}{\partial\mathbf{n}}\bigg|_{\partial V-} = -D(\mathbf{r}, E)\frac{\partial\phi(\mathbf{r}, E)}{\partial\mathbf{n}}\bigg|_{\partial V+}, \tag{3.37}$$

Conditions (3.36) are known as the *conditions of transmission* ([MK93, §12.13]).

Remark 3.2
In fact, the condition of current continuity is required only on interfaces between regions with different material composition, where $D(\mathbf{r}, E)$ will be discontinuous. Within homogeneous environments it will be satisfied automatically by the flux continuity condition. Nevertheless, it is essential for the diffusion term in (3.35) *to be mathematically correct.*

At the boundary of the reactor, only the albedo condition (3.20) will be considered. It allows us to model various types of reflector zones around the core with a single value without the need of thoroughly solving the diffusion equation for this special region. Omitting the energetic dependence to keep the notation simple, it can be written as follows:

$$j_n^-(\mathbf{r}) = \alpha j_n^+(\mathbf{r}), \quad \mathbf{r} \in \partial V, \tag{3.38}$$

where α is the albedo as defined in section 3.1.3 and j_n^+ and j_n^-, respectively, symbolize the partial currents of neutrons flowing in the direction, respectively in the opposite direction, of vector $\mathbf{n}$. Since $\mathbf{n}$ represents a unit normal to a given part of surface ∂V of some arbitrary volume V, pointing out of that volume, the two partial currents determine the number of neutrons escaping out of, respectively coming into, the region V through the given boundary. Their difference then represents the net current through the given side in the direction of its outward normal:

$$j_n(\mathbf{r}) = j_n^+(\mathbf{r}) - j_n^-(\mathbf{r}). \tag{3.39}$$

If I apply the same technique used to obtain diffusion expressions for partial currents through an elementary surface at the center of the x-y plane (eq. (3.29) and (3.30)) to ∂V and use the definition of diffusion coefficient (3.34), the net current through the volume surface may be approximated by

$$j_n(\mathbf{r}) = -D(\mathbf{r})\frac{\partial\phi(\mathbf{r})}{\partial\mathbf{n}}, \quad \mathbf{r} \in \partial V,$$

the partial inward current by

$$j_n^-(\mathbf{r}) \approx \frac{1}{4}\phi(\mathbf{r}) + \frac{1}{2}D(\mathbf{r})\frac{\partial\phi(\mathbf{r})}{\partial\mathbf{n}} = \frac{1}{4}\phi(\mathbf{r}) - \frac{1}{2}j_n(\mathbf{r}),$$

and the partial outward current by

$$j_n^+(\mathbf{r}) \approx \frac{1}{4}\phi(\mathbf{r}) - \frac{1}{2}D(\mathbf{r})\frac{\partial\phi(\mathbf{r})}{\partial\mathbf{n}} = \frac{1}{4}\phi(\mathbf{r}) + \frac{1}{2}j_n(\mathbf{r}).$$

Using these formulae, albedo condition (3.38) may be rewritten in terms of flux:

$$\frac{1-\alpha}{2(1+\alpha)}\phi(\mathbf{r}) + D(\mathbf{r})\frac{\partial\phi(\mathbf{r})}{\partial\mathbf{n}} = 0,$$

or

$$\gamma\phi(\mathbf{r}) + D(\mathbf{r})\frac{\partial\phi(\mathbf{r})}{\partial\mathbf{n}} = 0, \quad \gamma = \frac{1-\alpha}{2(1+\alpha)}, \tag{3.40}$$

exposing a boundary condition of Robin type.

Remark 3.3
Note that γ maps the interval $[0,1]$ of possible albedo values to the range $[0,0.5]$, such that values $\alpha = 0$ and $\alpha = 1$ (corresponding to the vacuum and the reflecting boundary conditions, respectively), are mapped to values $\gamma = 0.5$ and $\gamma = 0$, in that order.

Validity of diffusion approximation. In the derivation of neutron diffusion equation, various assumptions have been made, namely uniformity of material distribution, isotropy of scattering, flux being a slowly varying function of position and domination of scattering over absorption. There are many places in modern reactors where these conditions are not satisfied, e.g. around highly absorbing control elements or strong sources, near the boundaries or generally in largely inhomogeneous media. A more accurate treatment of transport theory is needed to correct the diffusion theory in these regions.

For instance, sophisticated homogenization methods are employed within the non-uniform core to obtain averaged cross sections and diffusion coefficients with which the diffusion approximation gives correct results. Also, a different approach leading to the standard set of diffusion and constitutive PDE's – the P_1 *approximation* – may be taken to account for anisotropy in scattering (see e.g. [Sta01, sec. 9.7], [Wil71, chap. 11]).

3.3 Multigroup approximation

Discretization with respect to energy is a final step of producing a computationally suitable model of neutron transport. To this end, the whole energy range is divided into G discrete intervals called *groups*. Indexing of these intervals is chosen so that group g contains neutrons with energies $E^g < E < E^{g-1}$. As a matter of convention, group index will be placed in superscript. The structure of multigroup discretization can then be written as $0 = E^g < E^{g-1} < \ldots < E^g < E^{g-1} < \ldots < E^1 \leq E^0 \to \infty$ (though in practical computation of real reactors, the whole range usually spans interval $[0, 10\,\mathrm{MeV}]$). Fission releases neutrons into group $g = 0$ and they then gradually lose their energy by diffusing through the core, passing to a group with a higher index.

Diffusion formulation of neutron balance within group g can be obtained by integrating eq. (3.35) over the group energy range:

$$
\begin{aligned}
-\int_{E^g}^{E^{g-1}} \nabla \cdot D(\mathbf{r},E)\nabla\phi(\mathbf{r},E)\,\mathrm{d}E \;+\; \int_{E^g}^{E^{g-1}} \big[\Sigma_s(\mathbf{r},E)+\Sigma_a(\mathbf{r},E)\big]\phi(\mathbf{r},E)\,\mathrm{d}E \;=& \\
\int_{E^g}^{E^{g-1}} \left(\sum_{g'=1}^{G} \int_{E^{g'}}^{E^{g'-1}} \Sigma_s(\mathbf{r},E'\to E)\phi(\mathbf{r},E')\,\mathrm{d}E' \right) \mathrm{d}E & \qquad (3.41)\\
+ \int_{E^g}^{E^{g-1}} \left(\sum_{g'=1}^{G} \int_{E^{g'}}^{E^{g'-1}} \chi(E'\to E)\nu(E')\Sigma_f(\mathbf{r},E')\phi(\mathbf{r},E')\,\mathrm{d}E' \right) \mathrm{d}E\,. &
\end{aligned}
$$

For thermal reactors, it is valid to assume that neither the energetic distribution of fission neutrons nor their count depends on energy of the fission-inducing neutron ([Wil71, p. 16]), hence

$$\chi(E' \to E) \equiv \chi(E), \quad \text{and also} \quad \nu(E') \equiv \nu. \tag{3.42}$$

The first expression allows to describe the fraction of neutrons released with energies in the group range (E^g, E^{g-1}) by the group fission spectrum

$$\chi^g = \int_{E^g}^{E^{g-1}} \chi(E)\,\mathrm{d}E\,. \tag{3.43}$$

To obtain the group-discretized expressions for the remaining terms of eq. (3.41), the group flux ϕ^g must first be defined:

$$\phi^g(\mathbf{r}) = \int_{E^g}^{E^{g-1}} \phi(\mathbf{r}, E)\,\mathrm{d}E\,. \tag{3.44}$$

The *multigroup constants*[9] may now be (at least theoretically) defined as in [Sta01, eqs. (4.39) and (4.74)]:

$$\begin{aligned}
\Sigma_a^g(\mathbf{r}) &= \frac{\int_{E^g}^{E^{g-1}} \Sigma_a(\mathbf{r}, E)\phi(\mathbf{r}, E)\,\mathrm{d}E}{\phi^g(\mathbf{r})},\\
\nu\Sigma_f^{g'}(\mathbf{r}) &= \frac{\int_{E^{g'}}^{E^{g'-1}} \nu\Sigma_f(\mathbf{r}, E')\phi(\mathbf{r}, E')\,\mathrm{d}E'}{\phi^{g'}(\mathbf{r})},\\
\Sigma_s^{g'\to g}(\mathbf{r}) &= \frac{\int_{E^g}^{E^{g-1}} \int_{E^{g'}}^{E^{g'-1}} \Sigma_s(\mathbf{r}, E' \to E)\phi(\mathbf{r}, E')\,\mathrm{d}E'\,\mathrm{d}E}{\phi^{g'}(\mathbf{r})},\\
\Sigma_s^g(\mathbf{r}) &= \sum_{g'=1}^{G} \Sigma_s^{g\to g'}(\mathbf{r}),\\
D^g(\mathbf{r}) &= \frac{\int_{E^g}^{E^{g-1}} D(\mathbf{r}, E)\nabla\phi(\mathbf{r}, E)\,\mathrm{d}E}{\int_{E^g}^{E^{g-1}} \nabla\phi(\mathbf{r}, E)\,\mathrm{d}E}.
\end{aligned} \tag{3.45}$$

Using assumptions (3.42), source term in (3.41):

$$\int_{E^g}^{E^{g-1}} \left(\sum_{g'=1}^{G} \int_{E^{g'}}^{E^{g'-1}} \chi(E' \to E)\nu(E')\Sigma_f(\mathbf{r}, E')\phi(\mathbf{r}, E')\,\mathrm{d}E' \right) \mathrm{d}E$$

[9] constant with respect to energy

can be rewritten as

$$\int_{E^{g}}^{E^{g-1}} \chi(E) \left(\sum_{g'=1}^{G} \int_{E^{g'}}^{E^{g'-1}} \nu\Sigma_f(\mathbf{r}, E')\phi(\mathbf{r}, E')\,\mathrm{d}E' \right) \mathrm{d}E\,.$$

Together with the group variables from equations (3.43), (3.44) and (3.45), this transformation leads to a more compact version of equation (3.41):

$$-\nabla \cdot D^g(\mathbf{r})\nabla\phi^g(\mathbf{r}) + \left[\Sigma_s^g(\mathbf{r}) + \Sigma_a^g(\mathbf{r})\right]\phi^g(\mathbf{r}) = \sum_{g'=1}^{G} \Sigma_s^{g'\to g}(\mathbf{r})\phi^{g'}(\mathbf{r}) + \chi^g \sum_{g'=1}^{G} \nu\Sigma_f^{g'}(\mathbf{r})\phi^{g'}(\mathbf{r}). \tag{3.46}$$

For $g = 1, \ldots, G$, eq. (3.46) specifies a system of the *multigroup diffusion equations*. To further clean up the notation, I will drop the spatial variable $\mathbf{r}$ from the following equations until sec. 3.3.1.1.

Note that both

$$\Sigma_s^g\phi^g = \sum_{g'=1}^{G} \Sigma_s^{g\to g'}\phi^g$$

and

$$\sum_{g'=1}^{G} \Sigma_s^{g'\to g}\phi^{g'}$$

contain terms characterizing neutrons that even after scattering stay within group g, thus they scatter neither out nor in. Since the two terms appear on opposite sides of the equation, they effectively cancel each other and pose no problem to the balance. However, it is accustomary to define the *removal cross section*:

$$\Sigma_r^g = \Sigma_a^g + \Sigma_s^g - \Sigma_s^{g\to g} \tag{3.47}$$

to represent the real net loss of neutrons from group g and rewrite eq. (3.46) as

$$-\nabla \cdot D^g\nabla\phi^g + \Sigma_r^g\phi^g = \sum_{g'=1,\, g'\neq g}^{G} \Sigma_s^{g'\to g}\phi^{g'} + \chi^g \sum_{g'=1}^{G} \nu\Sigma_f^{g'}\phi^{g'}. \tag{3.48}$$

Evaluation of multigroup constants. The problem with multigroup equations is that they involve terms defined via the unknown function ϕ^g. This raises a nonlinear problem that is usually solved in two steps. First, system (3.48) is solved with a fine energy resolution (e.g. $G = 100$) but only within a small representative area. This reduces the number of equations arising from spatial discretization and makes the numerical solution of the large number of group equations feasible. The result of this step are the fine-group fluxes which are then used to evaluate the multigroup constants for much coarser energy structure (usually $2 - 10$ groups for thermal reactors, [Sta01, p. 390]), according to eqns.

(3.45). The resulting few-group constants may finally be used in a smaller system of coarse-group equations (3.48) to calculate the spatially detailed flux distribution within the whole core.

In practice, the preparation of multigroup constants for the core-wise calculation, called *group data collapsing* ([Sch97, p. 18]), is a complex task that must take into account the heterogeneity of core composition as well as its changes. Precise treatment is beyond the scope of this thesis and I will further assume that the appropriate multigroup constants have already been obtained. Further details may be found e.g. in [Sta01, chap. 11].

3.3.1 The two group model

In PWR analyses, usually 2 to 4 groups are sufficient for performing the few-group core calculation ([Sta01, p. 390]). The 2-group model places neutrons with energies above 1 eV to a *fast group* ($g = 1$), while *thermal group* ($g = 2$) contains neutrons with $E \lesssim 1\,\mathrm{eV}$. Since fission processes release neutrons with energies in the MeV range (cf. section 2.3.4),

$$\chi^2 = \int_0^{1\,\mathrm{eV}} \chi(E)\,\mathrm{d}E = 0 \quad \text{and} \quad \chi^1 = 1.$$

Most neutrons lose energy when they scatter. Elastic collisions may increase energy of only low-energetic neutrons – this is called *up-scatter*. By setting the upper limit of thermal group to 1 eV, the energy of up-scattered thermal neutrons will still belong to the thermal group and hence $\Sigma_s^{2\to1} = 0$. Then

$$\Sigma_r^2 = \Sigma_a^2 + \Sigma_s^{1\to1} - \Sigma_s^{1\to1} = \Sigma_a^2,$$

i.e. the total number of neutrons removed from the thermal group is determined solely by the intragroup absorption, and there will also be no in-scattering of neutrons to the fast group. When these observations are applied to eq. (3.46), a system of steady-state, two-group diffusion equations is obtained[10]:

$$\begin{aligned} -\nabla \cdot D^1 \nabla\phi^1 + (\Sigma_a^1 + \Sigma_s^{1\to2})\phi^1 &= \nu\Sigma_f^1\phi^1 + \nu\Sigma_f^2\phi^2 \\ -\nabla \cdot D^2 \nabla\phi^2 + \Sigma_a^2\phi^2 &= \Sigma_s^{1\to2}\phi^1. \end{aligned} \tag{3.49}$$

For the interior of reactor core, the first equation describes balance in the fast group (in which fissions occur), while the latter governs the thermal neutrons whose only sources are the slowed down neutrons from the fast group. Albedo conditions on reactor boundaries (eq. (3.40)) are applicable:

$$\gamma^g\phi^g + D^g\frac{\partial\phi^g}{\partial\mathbf{n}} = 0, \quad \gamma^g = \frac{1-\alpha^g}{2(1+\alpha^g)}, \quad g = 1, 2. \tag{3.50}$$

[10] I choose not to use the removal cross section symbol for the moment as the number of terms is not too high in the 2-group model

3.3.1.1 Criticality as an eigenvalue problem

The trivial solution $\phi^1(\mathbf{r}) \equiv \phi^2(\mathbf{r}) \equiv 0$ will always fulfill the boundary value problem (3.49), (3.50). However, since we are modelling a running reactor, a nontrivial solution is sought that will describe realistic neutron densities (see sec. 3.1.3). Mathematical structure of the problem admits nontrivial solution only in certain cases that correspond to special values of a variable parameter added to eq. (3.49). These values are known as the *eigenvalues* of the problem and the solutions are called *eigenvectors*. In section 3.1.4 it has been suggested to put the parameter to the fission source term, so the *eigenvalue problem* for the steady-state, two-group diffusion equations with albedo boundary conditions reads:

$$\begin{aligned} -\nabla \cdot D^1(\mathbf{r})\nabla\phi^1(\mathbf{r}) + \left[\Sigma_a^1(\mathbf{r}) + \Sigma_s^{1\to 2}(\mathbf{r})\right]\phi^1(\mathbf{r}) &= \lambda\left[\nu\Sigma_f^1(\mathbf{r})\phi^1(\mathbf{r}) + \nu\Sigma_f^2(\mathbf{r})\phi^2(\mathbf{r})\right] && \text{in } V, \\ -\nabla \cdot D^2(\mathbf{r})\nabla\phi^2(\mathbf{r}) + \Sigma_a^2(\mathbf{r})\phi^2(\mathbf{r}) &= \Sigma_s^{1\to 2}(\mathbf{r})\phi^1(\mathbf{r}) && \text{in } V, \end{aligned} \tag{3.51a}$$

subject to boundary conditions

$$\gamma^1\phi^1(\mathbf{r}) + D^1(\mathbf{r})\frac{\partial\phi^1(\mathbf{r})}{\partial\mathbf{n}} = 0, \quad \gamma^2\phi^2(\mathbf{r}) + D^2(\mathbf{r})\frac{\partial\phi^2(\mathbf{r})}{\partial\mathbf{n}} = 0, \qquad \text{on } \partial V, \tag{3.51b}$$

Here V denotes the core area and ∂V its piece-wise smooth boundary.

Solutions to (3.51) are represented by the *eigenpairs* $\{\lambda_i, [\phi^1(\mathbf{r}), \phi^2(\mathbf{r})]_i\}$. Their existence has been thoroughly examined in works referred to e.g. in [Sch97, p. 19], [Pal97, p. 40] or [AC02]. It has been proven that under some physically justifiable requirements on the coefficients (see also [Cap99, sec. 3.2]), there exists a countable set of eigenvalues in which the first eigenvalue (smallest in modulus) is real, positive and algebraically simple. Its corresponding eigenvector is also real and can be chosen such that its components are everywhere positive. Moreover, the set contains no other eigenvalue for which an eigenvector with the same positivity property can be found.

The consequence is that the smallest eigenvalue λ_1 (also called *principal*) is the only eigenvalue whose eigenvector $(\phi^1, \phi^2)_1$ is capable of describing physically possible neutron distribution. The eigenvalue measures how close is the reactor governed by the equation to the critical state and the components of the eigenvector represent the fast and the thermal neutron fluxes, respectively, within this reactor. Note, however, that these components only allow determination of the relative flux shapes as any multiple of the eigenvector would also satisfy (3.51).

Chapter 4

Numerical solution

The two-group diffusion system developed in previous chapter is a model that is already suitable for numerical solution. The aim of the present chapter is to design a numerical scheme for such solution that would be efficient enough to fit into the encompassing optimization framework.

4.1 Overview

Finite difference scheme. Various methods have been developed in the past to numerically solve the two-group diffusion system (3.51). One of the first were the *finite difference methods* (FDM), in which a mesh of discrete points is laid over the continuous core domain and equations (3.51) are written for each point. The unknowns are the flux values at the discrete points and their derivatives are discretized using difference quotients. The discrete version of (3.51) is thus formed and can be written as a classical matrix eigenvalue problem.

The FDM is described in a greater detail e.g. in [Sta01, sec. 3.10]. On p. 87 in this reference there is also revealed one of its major limitations, namely the need for a very finely structured mesh to give accurate results. The requirement of sufficiently smooth coefficients in the equation in order for the diffusion model to be applicable (see discussion on the validity of diffusion theory, p. 33) even aggravates this need in cases of high core heterogeneity. This leads to a big number of unknowns in the discrete system and hence unacceptable computation times.

Finite volume scheme. To cope with the problems of FDM, more advanced schemes have been invented. Specifically, the *nodal methods* have matured into a very effective technique for whole-core neutronic calculations (e.g. [SA96], [Mou96]). They are based on the *finite volume* (FV) discretization scheme: the whole balance domain Ω is subdivided into so called *control volumes* and each volume is allowed to be much larger than the mesh boxes of the FDM discretization. In a typical nodal framework, one volume corresponds to a single assembly and is referred to as *node*. Material composition within each node

is assumed to be homogeneous, so that use of diffusion theory is justified for deriving the neccessary discrete relations for each node. If heterogeneity is present (almost always the case in real situations), a suitable homogenization procedure must be applied first. Advanced homogenization methods have been created for nodal methods and consequences of one that is particularly popular (known as the *generalized equivalence theory*, or *GET*) will be taken into account when deriving the nodal scheme. However, full description and implementation of the complex task of homogenization is beyond the scope of this thesis and interested reader is referred to [SA96, Sec. 2.2.4], [Mou96, Chap. 4] or [Cap99] for more details.

Discretization then proceeds by stating the conservation condition for every individual node and choosing the unknowns as integral averages of neutron flux over these nodes. Except intranodal average neutron fluxes, the balance equation will also contain neutron currents through the nodal boundaries. These are not known either and have to be related to the average fluxes to make the equation depend on one unknown quantity only. A typical FV procedure would use a constitutive relation (in this case the Fick's law) and approximate the derivatives of unknown flux at the boundaries with standard finite differences, so that the estimates of neutron currents are conservative and consistent. A scheme similar to the FDM is obtained which however uses the finite differences to approximate nodally-conserved integral quantities instead of the differential operator. Hence it preserves the original balance equality for every node. However, by still utilizing finite difference approximations, this method can not yield a sufficiently accurate solution over larger assembly-sized volumes.

Finite volume discretization of (3.51) will be described in section 4.3. For a more general explanation of the scheme, see e.g. [EGH03].

Nodal methods with transverse integration. The reduction of discretization errors resulting from the standard FV approximation can be achieved by a more accurate representation of the relationship between internal flux and surface current for each node. Modern nodal methods utilize the *transverse integration procedure* for this purpose, in which the nodal balance in each node is integrated over directions transverse to a particular coordinate direction. The result is a set of coupled second-order one-dimensional ODE's, one for each direction. These equations are solved for the transverse-averaged flux in every node using a higher order estimation of flux shape within that node. The solution is then used to determine the neccessary relationship between surface currents at the boundaries and average fluxes within the node. Section 4.4.2 provides more details on the procedure.

Actual methods employed in solving the transverse integrated ordinary differential equations distinguish the various nodal methods among each other. Two main approaches are widely used:

- *Analytic methods*: Solving the transverse integrated equations analytically is motivated by the requirement of high accuracy of the solution. However, due to their algebraic complexity, analytical methods do not scale well beyond problems with

more than two groups. Often mentioned in connection with this class are the *Analytic nodal method (ANM)* and the *Nodal Green's function method (NGFM)* (e.g. [FC02], [JJD98], [SA96]).

- *Polynomial expansion methods*: These methods approximate spatial variation of transverse integrated flux within the node by a higher-order polynomial expansion – e.g. the *Nodal expansion method (NEM)* expands the flux into a fourth-order polynomial ([SA96], [T$^+$94]). Polynomial methods are easily extensible to multigroup models.

Even the analytic method, however, does not avoid approximations completely. The only one that is necessary in this method stems from the fact that the coupling of each of the ODEs to the remaining ones cannot be determined precisely. Estimating the shape of the coupling term by a quadratic polynomial has exhibited good results and achieved a widespread use.

Semi-analytic method. Besides their complexity, analytic methods initially suffered from stability problems. Although recent developments successfully circumvented these problems ([JJD98], [FC02]), another research direction has also been taken which moreover simplifies the analytic formulation in order to make it amenable to multigroup calculations. It combines the expansion and analytic approaches - the former manifests in using a polynomial expansion of the inhomogeneous term of the transverse integrated balance equation. The latter shows up in the assumption that the intranodal flux takes a form of analytic solution to the balance equation with the polynomially-expanded right hand side. Arbitrary constants appearing in the solution are chosen such that appropriate physical and mathematical constraints are satisfied. This way of determining the transverse integrated flux within a node is known as *semi-analytic method* ([FC02]). It is used in this thesis (details in section 4.4.2.2) for its accuracy almost comparable to ANM and effortless scalability to multigroup problems.

Two-node problems. In either of the above mentioned nodal methods, the coefficients that determine the local flux profile within each node are subject to boundary conditions. This means that each node needs the information about the solution from its neighbouring node. This coupling forms a local *two-node problem*. Remaining coefficients are obtained from additional physically significant constraints. In the case of the semi-analytic method, also a mathematical requirement of satisfying the balance equation in a weak sense must be imposed on the flux[1].

Non-linear iteration. The transverse integrated fluxes may be used in conjunction with Fick's law to directly eliminate the surface currents in the local balance equality for each

[1]This condition is also required by all expansion methods in which flux is developed into polynomials of orders higher than two ([SA96, p.140])

node ([Mou96, chap. 3], [SA96]). Global neutron flux and critical eigenvalue may then be obtained in the same manner as in the FDM. However, an alternative technique has been developed which is more efficient from both memory and computational points of view ([T+94, sec. II.1.b], [SA96, p. 143]). It uses the higher-order surface current estimates from the local two-node problems to refine the low-order currents predicted by the coarse-mesh FV scheme, which is consequently used to advance the global solution. Since formulation of the two-node problems requires knowledge of this whole-core solution, the method is nonlinear – low-order solution of the global coarse-mesh problem is used to construct local nodal-coupling problems, these are solved by a high-order method and the solution finally provides corrections for the original coarse-mesh system. The procedure will be outlined in section 4.4.4.

4.2 Discretization

The task of the present section is to formulate a spatially discretized version of the two-group system of neutron diffusion equations involved in the steady-state eigenvalue problem (3.51). Let us write the equations in terms of neutron current, i.e. as a system of the exact balance equation and the approximate constitutive law (group-discretized form of equations (3.28) and (3.33), respectively):

$$\nabla \cdot \mathbf{j}^g(\mathbf{r}) + \Sigma_r^g(\mathbf{r})\phi^g(\mathbf{r}) = \sum_{g'=1,\, g' \neq g}^{2} \Sigma_s^{g' \to g}(\mathbf{r})\phi^{g'}(\mathbf{r}) + \frac{\chi^g}{k_{\text{eff}}} \sum_{g'=1}^{2} \nu\Sigma_f^{g'}(\mathbf{r})\phi^{g'}(\mathbf{r}), \tag{4.1a}$$

$$\mathbf{j}^g(\mathbf{r}) \approx -D^g(\mathbf{r})\nabla\phi^g(\mathbf{r}), \text{ for } \mathbf{r} \in \Omega; \tag{4.1b}$$

$$\gamma^g\phi^g(\mathbf{r}) + D^g(\mathbf{r})\nabla\phi^g(\mathbf{r}) \cdot \mathbf{n}(\mathbf{r}) = 0, \text{ for } \mathbf{r} \in \partial\Omega, \tag{4.1c}$$

where $\mathbf{r} = (x, y)$ is a point in the continuous core domain, $\mathbf{j}^g(\mathbf{r})$ is the group-discretized neutron current, $\mathbf{n}(\mathbf{r})$ represents the vector field of unit surface normals to $\partial\Omega$ pointing out of Ω, $\gamma^g = \frac{1-\alpha^g}{2(1+\alpha^g)}$ and $g = 1, 2$ (which will be assumed in the rest of the thesis where not specified otherwise). Note that relation (3.22) has been used to write the equation in a traditional form. Also recall that $\Sigma_s^{2\to1} = 0$, so the first term on the right-hand side will be present only for $g = 2$, and that $\chi^2 = 0$, so the second right-hand side term will appear only in the first equation.

The nodal method introduced in previous section will be used to discretize the equation. As it is based on the finite volume scheme, this fundamental building block will be described in detail first. Changes required to transform the FV scheme to a more accurate nodal scheme will be described in section 4.4.1.

4.2.1 Spatial domain discretization

Let us consider a planar reactor core, represented by a bounded subset Ω of $\mathbb{R}^2$. As already mentioned, the finite volume method utilizes a division of domain Ω into a mesh $\mathcal{T}$

of adjoining control "volumes" (planes in 2D), which I will call *nodes* (sometimes also *boxes* or *cells*). Derivation of the scheme for rectangular nodes can be found in many references, e.g. in [BK06, chap. 2], [Mou96, chap. 3] or [Sch97, sec. 3.1]. So instead, this thesis focuses on the case of hexagonally shaped nodes[2].

Discretization of domain Ω into the hexagonal lattice may be obtained as follows. Let us fix a row j, ($j = 1, \ldots, M$, $M \in \mathbb{N}$) spanning the domain extent in the x-direction, and lay over a grid of points $x_{ij} = [x_i, y_j]$, $i = 0, \ldots, N_j + 1$, $N_j \in \mathbb{N}$, such that

$$x_{0,j} = x_{\frac{1}{2},j} < x_{1,j} < x_{\frac{3}{2},j} < \cdots < x_{i-\frac{1}{2},j} < x_{i,j} < x_{i+\frac{1}{2},j} < \cdots x_{N,j} < x_{N_j+\frac{1}{2},j} = x_{N_j+1,j}.$$

A regular hexagon centered at x_{ij} and extending in the x-direction from $x_{i-1/2,j}$ to $x_{i+1/2,j}$ is then defined for each grid point x_{ij} ($1 \le i \le N_j$) in row j. If we set $h = x_{i+1/2,j} - x_{i-1/2,j}$, then h is the width of the hexagon and its edges perpendicular to the x-direction are placed at points $x_{i\pm1/2,j} = x_{ij} \pm h/2$. The top and bottom edges are given by functions $y_{t,ij}(x)$ and $-y_{t,ij}(x)$, respectively, where

$$y_{t,ij}(x) = \frac{1}{\sqrt{3}}(h - |x - x_{ij}|), \quad i = 1, \ldots, N_j. \tag{4.2}$$

One such hexagon is depicted in figure 4.1.

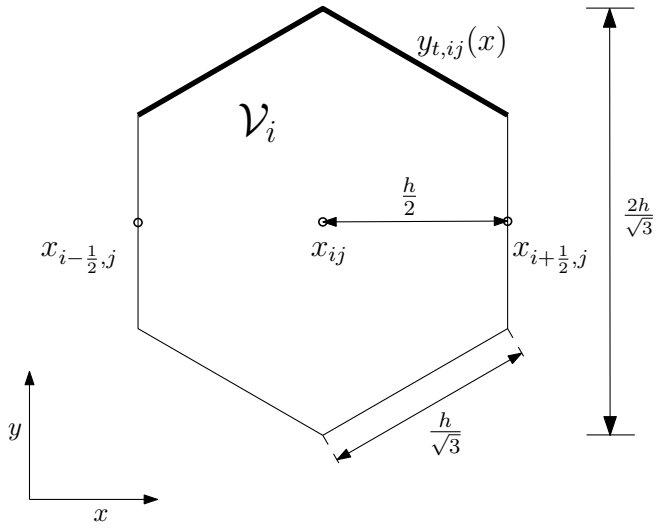

Figure 4.1: Hexagonal node with its dimensions

The row $j + 1$ above row j is put together in the same way so that the two rows join each other through the common segments of the bottom (respectively top) edges of their hexagons. When all rows are filled, a two-dimensional system of hexagonal nodes $\mathcal{V}_{ij}$ is created which fully covers Ω:

$$\mathcal{T} = \bigcup_{j=1,\ldots,M} \bigcup_{i=1,\ldots,N_j} \overline{\mathcal{V}_{ij}}, \quad \bigcup_{\mathcal{V}\in\mathcal{T}} \overline{\mathcal{V}} = \overline{\Omega}.$$

[2]such hexagonal assemblies are actually used in VVER-1000 type reactors ([ČEZ], [Heř81])

In the following, I adopt the accustomary linear indexing of the hexagons in system $\mathcal{T}$ from left to right and bottom to up as shown in figure 4.2. Denoting the total number of nodes by N ($N \in \mathbb{N}$, $N = \sum_{j=1}^{M} N_j$), then $\mathcal{T} = \bigcup_{k=1,\dots,N} \mathcal{V}_k$.

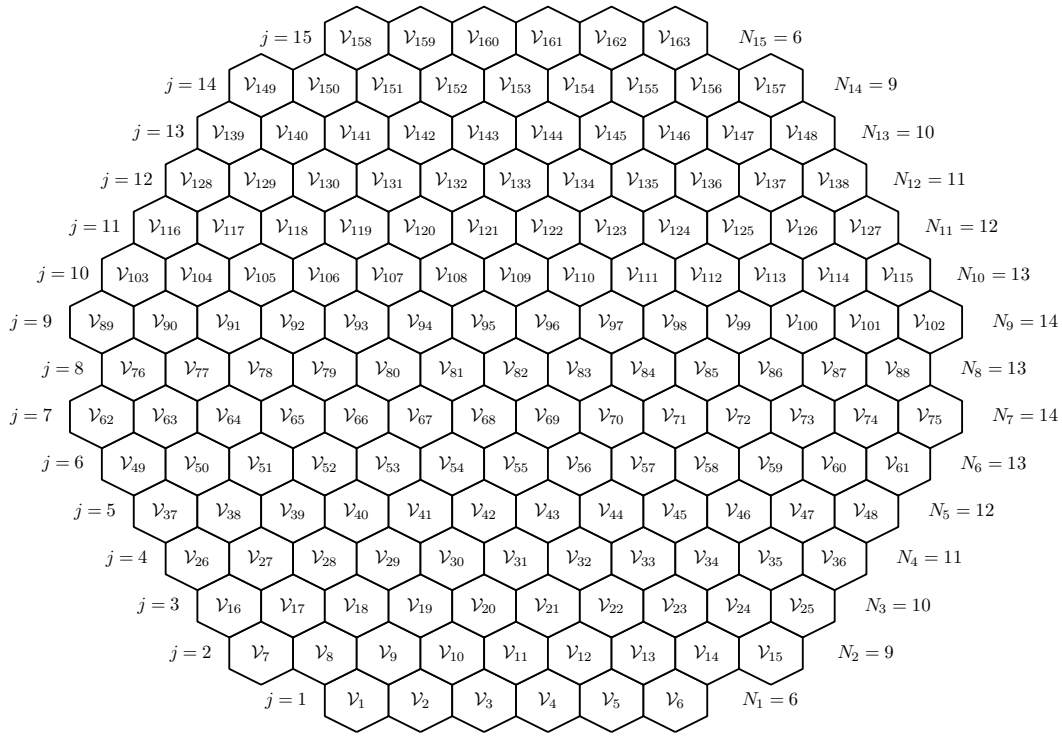

Figure 4.2: A core domain Ω composed of 163 nodes

Nodal symbolism and properties

Let $\mathcal{V}_i \in \mathcal{T}$ be an arbitrary hexagonal node of the mesh defined above. Node-wise spatial variables are defined as directions perpendicular to the faces of the hexagon, formally grouped under letter ξ: $\xi = (x, u, v)$. Quantities associated with node $\mathcal{V}_i$ will be marked with lower index i, i.e. as q_i. Neighbourhood of the node comprises nodes $\mathcal{V}_{i+x}, \mathcal{V}_{i+u}, \mathcal{V}_{i+v}, \mathcal{V}_{i-x}, \mathcal{V}_{i-u}, \mathcal{V}_{i-v}$ listed counter-clockwise beginning with node adjacent to $\mathcal{V}_i$ in the positive x-direction (see figure 4.3).

Faces of node $\mathcal{V}_i$ are represented by $\Gamma_{i,x\pm}$, $\Gamma_{i,u\pm}$, $\Gamma_{i,v\pm}$, where plus or minus sign is used to distinguish sides of the hexagon (left or right with respect to the given local direction). The complete boundary of the hexagon is denoted by $\partial\mathcal{V}_i$:

$$\partial\mathcal{V}_i = \bigcup_{s\in\{+,-\}} \left(\overline{\Gamma_{i,xs}} \cup \overline{\Gamma_{i,us}} \cup \overline{\Gamma_{i,vs}}\right).$$

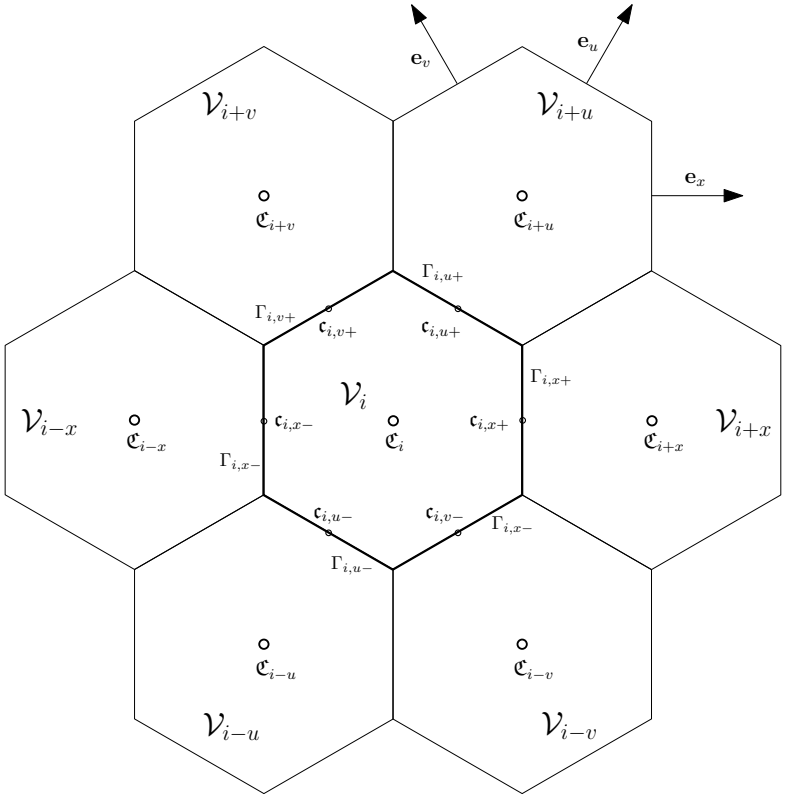

Figure 4.3: A neighbourhood of the hexagonal node (fraktur letters are used to denote centerpoints: $\mathfrak{C}_i = x_{ij}$, $\mathfrak{C}_{i\pm\xi} = \mathfrak{C}_i \pm \mathbf{e}_\xi h$, $\mathfrak{c}_{i,\xi\pm} = \mathfrak{C}_i \pm \frac{h}{2}\mathbf{e}_\xi$ $(\xi = (x, u, v))$

The faces are oriented by their respective normal vectors pointing outwards from the node:

$$\begin{aligned} \mathbf{n}_{i,x+} &= \mathbf{e}_x, \quad & \mathbf{n}_{i,x-} &= -\mathbf{e}_x, \\ \mathbf{n}_{i,u+} &= \mathbf{e}_u, \quad & \mathbf{n}_{i,u-} &= -\mathbf{e}_u, \\ \mathbf{n}_{i,v+} &= \mathbf{e}_v, \quad & \mathbf{n}_{i,v-} &= -\mathbf{e}_v, \end{aligned}$$

where $\mathbf{e}_\xi$ denotes the unit vector in the respective local direction ξ[3] (see figure 4.3). Similarly to face normals, any quantity q associated with faces $\Gamma_{i,\xi\pm}$ will be marked as $q_{i,\xi\pm}$. To stress the one-sided incidence of some quantity to the face, symbol $q_{i,\xi-}(\Gamma_{i,\xi-}+)$, respectively $q_{i,\xi+}(\Gamma_{i,\xi+}-)$, will be used in place of the right-sided, respectively left-sided, limit of the quantity approaching the given face from within the node along the local direction ξ, e.g.:

$$q_{i,\xi-}(\Gamma_{i,\xi-}+) = \lim_{\mathbf{r}\to\Gamma_{i,\xi-}+} q_{i,\xi-}(\mathbf{r}).$$

Any arbitrary face of $\mathcal{V}_i$ will be denoted by σ, i.e. $\sigma \in \partial V_i$, or formally $\sigma = \overline{\Gamma_{i,\xi\pm}}$. Symbol $\mathrm{d}\sigma$ will be used as the integration symbol for line integrals over the face.

[3]with Cartesian coordinates $\mathbf{e}_x = [1, 0]$, $\mathbf{e}_u = [\frac{1}{2}, \frac{\sqrt{3}}{2}]$, $\mathbf{e}_v = [-\frac{1}{2}, \frac{\sqrt{3}}{2}]$.

Dimensions of the hexagon that are of interest are given by the following measures (cf. figure 4.1):

- edge length:

$$m_e = \mu(\Gamma_{i,x\pm}) \equiv \mu(\Gamma_{i,u\pm}) \equiv \mu(\Gamma_{i,v\pm}) \equiv \frac{h}{\sqrt{3}}, \tag{4.3}$$

- node area:

$$m_N = \mu(\mathcal{V}_i) = 2 \int_{x_{ij}-\frac{h}{2}}^{x_{ij}+\frac{h}{2}} y_{t,ij}(x)\,\mathrm{d}x \;= \frac{h^2\sqrt{3}}{2}. \tag{4.4}$$

4.2.2 Discretization of the nodal balance relation

Both the finite volume scheme and the nodal scheme for discretizing boundary value problem (4.1) are based on preservation of neutron balance in each node $\mathcal{V}_i \in \mathcal{T}$. The exact derivation of the scheme starts from the global balance equality in balance domain $\mathcal{V}_i$, i.e. from eq. (3.16) where $V = \mathcal{V}_i$. This equation may be reduced to the steady-state two-group diffusion system by simply repeating the steps described in sections 3.1.2 through 3.3.1, with all spatial relations left in the original integral form (that is, not using the spatially local equation (3.18)). However, in a much simpler (although not so mathematically rigorous) procedure, one can derive the discrete expressions by formal manipulations with the local version of balance equations (4.1).

The formal procedure begins by integrating balance equation (4.1a) over node $\mathcal{V}_i$ and dividing it by the area of the node:

$$\frac{1}{m_N}\int_{\mathcal{V}_i} \nabla\cdot\mathbf{j}^g(\mathbf{r})\,\mathrm{d}\mathbf{r} \;+ \frac{1}{m_N}\int_{\mathcal{V}_i} \Sigma_r^g(\mathbf{r})\phi^g(\mathbf{r})\,\mathrm{d}\mathbf{r} \;= \\ = \frac{1}{m_N}\sum_{g'=1,\,g'\neq g}^{2}\int_{\mathcal{V}_i} \Sigma_s^{g'\to g}(\mathbf{r})\phi^{g'}(\mathbf{r})\,\mathrm{d}\mathbf{r} \;+ \frac{\chi^g}{k_{\mathrm{eff}}}\sum_{g'=1}^{2}\frac{1}{m_N}\int_{\mathcal{V}_i}\nu\Sigma_f^{g'}(\mathbf{r})\phi^{g'}(\mathbf{r})\,\mathrm{d}\mathbf{r}\,. \tag{4.5}$$

This equation naturally represents conservation of neutron flux in node $\mathcal{V}_i$. Its spatial discretization requires a choice of the discrete unknown for which it will be solved. The discrete solution should provide a reasonable approximation of the continuous quantity within each considered node. For this purpose, discrete variables in nodal schemes are typically assigned to mean values of continuous neutron flux over the respective nodes (the nodal averages):

$$\bar{\bar{\phi}}_i^g := \frac{1}{m_N}\int_{\mathcal{V}_i}\phi^g(\mathbf{r})\,\mathrm{d}\mathbf{r}\,, \quad i = 1,\ldots,N. \tag{4.6}$$

Two overbars denote the integral average over the whole node, contrary to one overbar that will be used later to symbolize the integral average over a face.

To obtain a numerically tractable version of eq. (4.5), let us choose a reference node $\mathcal{V}_i$ and spatially discretize each term of the equation.

4.2.2.1 Diffusion term

The first term can be rewritten with the help of divergence formula:

$$\frac{1}{m_N}\int\limits_{\mathcal{V}_i}\nabla\cdot\mathbf{j}^g(\mathbf{r})\,\mathrm{d}\mathbf{r}\;=\frac{1}{m_N}\oint\limits_{\partial\mathcal{V}_i}\mathbf{j}^g(\mathbf{r})\cdot\mathbf{n}_i(\mathbf{r})\,\mathrm{d}\sigma\;=\frac{1}{m_N}\sum_{\sigma\in\partial\mathcal{V}_i}\int\limits_{\sigma}\mathbf{j}^g(\mathbf{r})\cdot\mathbf{n}_{i,\sigma}\,\mathrm{d}\sigma\,, \tag{4.7}$$

where $\mathbf{n}_i(\mathbf{r})$ is the vector field of unit normals to nodal boundaries, pointing out of the node, and $\mathbf{n}_{i,\sigma}$ is the unit outward normal to a particular boundary edge σ. In the last term, $\mathbf{j}^g(\mathbf{r})\cdot\mathbf{n}_{i,\sigma}$ expresses the flow of neutrons through point $\mathbf{r}$ of some edge $\sigma\in\partial\mathcal{V}_i$ in the direction of its outward normal at that point. The average number of neutrons that leak out of the node through the given oriented face is then

$$\bar{j}^g_{i,\sigma,n_i}:=\frac{1}{\mu(\sigma)}\int\limits_{\sigma}\mathbf{j}^g(\mathbf{r})\cdot\mathbf{n}_{i,\sigma}\,\mathrm{d}\sigma\,.$$

In the case of hexagonal nodes, this quantity may be split into the following averages of neutron currents in the positive x, (resp. u, resp. v) directions across the respective pairs of edges (denoted by plus/minus signs) perpendicular to them:

$$\begin{aligned}\bar{j}^g_{i,x\pm}&:=\frac{1}{m_e}\int\limits_{\Gamma_{i,x\pm}}\mathbf{j}^g(\mathbf{r})\cdot\mathbf{e}_x\,\mathrm{d}\sigma\,,\\ \text{resp. }\bar{j}^g_{i,u\pm}&:=\frac{1}{m_e}\int\limits_{\Gamma_{i,u\pm}}\mathbf{j}^g(\mathbf{r})\cdot\mathbf{e}_u\,\mathrm{d}\sigma\,,\\ \text{resp. }\bar{j}^g_{i,v\pm}&:=\frac{1}{m_e}\int\limits_{\Gamma_{i,v\pm}}\mathbf{j}^g(\mathbf{r})\cdot\mathbf{e}_v\,\mathrm{d}\sigma\,.\end{aligned} \tag{4.8}$$

By continuing the discretization process started in (4.7):

$$\begin{aligned}\frac{1}{m_N}\sum_{\sigma\in\partial\mathcal{V}_i}\int_{\sigma}&\mathbf{j}^g(\mathbf{r})\cdot\mathbf{n}_{i,\sigma}\,\mathrm{d}\sigma\;=\\ &=\frac{1}{m_N}\sum_{\xi\in\{x,u,v\}}\left(\int_{\Gamma_{i,\xi+}}\mathbf{j}^g(\mathbf{r})\cdot\mathbf{n}_{i,\xi+}\,\mathrm{d}\sigma\;+\int_{\Gamma_{i,\xi-}}\mathbf{j}^g(\mathbf{r})\cdot\mathbf{n}_{i,\xi-}\,\mathrm{d}\sigma\right)=\\ &=\frac{1}{m_N}m_e\sum_{\xi\in\{x,u,v\}}\left(\frac{1}{m_e}\int_{\Gamma_{i,\xi+}}\mathbf{j}^g(\mathbf{r})\cdot\mathbf{e}_\xi\,\mathrm{d}\sigma\;+\frac{1}{m_e}\int_{\Gamma_{i,\xi-}}\mathbf{j}^g(\mathbf{r})\cdot(-\mathbf{e}_\xi)\,\mathrm{d}\sigma\right)\end{aligned}$$

and using (4.8), the total neutron leakage out of node $\mathcal{V}_i$ averaged over the area of the node is obtained as a superposition of the face-averaged net leakages in the respective directions,

which are given by $\bar{l}^g_{i,\xi} = \bar{j}^g_{i,\xi+} - \bar{j}^g_{i,\xi-}$:

$$\bar{\bar{l}}^g_i := \frac{1}{m_N}\int_{\mathcal{V}_i} \nabla\cdot\mathbf{j}^g(\mathbf{r})\,\mathrm{d}\mathbf{r} = \frac{2}{h^2\sqrt{3}}\frac{h}{\sqrt{3}}\sum_{\xi\in\{x,u,v\}}\left(\bar{j}^g_{i,\xi+} - \bar{j}^g_{i,\xi-}\right) = \frac{2}{3h}\sum_{\xi\in\{x,u,v\}}\bar{l}^g_{i,\xi} =$$
$$= \frac{2}{3h}(\bar{j}^g_{i,x+} - \bar{j}^g_{i,x-}) + \frac{2}{3h}(\bar{j}^g_{i,u+} - \bar{j}^g_{i,u-}) + \frac{2}{3h}(\bar{j}^g_{i,v+} - \bar{j}^g_{i,v-}). \quad (4.9)$$

Note that by imposing the flow of neutrons in positive direction (from left to right), neutrons actually flow *into* the node through the left (minus) side of boundary and thus the partial leakage through that side must be negative.

Equation (4.9) may be thought about as an *exact* discretization, since no approximation had to be employed yet. However, it involves a secondary discrete unknown, namely the edge-averaged net neutron current $\bar{j}^g_{i,\sigma}$. In order for the scheme to be well-defined an expression relating the primary and secondary unknowns must be worked out, so that the final system resulting from the discretization contains only one family of unknowns per group. As will be shown in section 4.3, this relationship will already require some approximations and hence when used to close (4.5), it will produce an equation whose solution may no longer represent the exact integral averages of neutron flux. For this moment, however, let us assume that the exact relationship $\bar{j}^g_{i,\sigma} = \bar{j}^g_{i,\sigma}(\bar{\bar{\phi}}^g_i)$ is obtainable for each face σ and proceed with exact discretization of (4.5).

4.2.2.2 Reaction terms

The remaining terms in (4.5) represent various reaction rates. Principially, we wish to replace

$$\frac{1}{m_N}\int_{\mathcal{V}_i}\Sigma^g_*(\mathbf{r})\phi^g(\mathbf{r})\,\mathrm{d}\mathbf{r}$$

in the equation for node $\mathcal{V}_i$ by

$$\Sigma^g_{i,*}\bar{\bar{\phi}}^g_i = \Sigma^g_{i,*}\frac{1}{m_N}\int_{\mathcal{V}_i}\phi^g(\mathbf{r})\,\mathrm{d}\mathbf{r}\,,$$

for each reaction type (removal, scattering, fission). If we continued the exact procedure, discrete values of cross sections in the given node would have to be defined by

$$\Sigma^g_{i,*} = \frac{\int_{\mathcal{V}_i}\Sigma^g_*(\mathbf{r})\phi^g(\mathbf{r})\,\mathrm{d}\mathbf{r}}{\int_{\mathcal{V}_i}\phi^g(\mathbf{r})\,\mathrm{d}\mathbf{r}}. \quad (4.10)$$

This would be possible in the case where real cross sections represented by $\Sigma^g_*(\mathbf{r})$ were constant within each node, since the integral values of unknown neutron flux would cancel out. However, recall from the overview of the finite volume scheme (p. 39) that in the nodal framework used with the FV method for neutron diffusion problems, each control

volume is identified with a single assembly. Since the material distribution is usually non-uniform within each assembly, the macroscopic cross sections will certainly not be node-wise constant functions. In this case, a direct application of (4.10) is not possible since it involves the very unknown we are solving for. However, a homogenization procedure may be employed to define constant cross sections over each node even on this coarse mesh. As this complicated task exceeds the scope of this thesis, I assume every node $\mathcal{V}_i \in \mathcal{T}$ to be homogeneous, so that

$$\Sigma_*^g(\mathbf{r})\big|_{\mathbf{r}\in\mathcal{V}_i} = \text{ const.} =: \Sigma_{i,*}^g. \tag{4.11}$$

Note that the constant may be different for different nodes and hence the homogenized cross-section is generally a function discontinuous at nodal interfaces. Using this node-wise constant function in (4.10), one may now define the exact discrete reaction rates for:

- *total neutron removal*:

$$\Sigma_{i,r}^g \bar{\bar{\phi}}_i^g = \frac{1}{m_N} \int_{\mathcal{V}_i} \Sigma_r^g(\mathbf{r}) \phi^g(\mathbf{r}) \,\mathrm{d}\mathbf{r}\,, \tag{4.12}$$

- *neutron in-scatter from fast group to thermal*:

$$\Sigma_{i,s}^{1\to 2} \bar{\bar{\phi}}_i^1 = \frac{1}{m_N} \int_{\mathcal{V}_i} \Sigma_s^{1\to 2}(\mathbf{r}) \phi^1(\mathbf{r}) \,\mathrm{d}\mathbf{r}\,, \tag{4.13}$$

- *fission*:

$$\nu\Sigma_{i,f}^g \bar{\bar{\phi}}_i^g = \frac{1}{m_N} \int_{\mathcal{V}_i} \nu\Sigma_f^g(\mathbf{r}) \phi^g(\mathbf{r}) \,\mathrm{d}\mathbf{r}\,. \tag{4.14}$$

4.2.2.3 A complete discretized equation

The discrete version of (4.5) that exactly preserves neutron balance in node $\mathcal{V}_i,\ i = 1, \ldots, N$, is obtained by inserting (4.9), (4.12), (4.13) and (4.14) into (4.5):

$$\begin{aligned} \frac{2}{3h}(\bar{j}_{i,x+}^g - \bar{j}_{i,x-}^g) + \frac{2}{3h}(\bar{j}_{i,u+}^g - \bar{j}_{i,u-}^g) + \frac{2}{3h}(\bar{j}_{i,v+}^g - \bar{j}_{i,v-}^g) + \Sigma_{i,r}^g \bar{\bar{\phi}}_i^g = \\ = \sum_{g'=1,\, g'\neq g}^{2} \Sigma_{i,s}^{g'\to g} \bar{\bar{\phi}}_i^{g'} + \frac{\chi^g}{k_{\mathrm{eff}}} \sum_{g'=1}^{2} \nu\Sigma_{i,f}^{g'} \bar{\bar{\phi}}_i^{g'}\,, \end{aligned} \tag{4.15}$$

A crucial step in construction of the numerical scheme is finding how to eliminate the edge-averaged neutron currents $\bar{j}_{i,\xi\pm}^g$ from (4.15) in favor of the node-averaged fluxes $\bar{\bar{\phi}}_i^g$. The way of doing so distinguishes from the most part various nodal methods from each other and also from the classical FV-based methods. The following section will describe the finite volume approach, while section 4.4 in the sequel will present the semi-analytic nodal technique.

4.3 Finite volume scheme

A big advantage of the classical FV scheme is its theoretically well-founded numerical behaviour. A detailed presentations of FV theory for relevant problems are given in the book [EGH03] or in the paper [GHV00]. This section borrows ideas from the two references to obtain from eq. (4.15) a stable and convergent FV scheme. Proving the two properties exceeds the scope of this thesis, however, and only references to literature where more details can be found will be given at the end of the section.

As a convention, approximations of the unknown variables in eq. (4.15) that the scheme introduces will be denoted by corresponding capital letters.

4.3.1 Basic assumptions

The two fundamental conditions neccessary for constructing a well-posed FV scheme are placed on the discretization mesh and the approximation of integral averages of neutron currents (in literature on finite volumes called *numerical fluxes*). The former is automatically satisfied by set $\mathcal{T}$ of hexagonal nodes from section 4.2.1 since it posesses all the properties of the so-called *restricted admissible mesh* for the given problem (in the sense of definition 2.1, p. 1936, and remark 1, p. 1937, in [GHV00]).

The latter requires that the approximation of edge-averaged neutron currents in terms of the cell-averaged neutron fluxes (the primary unknowns of the problem) be

1. *conservative*: for any two consecutive nodes $\mathcal{V}_i$ and $\mathcal{V}_k$ ($\mathcal{V}_i, \mathcal{V}_k \in \mathcal{T}$) with a common interface σ ($\sigma = \overline{\mathcal{V}_i} \cap \overline{\mathcal{V}_k}$),
$$\bar{J}^g_{i,\sigma}(\sigma-) = \bar{J}^g_{k,\sigma}(\sigma+), \tag{4.16}$$
where $\bar{\bar{j}}^g_{i,\sigma} \approx \bar{J}^g_{i,\sigma}(\bar{\bar{\Phi}}^g_i)$ and $\bar{\bar{\Phi}}^g_i$ is also some suitable numerical approximation of the exact integral average $\bar{\bar{\phi}}^g_i$ (will be determined later). This condition describes the discrete approximate equivalent of neutron current continuity (second part of (3.36), p. 31).

2. *consistent*: the error introduced by replacing the exact edge-averaged neutron current $\bar{\bar{j}}^g_{i,\sigma}$ with its approximation $\bar{J}^g_{i,\sigma}$ in node $\mathcal{V}_i \in \mathcal{T}$ tends to zero as the size of the node diminishes.

4.3.2 Approximation of integral averages of neutron currents

FV expressions for average neutron current through nodal boundary will be derived here first for edge σ separating two nodes $\mathcal{V}_i, \mathcal{V}_{i+x} \in \mathcal{T}$ in the x direction. Hence $\sigma = \Gamma_{i,x+} = \Gamma_{i+x,x-}$. Expressions for other interior faces separating the two hexagons in $\pm\xi$ directions may be obtained in a similar manner. At the end of this section, average currents through outer boundaries of the core will be specified by using boundary conditions (3.50).

4.3.2.1 Nodal interfaces

Problem setting. Since only one direction will be considered, I will refer to the right node by a more common index $i+1$ instead of $i+x$. By construction of mesh $\mathcal{T}$ (see section 4.2.1), the center-points of the involved nodes are located at points with Cartesian coordinates $[x_i, y_j]$ and $[x_{i+1}, y_j]$, respectively, and the considered edge crosses perpendicularly the line connecting the centres through its midpoint at $[x_{i+1/2}, y_j]$. Distance from the interface cross-point to the center of each of the two nodes is $x_{i+1/2,j} - x_{ij} = x_{i+1,j} - x_{i+1/2,j} = h/2$ (see figure 4.3).

Approximate relations. Assuming conservativity, a consistent approximation of the edge-averaged neutron current in terms of the approximate cell-averaged neutron fluxes may be written to close (4.15). For this purpose, Fick's law (4.1b) describing a connection between the continuous quantities is discretized in the FV sense to also yield the corresponding discrete relationship.

Writing the Fick's law for neutron current in the direction of $\mathbf{e}_x$ and averaging over face $\Gamma_{i,x+}$ yields

$$\bar{j}_{i,x+} = \frac{1}{m_e} \int\limits_{\Gamma_{i,x+}} \mathbf{j}^g(\mathbf{r}) \cdot \mathbf{e}_x \,\mathrm{d}\sigma \;\approx \frac{1}{m_e} \int\limits_{\Gamma_{i,x+}} -D^g(\mathbf{r}) \nabla\phi^g(\mathbf{r}) \cdot \mathbf{e}_x \,\mathrm{d}\sigma \,. \tag{4.17}$$

Since we are working on a homoegeneous problem, we may use the average homogenized diffusion constant D_i^g in place of $D^g(\mathbf{r})$ in node $\mathcal{V}_i$. The actual constant suitably representing $D^g(\mathbf{r})$ within the node is obtained by some homogenization procedure, as in the case of cross sections. This leads to the following transcription of (4.17) for node $\mathcal{V}_i$

$$\frac{1}{m_e} \int\limits_{\Gamma_{i,x+}} \mathbf{j}^g(\mathbf{r}) \cdot \mathbf{e}_x \,\mathrm{d}\sigma \;\approx -\frac{1}{m_e} D_i^g \int\limits_{\Gamma_{i,x+}} \nabla\phi^g(\mathbf{r}) \cdot \mathbf{e}_x \,\mathrm{d}\sigma \,. \tag{4.18}$$

Since the diffusion coefficient attains different values in the two adjoining nodes, approximation of the edge-based derivative on the right-hand side needs to be performed from both sides of the interface. Conservativity condition can then be used to obtain the relationship.

Let us first consider node $\mathcal{V}_i$. Average neutron current coming from its interior to face $\Gamma_{i,x+}$ in the positive x-direction may be approximated using (4.18) as follows:

$$\begin{aligned} \bar{j}_{i,x+} \approx -\frac{1}{m_e} D_i^g \int\limits_{\Gamma_{i,x+}} \nabla\phi^g(\mathbf{r}) \cdot \mathbf{e}_x \,\mathrm{d}\sigma \;&= -\frac{1}{m_e} D_i^g \int\limits_{y_1}^{y_2} \left(\frac{\partial \phi^g(x,y)}{\partial x}\bigg|_{x \to x_{i+\frac{1}{2}}-} \right) \mathrm{d}y \;= \\ &= -D_i^g \frac{\partial}{\partial x} \left(\frac{1}{m_e} \int\limits_{y_1}^{y_2} \phi^g(x,y) \,\mathrm{d}y \right) \bigg|_{x \to x_{i+\frac{1}{2}}-} . \end{aligned} \tag{4.19}$$

The last expression involves derivative at point $x_{i+1/2}$ of flux averaged over the face $\Gamma_{i,x+}$ which extends at that point from $y_1 = -y_{t,ij}(x_{i+1/2})$ to $y_2 = y_{t,ij}(x_{i+1/2})$. Estimating the

integral by midpoint rule,

$$\frac{1}{m_e}\int_{y_1}^{y_2}\phi^g(x,y)\,\mathrm{d}y \approx \frac{1}{m_e}\phi^g(x,y_j)(y_2-y_1)=\phi^g(x,y_j), \tag{4.20}$$

we obtain the following expression for the average neutron current approximated at given face:

$$\bar{j}^g_{i,x+} \approx -D^g_i \left.\frac{\partial\phi^g(x,y_j)}{\partial x}\right|_{x\to x_{i+\frac{1}{2}}-}. \tag{4.21}$$

For approximation of the derivative, we can use the finite-difference principle on interval $[x_i, x_{i+\frac{1}{2}}]$ corresponding to node $\mathcal{V}_i$:

$$\left.\frac{\partial\phi^g(x,y_j)}{\partial x}\right|_{x\to x_{i+\frac{1}{2}}-} \approx \frac{\phi^g(x_{i+\frac{1}{2}},y_j)-\phi^g(x_i,y_j)}{\frac{h}{2}}. \tag{4.22}$$

The first term in the nominator is the approximation of face-averaged flux at $\Gamma_{i,x+}$, which I denote by $\bar{\Phi}^g_{i,x+}$ (see also remark 4.2). The second term is the midpoint approximation of the unknown node-averaged flux (4.6):

$$\frac{1}{m_N}\int_{\mathcal{V}_i}\phi^g(\mathbf{r})\,\mathrm{d}\mathbf{r} \approx \phi^g(x_i,y_j) =: \bar{\bar{\Phi}}^g_i. \tag{4.23}$$

The final numerical approximation of the face averaged neutron current through $\Gamma_{i,x+}$ is:

$$\bar{J}^g_{i,x+} := -D^g_i \frac{\bar{\Phi}^g_{i,x+}-\bar{\bar{\Phi}}^g_i}{\frac{h}{2}}. \tag{4.24}$$

Now let us move to the neighbouring node $\mathcal{V}_{i+1}$ and perform an analogous procedure as above, only with x located in the appropriate interval $[x_{i+1/2}, x_{i+1}]$ and using the relevant diffusion parameter. This yields the following estimate for the interfacial current associated with $\mathcal{V}_{i+1}$:

$$\bar{j}^g_{i+1,x-} \approx -D^g_{i+1}\frac{\bar{\bar{\Phi}}^g_{i+1}-\bar{\Phi}^g_{i,x+}}{\frac{h}{2}} =: \bar{J}^g_{i+1,x-}. \tag{4.25}$$

The value of neutron flux at the interface between the two nodes may now be obtained by imposing the conservativity condition:

$$\bar{J}^g_{i,x+}=\bar{J}^g_{i+1,x-} \Longrightarrow \bar{\Phi}^g_{i,x+}=\frac{D^g_i\bar{\bar{\Phi}}^g_i + D^g_{i+1}\bar{\bar{\Phi}}_{i+1}}{D^g_i+D^g_{i+1}}$$

and used to specify the numerical approximation of neutron current at face $\Gamma_{i,x+}$ in terms of only the primary discrete unknowns, the nodal averages of neutron flux:

$$\bar{J}^g_{i,x+} = -\frac{2D^g_iD^g_{i+1}}{D^g_i+D^g_{i+1}}\,\frac{\bar{\bar{\Phi}}^g_{i+1}-\bar{\bar{\Phi}}^g_i}{h}. \tag{4.26}$$

Proof that $\bar{J}^g_{i,x+}$ is a consistent approximation of the exact integral average $\bar{j}^g_{i,x+}$ may be done using Taylor expansions as in the second step in the proof of Theorem 2.3, [EGH03, Sec. 2.3]. This property is neccessary for proving convergence of the FV scheme.

Remark 4.1 (Approximations)
Note that the various approximations undertaken in the course of the scheme development were not always of the same type. The approximation in (4.17) *is due to the inexact nature of Fick's law (recall its derivation, p. 30). The following approximate equality,* (4.18)*, contains also inaccuracies from the homogenization process. The third type of approximations appears in eqs.* (4.20) *and* (4.23) *and is of numerical kind. In the end, the resulting approximate quantity, i.e. the integral average of neutron current given by* (4.24)*, is burdened by errors from all the mentioned approximations.*

Remark 4.2
Note that the actual choice of discrete variable approximation at an interface is unimportant for the derivation, since it may be eliminated by the condition of conservativity. Any expected value of solution ϕ^g at the interface could have been used.

The result of the just completed derivation is the finite volume expression for neutron leakage through one face of the hexagonal meshbox. Repeating the procedure for the opposite face ($\Gamma_{i,x-}$) and then for the remaining directions (by formally replacing x with u and v, respectively) leads to similar approximations of the remaining current averages in (4.15), symbolically written as

$$\begin{aligned}
\bar{J}^g_{i,\xi+} &= -\frac{2D^g_i D^g_{i+\xi}}{D^g_i + D^g_{i+\xi}} \frac{\bar{\bar{\Phi}}^g_{i+\xi} - \bar{\bar{\Phi}}^g_i}{h} = -D^g_{i,\xi+} \frac{\bar{\bar{\Phi}}^g_{i+\xi} - \bar{\bar{\Phi}}^g_i}{h} \\
\bar{J}^g_{i,\xi-} &= -\frac{2D^g_{i-\xi} D^g_i}{D^g_{i-\xi} + D^g_i} \frac{\bar{\bar{\Phi}}^g_i - \bar{\bar{\Phi}}^g_{i-\xi}}{h} = -D^g_{i,\xi-} \frac{\bar{\bar{\Phi}}^g_i - \bar{\bar{\Phi}}^g_{i-\xi}}{h}, \quad \xi = (x,u,v).
\end{aligned} \tag{4.27}$$

Harmonic mean of diffusion coefficients of the two neighbouring cells, $D^g_{i,\xi\pm}$, is thus considered as an approximation of diffusion at their common interface. These expressions hold for nodes $\mathcal{V}_i$ and their faces $\Gamma_{i,\xi\pm}$ that separate them in the respective direction from some neighbouring node, i.e. there exists node $\mathcal{V}_{i+\xi} \in \mathcal{T}$, respectively $\mathcal{V}_{i-\xi} \in \mathcal{T}$, such that $\overline{\mathcal{V}_i} \cap \overline{\mathcal{V}_{i+\xi}} = \overline{\Gamma_{i,\xi+}}$, respectively $\overline{\mathcal{V}_i} \cap \overline{\mathcal{V}_{i-\xi}} = \overline{\Gamma_{i,\xi-}}$. For nodes that lie on the boundary of the core, boundary conditions must be used to determine neutron currents across faces that do not have any node on their outer side.

4.3.2.2 Boundary edges

Albedo type boundary conditions given by (3.50) are considered in this thesis. Their derivation is based on diffusion theory and is described in section 3.2.4, p. 31 (eq. (3.40)). For node $\mathcal{V}_i$ lying at the outer rim of the core, we can write the conditions for right, respectively left, boundary faces ($\Gamma_{i,\xi+}$, resp. $\Gamma_{i,\xi-}$) in the following symbolic form:

$$0 = \gamma^g \phi^g(\mathbf{r}) + D^g(\mathbf{r}) \nabla \phi^g(\mathbf{r}) \cdot \mathbf{n}_{i,\xi\pm} = \gamma^g \phi^g(\mathbf{r}) - \mathbf{j}^g(\mathbf{r}) \cdot \mathbf{n}_{i,\xi\pm}, \quad \mathbf{r} \in \Gamma_{i,\xi\pm}, \tag{4.28}$$

where $\mathbf{n}_{i,\xi\pm}$ are the outward normal vectors to $\Gamma_{i,\xi\pm}$. Recall from section 3.1.3 that coefficient γ is defined by

$$\gamma^g = \frac{1-\alpha^g}{2(1+\alpha^g)},$$

where α is the albedo, i.e. the ratio between the number of neutrons that enter the node through the face and the number of neutrons that leave it through the same face.

As in the interior case investigated in previous paragraph, discretization of the boundary condition will be carried out in detail only in the $\xi = x$ direction and only for the right boundary. To keep the notation simple, let the rightmost node in the last row, i.e. $\mathcal{V}_i = \mathcal{V}_N$, serve as the reference node for which the derivation will be performed. To use the discrete variables, let us first write (4.28) in terms of neutron current oriented in the positive x direction:

$$\gamma^g \phi^g(\mathbf{r}) - \mathbf{j}^g(\mathbf{r}) \cdot \mathbf{e}_x = 0.$$

Averaging over face $\Gamma_{N,x+}$ and using eq. (4.18) then gives

$$0 = \gamma^g \frac{1}{m_e} \int\limits_{\Gamma_{N,x+}} \phi^g(\mathbf{r})\,\mathrm{d}\sigma \; - \frac{1}{m_e} \int\limits_{\Gamma_{N,x+}} \mathbf{j}^g(\mathbf{r}) \cdot \mathbf{e}_x \,\mathrm{d}\sigma\,, \tag{4.29}$$

which, following steps (4.18) through (4.24), leads to the approximate boundary condition

$$\gamma^g \bar{\Phi}^g_{N,x+} - \bar{J}^g_{N,x+} = 0. \tag{4.30}$$

To determine the value of the approximate neutron current through the boundary with respect to the primary discrete unknown in $\mathcal{V}_N$ (i.e. relation of type $\bar{J}^g_{N,x+} = \bar{J}^g_{N,x+}(\bar{\bar{\Phi}}^g_N)$), second term in the above equation must be replaced with the expression from eq. (4.24) and the equation thus formed:

$$\gamma^g \bar{\Phi}^g_{N,x+} + \frac{2D^g_N}{h}(\bar{\Phi}^g_{N,x+} - \bar{\bar{\Phi}}^g_N) = 0 \tag{4.31}$$

solved for the approximation of neutron flux average at the face:

$$\bar{\Phi}^g_{N,x+} = \frac{2D^g_N}{h\gamma^g + 2D^g_N} \bar{\bar{\Phi}}^g_N. \tag{4.32}$$

The required relationship is then obtained by substituting the solution back into (4.30):

$$\bar{J}^g_{N,x+} = \gamma^g \bar{\Phi}^g_{N,x+} = \frac{2D^g_N \gamma^g}{h\gamma^g + 2D^g_N} \bar{\bar{\Phi}}^g_N. \tag{4.33}$$

For the left boundary, e.g. for node V_1, the procedure is exactly the same, only equation

$$\gamma^g \phi^g(\mathbf{r}) + \mathbf{j}^g(\mathbf{r}) \cdot \mathbf{e}_x = 0$$

is used as a starting point and eq. (4.25) (with $i = 0$ and obviously $\bar{\Phi}^g_{0,x+} \equiv \bar{\Phi}^g_{1,x-}$) must be used instead of eq. (4.24) to obtain the dependence relation $\bar{J}^g_{1,x-} = \bar{J}^g_{1,x-}(\bar{\bar{\Phi}}^g_1)$. The resulting expression is:

$$\bar{J}^g_{1,x-} = -\gamma^g \bar{\Phi}^g_{1,x-} = -\frac{2D^g_1\gamma^g}{h\gamma^g + 2D^g_1}\bar{\bar{\Phi}}^g_1. \tag{4.34}$$

General case of boundary node $\mathcal{V}_i$ such that $\partial\mathcal{V}_i \cap \partial\Omega = \Gamma_{i,\xi+}$ (or $\partial\mathcal{V}_i \cap \partial\Omega = \Gamma_{i,\xi-}$) is handled in the same manner and produces

$$\bar{J}^g_{i,\xi\pm} = \pm\frac{2D^g_i\gamma^g}{h\gamma^g + 2D^g_i}\bar{\bar{\Phi}}^g_i. \tag{4.35}$$

4.3.2.3 A complete numerical scheme

One obtains the final FV discretization of (4.1) by using the approximations of integral averages of neutron currents with respect to the discrete unknowns ((4.27) and (4.35) for nodes at the outer boundary of the core) in the discrete balance system (4.15):

$$\begin{aligned}\frac{2}{3h}(\bar{J}^g_{i,x+} - \bar{J}^g_{i,x-}) + \frac{2}{3h}(\bar{J}^g_{i,u+} - \bar{J}^g_{i,u-}) + \frac{2}{3h}(\bar{J}^g_{i,v+} - \bar{J}^g_{i,v-}) + \Sigma^g_{i,r}\bar{\bar{\Phi}}^g_i = \\ = \sum_{g'=1,\, g'\neq g}^{2} \Sigma^{g'\to g}_{i,s}\bar{\bar{\Phi}}^{g'}_i + \frac{\chi^g}{K_{\text{eff}}}\sum_{g'=1}^{2}\nu\Sigma^{g'}_{i,f}\bar{\bar{\Phi}}^{g'}_i,\end{aligned} \tag{4.36}$$

where $\bar{J}^g_{i,\xi\pm}$ depend only on discrete diffusion coefficients and the primary discrete unknowns and K_{eff} is the approximation of the exact criticality factor k_{eff}.

For further exposition, I will rewrite the scheme in terms of approximations of the face averaged net leakages in the respective directions. According to (4.9), they are given by

$$\bar{L}^g_{i,\xi} := \bar{J}^g_{i,\xi+} - \bar{J}^g_{i,\xi-} \tag{4.37}$$

and transform eq. (4.36) into

$$\frac{2}{3h}\sum_{\xi\in\{x,u,v\}}\bar{L}^g_{i,\xi} + \Sigma^g_{i,r}\bar{\bar{\Phi}}^g_i = \sum_{g'=1,\, g'\neq g}^{2}\Sigma^{g'\to g}_{i,s}\bar{\bar{\Phi}}^{g'}_i + \frac{\chi^g}{K_{\text{eff}}}\sum_{g'=1}^{2}\nu\Sigma^{g'}_{i,f}\bar{\bar{\Phi}}^{g'}_i, \tag{4.38}$$

Using (4.27) and (4.35), the approximations of average ξ-directed leakages for different types of nodes follow:

- *interior nodes*: nodes $\mathcal{V}_i \in \mathcal{T}$, for which there exist $\mathcal{V}_{i-\xi}, \mathcal{V}_{i+\xi} \in \mathcal{T}$ such that $\partial\mathcal{V}_i \cap \partial\mathcal{V}_{i\pm\xi} = \Gamma_{i,\xi\pm}$:

$$\begin{aligned}\bar{L}^g_{i,\xi} &= \frac{1}{h}\left[-D^g_{i,\xi-}\bar{\bar{\Phi}}^g_{i-\xi} + (D^g_{i,\xi-} + D^g_{i,\xi+})\bar{\bar{\Phi}}^g_i - D^g_{i,\xi+}\bar{\bar{\Phi}}^g_{i+\xi}\right], \\ D^g_{i,\xi\pm} &= \frac{2D^g_i D^g_{i\pm\xi}}{D^g_i + D^g_{i\pm\xi}}, \quad \xi = (x,u,v);\end{aligned} \tag{4.39}$$

- *nodes on the "left" boundary (boundary in the negative ξ-direction)*: nodes $\mathcal{V}_i \in \mathcal{T}$, for which there exists $\mathcal{V}_{i+\xi} \in \mathcal{T}$ such that $\partial\mathcal{V}_i \cap \partial\mathcal{V}_{i+\xi} = \Gamma_{i,\xi+}$ and $\partial\mathcal{V}_i \cap \partial\Omega = \Gamma_{i,\xi-}$:

$$\begin{aligned} \bar{L}^g_{i,\xi} &= \frac{1}{h}\left[(D^g_{i,\xi-} + D^g_{i,\xi+})\bar{\bar{\Phi}}^g_i - D^g_{i,\xi+}\bar{\bar{\Phi}}^g_{i+\xi}\right], \\ D^g_{i,\xi+} &= \frac{2D^g_i D^g_{i+\xi}}{D^g_i + D^g_{i+\xi}}, \quad D^g_{i,\xi-} = h\frac{2D^g_i\gamma^g}{h\gamma^g + 2D^g_i}, \quad \xi = (x,u,v); \end{aligned} \tag{4.40}$$

- *nodes on the "right" boundary (boundary in the positive ξ-direction)*: nodes $\mathcal{V}_i \in \mathcal{T}$, for which there exists $\mathcal{V}_{i-\xi} \in \mathcal{T}$ such that $\partial\mathcal{V}_i \cap \partial\mathcal{V}_{i-\xi} = \Gamma_{i,\xi-}$ and $\partial\mathcal{V}_i \cap \partial\Omega = \Gamma_{i,\xi+}$:

$$\begin{aligned} \bar{L}^g_{i,\xi} &= \frac{1}{h}\left[-D^g_{i,\xi-}\bar{\bar{\Phi}}^g_{i-\xi} + (D^g_{i,\xi-} + D^g_{i,\xi+})\bar{\bar{\Phi}}^g_i\right], \\ D^g_{i,\xi+} &= h\frac{2D^g_i\gamma^g}{h\gamma^g + 2D^g_i}, \quad D^g_{i,\xi-} = \frac{2D^g_{i-\xi}D^g_i}{D^g_{i-\xi} + D^g_i}, \quad \xi = (x,u,v). \end{aligned} \tag{4.41}$$

4.3.3 Numerical properties

The scheme given by (4.38–4.41) has the form of that developed in [GHV00, Sec. 5] for general advection-diffusion equations with Robin boundary conditions. A correspondence can be spotted between these problems and the fixed-source version of the neutron diffusion problem with homogenized data, discretized by eq. (4.38) with a given right hand side. As I will proceed to show in the following section, the fixed-source case is truly the problem which the scheme will be applied to. The discontinuous diffusion coefficients inherent to the homogenized problem are addressed in the remarks throughout the paper and also in section 3.3, p. 78 in [EGH03]. Hence the numerical analysis of scheme (4.38–4.41) can be performed in the same spirit as in the referenced publications. It reveals that a unique discrete non-negative solution exists, is stable with respect to an appropriate discrete norm and thanks to the conservativity and consistency of the current approximations also converges to the unique variational solution of the original continuous problem in the limit of infinitely fine mesh spacing.

4.3.4 Solution procedure

Matrix notation. If we express the average total leakage of neutrons out of node $\mathcal{V}_i$ (an approximation of the node-averaged divergence term in (4.1a), according to eq. (4.9)) by

$$\bar{\bar{L}}^g_i = \frac{2}{3h}\sum_{\xi\in\{x,u,v\}} \bar{L}^g_{i,\xi} \tag{4.42}$$

and order the group g flux averages into an $N \times 1$ column vector $\bar{\bar{\mathbf{\Phi}}}^g$ (using the linear indexing from figure 4.2), then according to (4.39), (4.40) and (4.41),

$$\bar{\bar{L}}_i^g = \mathbf{L}^g \bar{\bar{\mathbf{\Phi}}}^g.$$

The $N \times N$ matrix $\mathbf{L}^g$ will have a block heptadiagonal structure with non-adjacent diagonals and consist of the interface diffusion coefficients $D^g_{i,\xi\pm}$. If we also order the macroscopic cross sections into $N \times N$ diagonal matrices $\mathbf{\Sigma}^g_*$, we can rewrite (4.38) for the two energy groups in the following group-block form:

$$\begin{bmatrix} \mathbf{L}^1 + \mathbf{\Sigma}^1_r & \mathbf{0} \\ -\mathbf{\Sigma}^{1\to 2}_s & \mathbf{L}^2 + \mathbf{\Sigma}^2_r \end{bmatrix} \cdot \begin{bmatrix} \bar{\bar{\mathbf{\Phi}}}^1 \\ \bar{\bar{\mathbf{\Phi}}}^2 \end{bmatrix} = \frac{1}{K_{\text{eff}}} \begin{bmatrix} \nu\mathbf{\Sigma}^1_f & \nu\mathbf{\Sigma}^2_f \\ \mathbf{0} & \mathbf{0} \end{bmatrix} \cdot \begin{bmatrix} \bar{\bar{\mathbf{\Phi}}}^1 \\ \bar{\bar{\mathbf{\Phi}}}^2 \end{bmatrix} \tag{4.43}$$

($\mathbf{0}$ is an $N \times N$ zero matrix, or more compactly as

$$\mathbf{M}\bar{\bar{\mathbf{\Phi}}} = \frac{1}{K_{\text{eff}}} \mathbf{S}_{\text{f}} \bar{\bar{\mathbf{\Phi}}} \tag{4.44}$$

with $2N \times 2N$ matrices $\mathbf{M}$ and $\mathbf{S}_{\text{f}}$ and $2N \times 1$ vector $\bar{\bar{\mathbf{\Phi}}}$. Thanks to the physical nature of the problem, the homogenized cross sections as well as diffusion coefficients are positive constants which may be used to show that matrix $\mathbf{M}$ has the following properties ([Pal97, p. 40]):

1. $\mathbf{M}$ is real,
2. $\mathbf{M}$ has positive diagonal elements,
3. off-diagonal elements of $\mathbf{M}$ are non-positive,
4. $\mathbf{M}$ is diagonally dominant,
5. $\mathbf{M}$ is irreducible.

It follows from properties 2, 3 and 4 that the "neutron migration" matrix $\mathbf{M}$ is an M-matrix and as such, its inverse exists and is non-negative ([Axe96, Sec. 6.1]). Since the elements of the fission matrix $\mathbf{S}_{\text{f}}$ are also non-negative the product $\mathbf{M}^{-1}\mathbf{S}_{\text{f}}$ is a non-negative matrix which is also irreducible ([Geh92, p. 65]). It then follows from the Perron-Frobenius theorem ([Axe96, Thm. 4.11]) that $\mathbf{M}^{-1}\mathbf{S}_{\text{f}}$ has a unique eigenvector with all positive entries, corresponding to the approximation of real physical neutron flux. This eigenvector is associated with the spectral radius of the matrix, which is the largest-modulus eigenvalue of the matrix. This result is also acknowledged in [Pal97] or [Sch97].

Rewriting (4.44) as

$$K_{\text{eff}}\bar{\bar{\mathbf{\Phi}}} = \mathbf{M}^{-1}\mathbf{S}_{\text{f}}\bar{\bar{\mathbf{\Phi}}}, \tag{4.45}$$

reveals that actually the approximation of the multiplication factor k_{eff} has the role of the eigenvalue. So in order to obtain a physically realistic eigenvector, we look for such K_{eff} that will have the largest magnitude of all for which (4.45) holds nontrivially. Since

by (3.22) we have $\lambda = \frac{1}{k_{\text{eff}}} \approx \frac{1}{K_{\text{eff}}}$, this corresponds to results acknowledged at the end of section 3.3.1 for the continuous eigenvalue problem (3.51a), where the unique positive eigenvector was associated with the smallest eigenvalue λ and hence the largest value of k_{eff}.

Fission source iteration. Spectral structure of $\mathbf{M}^{-1}\mathbf{S}_{\text{f}}$ admits the use of the *power method* to compute the largest eigenvalue. In reactor calculations, the method is called *fission source iteration* ([Pal97, p. 40], [Sta01, p. 83]) and proceeds as follows:

1. *Initialization*
$$K_{\text{eff}}^{(0)} := {}^0K_{\text{eff}}, \quad \bar{\bar{\mathbf{\Phi}}}^{(0)} := {}^0\bar{\bar{\mathbf{\Phi}}}; \tag{4.46}$$
${}^0K_{\text{eff}}$ and ${}^0\bar{\bar{\mathbf{\Phi}}}$ are arbitrary initial criticality and flux distribution

2. *Outer eigenvalue iteration* – the power method

for $p = 1, 2, \ldots$

(a) *flux update*
$$\bar{\bar{\mathbf{\Phi}}}^{(p)} := \frac{1}{K_{\text{eff}}^{(p-1)}} \mathbf{M}^{-1}\mathbf{S}_{\text{f}}\bar{\bar{\mathbf{\Phi}}}^{(p-1)}, \tag{4.47}$$

- *inner iteration* – solution of the system
$$\mathbf{M}\bar{\bar{\mathbf{\Phi}}}^{(p)} = \frac{1}{K_{\text{eff}}^{(p-1)}} \mathbf{S}_{\text{f}}\bar{\bar{\mathbf{\Phi}}}^{(p-1)}, \tag{4.48}$$

(b) *eigenvalue update*
$$K_{\text{eff}}^{(p)} := K_{\text{eff}}^{(p-1)} \frac{\mathbf{w}^T \mathbf{S}_{\text{f}}\bar{\bar{\mathbf{\Phi}}}^{(p)}}{\mathbf{w}^T \mathbf{S}_{\text{f}}\bar{\bar{\mathbf{\Phi}}}^{(p-1)}}, \tag{4.49}$$

(c) *stopping condition* (ε is an appropriate convergence criterion)
$$\left| \frac{K_{\text{eff}}^{(p)} - K_{\text{eff}}^{(p-1)}}{K_{\text{eff}}^{(p)}} \right| < \varepsilon. \tag{4.50}$$

Remark 4.3
Multiple choices of weighting vector $\mathbf{w}$ *in the power method step 2-(b) are possible, although they have some effects on the speed of convergence. Specifically, it can be shown that by setting* $\mathbf{w} := \mathbf{S}_{\text{f}}\bar{\bar{\mathbf{\Phi}}}^{(p)}$ *in each iteration, the procedure converges twice as fast than with the most simple choice of* $\mathbf{w}$ *being a unity vector.*

As noted in step 2-(a), matrix $\mathbf{M}$ is not directly inverted in practice since it is quite big (of order $2N$ for a two-group problem with N assemblies). Instead, a system given by (4.48) is solved at each outer iteration by a suitable iterative solution method. Right hand side of (4.48) has been computed in the previous outer iteration and remains constant

during the inner solution process. Step 2-(a) thus requires a solution of the *fixed source problem*

$$\mathbf{M}\bar{\bar{\mathbf{\Phi}}}^{(p)} = \mathbf{S}^{(p)}, \quad \mathbf{S}^{(p)} := \frac{1}{K_{\text{eff}}^{(p-1)}}\mathbf{S}_{\text{f}}\bar{\bar{\mathbf{\Phi}}}^{(p-1)}.$$

The two-group structure of the matrices (cf. (4.43)) can be utilized to further split the problem into two $N \times N$ linear systems

$$\left(\mathbf{L}^1 + \mathbf{\Sigma}_r^1\right)\bar{\bar{\mathbf{\Phi}}}^{1,(p)} = \mathbf{S}^{1,(p)}, \tag{4.51a}$$

$$\left(\mathbf{L}^2 + \mathbf{\Sigma}_r^2\right)\bar{\bar{\mathbf{\Phi}}}^{2,(p)} = \mathbf{\Sigma}_s^{1\text{—}2}\bar{\bar{\mathbf{\Phi}}}^{1,(p)}, \tag{4.51b}$$

where for each iteration p, the first-group fission source vector $\mathbf{S}^1$ contains first N elements of the $N \times 1$ vector $\mathbf{S}$ (note that $\mathbf{S}^2 \equiv \mathbf{0}_{N\times 1}$). The fast group system (4.51a) is solved first for fast flux approximations in grid cells (components of $\bar{\bar{\mathbf{\Phi}}}^1$). The solution is then used on the right side of the second system to define the fixed-source problem for the p-th iteration of thermal flux ($\bar{\bar{\mathbf{\Phi}}}^2$). Note that these decompositions into fixed-source problems allow us to apply the numerical properties of the scheme represented by matrices $\mathbf{L}^g + \mathbf{\Sigma}_r^g$ (discussed on p. 56) to once again confirm the existence of $\mathbf{M}^{-1}\mathbf{S}_{\text{f}}$ in (4.45) and physical reality of the solution.

4.4 Nodal methods

The fundamental problem of the FV scheme is that its pleasing numerical properties are derived for inifinitely small mesh-boxes (as $h \to 0$). With increasing coarsity of the mesh, the errors introduced by neutron face current approximations via eq. (4.27) grow severely. Since in practical calculations the mesh-boxes are identified with relatively large assemblies with fixed geometry, the fine mesh granularity required for sufficient accuracy is hard to achieve and would be computationally too costly ([Mou96, chap. 3]).

4.4.1 Modification of the FV scheme

Instead of many mesh subdivisions, nodal methods propose a different solution to the problem. They utilize a "corrected" approximation of average face currents:

$$\begin{aligned} {}^{\text{C}}\bar{J}^g_{i,\xi+} &= -D^g_{i,\xi+}\frac{\bar{\bar{\Phi}}^g_{i+\xi} - \bar{\bar{\Phi}}^g_i}{h} + {}^{\text{C}}D^g_{i,\xi+}(\bar{\bar{\Phi}}^g_i + \bar{\bar{\Phi}}^g_{i+\xi}) \\ {}^{\text{C}}\bar{J}^g_{i,\xi-} &= -D^g_{i,\xi-}\frac{\bar{\bar{\Phi}}^g_i - \bar{\bar{\Phi}}^g_{i-\xi}}{h} + {}^{\text{C}}D^g_{i,\xi-}(\bar{\bar{\Phi}}^g_{i-\xi} + \bar{\bar{\Phi}}^g_i), \quad \xi = (x,u,v). \end{aligned} \tag{4.52}$$

where ${}^{\text{C}}D^g_{i,\xi\pm}$ are the so-called *coupling correction factors* supposed to remedy the errors from coarse discretization. This form of their appearance is standard (e.g. [BK06], [FC02], [T$^+$94], a similar expression can be also found in [SA96]) with the plus sign between the

fluxes in the correction part supposed to have positive influence on the convergence behaviour ([T+94, p. 15]). Also note the manifestation of the standard FVM approximations of current (4.27) in the definition:

$$^{\mathrm{C}}\bar{J}^g_{i,\xi\pm} = \bar{J}^g_{i,\xi\pm} + {}^{\mathrm{C}}D^g_{i,\xi\pm}(\bar{\bar{\Phi}}^g_i + \bar{\bar{\Phi}}^g_{i+\xi}). \tag{4.53}$$

In analogy to eq. (4.53), boundary currents are corrected using the following expression:

$$^{\mathrm{C}}\bar{J}^g_{i,\xi\pm} = \bar{J}^g_{i,\xi\pm} + {}^{\mathrm{C}}D^g_{i,\xi\pm}\bar{\bar{\Phi}}^g_i = \pm\frac{2D^g_i\gamma^g}{h\gamma^g + 2D^g_i}\bar{\bar{\Phi}}^g_i + {}^{\mathrm{C}}D^g_{i,\xi\pm}\bar{\bar{\Phi}}^g_i, \quad \partial\mathcal{V}_i \cap \partial\Omega \neq \emptyset. \tag{4.54}$$

A modified FV scheme can now be obtained by using eq. (4.37) with the corrected approximations of average face currents in eq. (4.36):

$$\frac{2}{3h}\sum_{\xi\in\{x,u,v\}} {}^{\mathrm{C}}\bar{L}^g_{i,\xi} + \Sigma^g_{i,r}\bar{\bar{\Phi}}^g_i = \sum_{g'=1,\, g'\neq g}^{2} \Sigma^{g'\to g}_{i,s}\bar{\bar{\Phi}}^{g'}_i + \frac{\chi^g}{K_{\mathrm{eff}}}\sum_{g'=1}^{2}\nu\Sigma^{g'}_{i,f}\bar{\bar{\Phi}}^{g'}_i, \tag{4.55}$$

- *inside*: $\forall\mathcal{V}_i \in \mathcal{T}$ such that $\exists\mathcal{V}_{i-\xi}, \mathcal{V}_{i+\xi} \in \mathcal{T} : \partial\mathcal{V}_i \cap \partial\mathcal{V}_{i\pm\xi} = \Gamma_{i,\xi\pm}$:

$$\begin{aligned} {}^{\mathrm{C}}\bar{L}^g_{i,\xi} = \frac{1}{h}\Big[&-(D^g_{i,\xi-} + {}^{\mathrm{C}}D^g_{i,\xi-})\bar{\bar{\Phi}}^g_{i-\xi} \\ &+ (D^g_{i,\xi-} + D^g_{i,\xi+} - {}^{\mathrm{C}}D^g_{i,\xi-} + {}^{\mathrm{C}}D^g_{i,\xi+})\bar{\bar{\Phi}}^g_i \\ &- (D^g_{i,\xi+} - {}^{\mathrm{C}}D^g_{i,\xi+})\bar{\bar{\Phi}}^g_{i+\xi}\Big], \\ D^g_{i,\xi\pm} = \frac{2D^g_i D^g_{i\pm\xi}}{D^g_i + D^g_{i\pm\xi}}, &\quad \xi = (x,u,v); \end{aligned} \tag{4.56}$$

- *negative boundary*: $\forall\mathcal{V}_i \in \mathcal{T}$, such that $\exists\mathcal{V}_{i+\xi} \in \mathcal{T} : \partial\mathcal{V}_i \cap \partial\mathcal{V}_{i+\xi} = \Gamma_{i,\xi+}$ and $\partial\mathcal{V}_i \cap \partial\Omega = \Gamma_{i,\xi-}$:

$$\begin{aligned} {}^{\mathrm{C}}\bar{L}^g_{i,\xi} &= \frac{1}{h}\left[(D^g_{i,\xi-} + D^g_{i,\xi+} - {}^{\mathrm{C}}D^g_{i,\xi-} + {}^{\mathrm{C}}D^g_{i,\xi+})\bar{\bar{\Phi}}^g_i - (D^g_{i,\xi+} - {}^{\mathrm{C}}D^g_{i,\xi+})\bar{\bar{\Phi}}^g_{i+\xi}\right], \\ D^g_{i,\xi+} &= \frac{2D^g_i D^g_{i+\xi}}{D^g_i + D^g_{i+\xi}}, \quad D^g_{i,\xi-} = h\frac{2D^g_i\gamma^g}{h\gamma^g + 2D^g_i}, \quad \xi = (x,u,v); \end{aligned} \tag{4.57}$$

- *positive boundary*: $\forall\mathcal{V}_i \in \mathcal{T}$, such that $\exists\mathcal{V}_{i-\xi} \in \mathcal{T} : \partial\mathcal{V}_i \cap \partial\mathcal{V}_{i-\xi} = \Gamma_{i,\xi-}$ and $\partial\mathcal{V}_i \cap \partial\Omega = \Gamma_{i,\xi+}$:

$$\begin{aligned} {}^{\mathrm{C}}\bar{L}^g_{i,\xi} &= \frac{1}{h}\left[-(D^g_{i,\xi-} + {}^{\mathrm{C}}D^g_{i,\xi-})\bar{\bar{\Phi}}^g_{i-\xi} + (D^g_{i,\xi-} + D^g_{i,\xi+} - {}^{\mathrm{C}}D^g_{i,\xi-} + {}^{\mathrm{C}}D^g_{i,\xi+})\bar{\bar{\Phi}}^g_i\right], \\ D^g_{i,\xi+} &= h\frac{2D^g_i\gamma^g}{h\gamma^g + 2D^g_i}, \quad D^g_{i,\xi-} = \frac{2D^g_{i-\xi}D^g_i}{D^g_{i-\xi} + D^g_i}, \quad \xi = (x,u,v). \end{aligned} \tag{4.58}$$

The scheme may be written in group-block matrix form:

$$\begin{bmatrix} {}^{\mathrm{C}}\mathbf{L}^1 + \boldsymbol{\Sigma}_r^1 & \mathbf{0} \\ -\boldsymbol{\Sigma}_s^{1\to 2} & {}^{\mathrm{C}}\mathbf{L}^2 + \boldsymbol{\Sigma}_r^2 \end{bmatrix} \cdot \begin{bmatrix} \bar{\bar{\boldsymbol{\Phi}}}^1 \\ \bar{\bar{\boldsymbol{\Phi}}}^2 \end{bmatrix} = \frac{1}{K_{\mathrm{eff}}} \begin{bmatrix} \nu\boldsymbol{\Sigma}_f^1 & \nu\boldsymbol{\Sigma}_f^2 \\ \mathbf{0} & \mathbf{0} \end{bmatrix} \cdot \begin{bmatrix} \bar{\bar{\boldsymbol{\Phi}}}^1 \\ \bar{\bar{\boldsymbol{\Phi}}}^2 \end{bmatrix} \tag{4.59}$$

or shortly

$${}^{\mathrm{C}}\mathbf{M}\bar{\bar{\boldsymbol{\Phi}}} = \frac{1}{K_{\mathrm{eff}}}\mathbf{S}_{\mathrm{f}}\bar{\bar{\boldsymbol{\Phi}}}. \tag{4.60}$$

Comparing eqs. (4.56–4.58) and (4.39–4.41), the corrected system (4.60) may be split into:

$$(\mathbf{M} + {}^{\mathrm{C}}\mathbf{D})\bar{\bar{\boldsymbol{\Phi}}} = \frac{1}{K_{\mathrm{eff}}}\mathbf{S}_{\mathrm{f}}\bar{\bar{\boldsymbol{\Phi}}}, \tag{4.61}$$

where $\mathbf{M}$ is the standard FV matrix with known coefficients (given by the diffusion coefficients and removal and scattering cross sections), while the block-heptadiagonal $2N \times 2N$ matrix ${}^{\mathrm{C}}\mathbf{D}$ contains the nodal coupling correction factors. The same decomposition of the matrix $\mathbf{M}$ into two single-group fixed source problems as shown in eqs. (4.51) may be used to yield the two decoupled systems with block-heptadiagonal matrices (see figure 5.3 in chap. 5):

$$\begin{aligned} \left(\mathbf{L}^1 + \boldsymbol{\Sigma}_r^1 + {}^{\mathrm{C}}\mathbf{D}^1\right)\bar{\bar{\boldsymbol{\Phi}}}^1 &= \mathbf{S}^1, \\ \left(\mathbf{L}^2 + \boldsymbol{\Sigma}_r^2 + {}^{\mathrm{C}}\mathbf{D}^2\right)\bar{\bar{\boldsymbol{\Phi}}}^2 &= \boldsymbol{\Sigma}_s^{1\to 2}\bar{\bar{\boldsymbol{\Phi}}}^1, \end{aligned} \tag{4.62}$$

When used in the global fission source iteration described by eqs. (4.46–4.50), the correction factors need to be iteratively determined to progressively refine the matrix ${}^{\mathrm{C}}\mathbf{M}$, so that the average fluxes determined by power-method iterations with this matrix converge to those predicted by the highly-accurate solution of local problems. Since the whole-core matrix ${}^{\mathrm{C}}\mathbf{M}$ updated with the correction matrix ${}^{\mathrm{C}}\mathbf{D}$ formally resembles the standard FV matrix derived using finite-difference techniques (see section 4.3.2), the core-wise iteration on fission source and global average flux is commonly referred to as *CMFD (Coarse Mesh Finite Difference)* iteration.

4.4.2 Two-node subdomain problems

After the initial CMFD iteration in which ${}^{\mathrm{C}}\mathbf{D} = \mathbf{0}$ and which hence uses the standard FV matrix $\mathbf{M}$, the correction factors need to be determined so that the errors due to large node sizes do not propagate to further stages. They are obtained by solving auxiliary nodal balance problems with a higher-order scheme on local overlapping subdomains, each consisting of two consecutive nodes. This task consists of two main parts – formulation of the auxiliary problems by transverse integration and their suitably accurate solution by some higher order nodal method.

These two building blocks will be described in this section, drawing upon two fundamental references. Wagner's approach to transverse integration in hexagonal geometry is described first according to paper [Wag89]. The second reference is the article by Fu and Cho, [FC02], which presents the advanced semi-analytic method for solving the transverse

integrated equations. Since the authors assumed Cartesian geometry, derivation found in their paper must be modified. One possible generalization to hexagonal mesh is outlined in [BK06, Chap. 4] and requires only slight changes to the original Fu and Cho's approach. Nevertheless, I will repeat and modify it here to put the method into the context of this thesis.

4.4.2.1 Transverse integration

Balance equations for each node in the considered subdomain are formed by integrating the general two-dimensional neutron balance (4.1) over full hexagonal extent in directions transverse to x, u and v, respectively. The result are three one-dimensional diffusion equations which are easier to solve, but can not naturally provide detailed information on spatial flux distribution within the node any more. However, it suffices that nodal averages can be preserved by the method as it is employed to correct the FV solution already approximated by integrally averaged quantities.

Exact equation. The procedure will be outlined here for reference node $\mathcal{V}_i$ placed at the origin (assumed to be inside the core), which is hence described by

$$\xi \in \left[-\frac{h}{2}, \frac{h}{2}\right],$$
$$y \in [-y_{t,i}(\xi), y_{t,i}(\xi)], \quad y_{t,i}(\xi) = \frac{1}{\sqrt{3}}(h - |\xi|), \quad \xi = (x, y, z).$$

Only direction $\xi = x$ will be considered in following derivation. I shall also refer to this direction as to *principal direction*.

Transverse integration that yields the x-direction ODE consists of operating with $\int_{-y_{t,i}(x)}^{y_{t,i}(x)} (\bullet)\,\mathrm{d}y$ on the two-dimensional balance equations (4.1a) and (4.1b). Following Wagner, the combined flux formulation of the diffusion equation in node $\mathcal{V}_i$ will be used as a starting point:

$$-D_i^g \frac{\partial^2}{\partial x^2}\phi^g(x,y) - D_i^g \frac{\partial^2}{\partial y^2}\phi^g(x,y) + \Sigma_{i,r}^g \phi^g(x,y) = s_i^g(x,y), \quad [x,y] \in \mathcal{V}_i, \tag{4.63}$$

where the group source terms have been collected under s_i^g:

$$s_i^g(x,y) := \sum_{g'=1,\, g' \neq g}^{2} \Sigma_{i,s}^{g' \to g} \phi^{g'}(x,y) + \frac{\chi^g}{k_{\mathrm{eff}}} \sum_{g'=1}^{2} \nu \Sigma_{i,f}^{g'} \phi^{g'}(x,y), \tag{4.64}$$

and homogenized parameters have been used. Transverse integrating eq. (4.63) along the y-axis yields the following one-dimensional equation:

$$-D_i^g \frac{\mathrm{d}^2 \phi_{t,i}^g(x)}{\mathrm{d}x^2} + \Sigma_{i,r}^g \phi_{t,i}^g(x) = s_{t,i}^g(x) - l_{t,i}^g(x), \tag{4.65}$$

for the unknown *transverse integrated flux*

$$\phi^g_{t,i}(x) := \int\limits_{-y_{t,i}(x)}^{y_{t,i}(x)} \phi^g(x,y)\,\mathrm{d}y\,, \tag{4.66}$$

which is also used to define the transverse integrated group source term $s^g_{t,i}(x)$ according to (4.64). The new term that emerged on the right side, $l^g_{t,i}(x)$, comprises two parts. The first contains surface normal components of net neutron currents at transverse boundaries $\pm y_{t,i}(x)$ and is the result of transverse integration of the $-D^g_i \frac{\partial^2}{\partial y^2}\phi^g(x,y)$ term in eq. (4.63). It is formally the same as in Cartesian geometry and gives the term its common name *transverse leakage*. Since information on transverse currents can not be rigorously extracted from the one-dimensional equation, its suitable approximation will be needed. In order to find its proper form, however, the other part of the term specific to the hexagonal geometry should be taken into account.

That part involves derivatives of flux with respect to x at transverse boundaries and first and second order derivatives of the transverse profile function $y_{t,i}(x)$ ([Wag89]). It originates from transverse integration of the $-D^g_i \frac{\partial^2}{\partial x^2}\phi^g(x,y)$ term of the 2D diffusion equation (4.63) in the hexagonal domain. Since $y_{t,i}(x)$ has a cusp at the origin, these terms introduce non-physical singularities to the balance relation in 1D. Although they may be rigorously approximated (as remarked both in [CS95] and [Wag89] where references are given for further details), Wagner chose to neglect the singularities and rather developed a novel approach to enforcing the nodal balance relation even with such an inaccurate approximation of transverse integrated flux.

The transverse integrated equation in its exact form truly agrees with the original full-hexagonal balance on a node-average basis as mentioned at the beginning of this section. That is, if eq. (4.65) is integrated over nodal extent in x-direction and divided by its area it matches eq. (4.63) averaged over both dimensions (eq. (4.5)). This follows from the average flux preservation property:

$$\frac{1}{m_N}\int\limits_{-h/2}^{h/2} \phi^g_{t,i}(x)\,\mathrm{d}x \;=\; \frac{1}{m_N}\int\limits_{-h/2}^{h/2}\int\limits_{-y_{t,i}(x)}^{y_{t,i}(x)} \phi^g(x,y)\,\mathrm{d}y\;\mathrm{d}x \;=\; \frac{1}{m_N}\int\limits_{\mathcal{V}_i} \phi^g(\mathbf{r})\,\mathrm{d}\mathbf{r} \;=\; \bar{\bar{\phi}}^g_i \tag{4.67}$$

and the average total leakage preservation property

$$\begin{aligned}
&\frac{1}{m_N}\int\limits_{-h/2}^{h/2} -D^g_i \frac{\mathrm{d}^2\phi^g_{t,i}(x)}{\mathrm{d}x^2}\,\mathrm{d}x \;+\; \frac{1}{m_N}\int\limits_{-h/2}^{h/2} l^g_{t,i}(x)\,\mathrm{d}x \;= \\
&= \frac{1}{m_N}\int\limits_{-h/2}^{h/2}\int\limits_{-y_{t,i}(x)}^{y_{t,i}(x)} -D^g_i \frac{\partial^2}{\partial x^2}\phi^g(x,y) - D^g_i \frac{\partial^2}{\partial y^2}\phi^g(x,y)\,\mathrm{d}y\;\mathrm{d}x \;=\; \frac{1}{m_N}\int\limits_{\mathcal{V}_i} -\nabla\cdot D^g_i \nabla\phi^g(\mathbf{r})\,\mathrm{d}\mathbf{r}
\end{aligned} \tag{4.68}$$

(which is exactly the node-averaged neutron leakage $\bar{\bar{l}}_i^g$ due to diffusion as defined in eq. (4.9)), since equivalence of group sources is implied by the former. The second identity represents the obvious fact that average leakage in the principal direction (the one-dimensional diffusion term, first term in eq. (4.68)) must add with the average leakage in transverse direction to make the total average leakage of neutrons out of the node.

Approximation of the exact equation. Since the one-dimensional equations obtained by transverse integration will be solved in conjunction with the two-dimensional FV-based method, approximations of both methods must be consistent. Wagner showed how this consistency implied the form of transverse leakage term corresponding to the approximation of the rest of the one-dimensional equation.

First he noted that for the purposes of approximation, the one-dimensional diffusion equation should be formulated in terms of flux *averaged* (in integral sense) over the transverse cross section of the node at given point x. This is reasonable since the original 2D balance relation we wish to adequately represent in 1D has been approximated using averaged quantities. The transverse averaged flux is defined by

$$\tilde{\phi}_i^g(x) := \frac{1}{2y_{t,i}(x)} \int_{-y_{t,i}(x)}^{y_{t,i}(x)} \phi^g(x,y)\,\mathrm{d}y = \frac{1}{2y_{t,i}(x)} \phi_{t,i}^g(x) \tag{4.69}$$

and thus we have $\phi_{t,i}^g(x) = 2y_{t,i}(x)\tilde{\phi}_i^g(x)$. Inserting this into eq. (4.65) and dividing by $2y_{t,i}(x)$ yields the one-dimensional diffusion equation for the transverse averaged flux:

$$-D_i^g \frac{\mathrm{d}^2\tilde{\phi}_i^g(x)}{\mathrm{d}x^2} + \Sigma_{i,r}^g \tilde{\phi}_i^g(x) = \tilde{s}_i^g(x) - \tilde{l}_i^g(x), \tag{4.70}$$

where the group source term $\tilde{s}_i^g(x)$ is defined in an obvious way by $\tilde{\phi}_i^g(x)$. The transverse leakage term $\tilde{l}_i^g(x)$ in this equation may be symbolically written as

$$\tilde{l}_i^g(x) = \frac{1}{2y_{t,i}(x)} (l_{t,i}^g(x) + \rho(x)), \tag{4.71}$$

where $\rho(x)$ emerges from double differentiation of the product $2y_{t,i}(x)\tilde{\phi}_i^g(x)$ and represents singularities of $\tilde{\phi}_i^g(x)$ and its first derivative. Realizing that this term can't be exact for the one-dimensional equation, we can satisfy the equality only approximately:

$$-D_i^g \frac{\mathrm{d}^2\tilde{\Phi}_i^g(x)}{\mathrm{d}x^2} + \Sigma_{i,r}^g \tilde{\Phi}_i^g(x) = \tilde{S}_i^g(x) - \tilde{L}_i^g(x). \tag{4.72}$$

As a first approximation, Wagner neglected the additional $\rho(x)$ term in (4.71), so that

$$2y_{t,i}(x)\tilde{L}_i^g(x) \approx l_{t,i}^g(x).$$

The final approximation $\tilde{L}_i^g(x)$ must be sought so that at least the approximate nodal averages of the FV-based 2D model (eq. (4.36), p. 55 [4]) are preserved by the one-dimensional equation (4.72). This means that its solution must satisfy the nodal average preservation property (4.67) for the FV approximation of average flux (def. (4.23), p. 52):

$$\frac{1}{m_N} \int_{-h/2}^{h/2} 2y_{t,i}(x)\tilde{\Phi}_i^g(x)\,\mathrm{d}x = \bar{\bar{\Phi}}_i^g \tag{4.73}$$

and that the 1D average transverse leakage represented by $\tilde{L}_i^g(x)$ must reproduce, after appropriate normalization by nodal area, the transverse part of the 2D whole-node average leakage ${}^{\mathrm{C}}\bar{\bar{L}}_i^g$ (def. (4.42), p. 56 [5]). If I denote this transverse component by ${}^{\mathrm{C}}\bar{\bar{L}}_{i,y_t}^g$ then the condition can be stated as

$$\frac{1}{m_N} \int_{-h/2}^{h/2} 2y_{t,i}(x)\tilde{L}_i^g(x)\,\mathrm{d}x = {}^{\mathrm{C}}\bar{\bar{L}}_{i,y_t}^g. \tag{4.74}$$

The non-transverse (i.e. x-directed) contribution to 2D average leakage ${}^{\mathrm{C}}\bar{\bar{L}}_i^g$ is left to the diffusion term, so that adding the diffusion and the transverse leakage terms together as in eq. (4.68) again leads to perservation of whole-node average total leakage.

Note that unlike the Cartesian case, the transverse part of total average leakage will not contain just the average leakages through transverse boundaries $\pm y_{t,i}(x)$, that is

$${}^{\mathrm{C}}\bar{\bar{L}}_{i,y_t}^g \neq \frac{2}{3h}{}^{\mathrm{C}}\bar{L}_{i,u}^g + \frac{2}{3h}{}^{\mathrm{C}}\bar{L}_{i,v}^g.$$

This can be intuitively explained that since these boundaries are not in hexagonal geometry perpendicular to the transverse integration axis y, the transverse boundaries $\pm y_{t,i}(x)$ will contain also leakages in the non-transverse x-direction (repr. by net currents with nonzero dot product with face normal but zero dot product with the y-axis unit vector). These components are already contained in the x-direction diffusion term, so the transverse-direction-only part of the transverse leakage must subtract them in a way that preserves the 2D nodal balance, so that a correct form of transverse leakage results, that is formally identical to that from Cartesian geometry.

Determination of the form of transverse leakage term. In order to find the expression for the correct form of the y-directed part of the total average leakage, Wagner noted that the one-dimensional nodal balance constructed with transverse averaged flux, eq. (4.72), must give the original two-dimensional balance (4.55) after being averaged in

[4] or, more precisely, eq. (4.55) since we work with corrected currents approximations

[5] using corrected approximations for currents

the remaining dimension, that is after being integrated from $-h/2$ to $h/2$ and divided by h. Using the one-dimensional analogy of Fick's law with the transverse averaged flux:

$$\tilde{J}^g_{i,x\pm} = -D^g \frac{\mathrm{d}\tilde{\Phi}^g_i(x)}{\mathrm{d}x}\bigg|_{x=\pm\frac{h}{2}}, \tag{4.75}$$

we obtain the approximate transverse averaged currents at nodal faces in x-direction. The resulting one dimensional average balance then writes

$$\frac{1}{h}\left(\tilde{J}^g_{i,x+} - \tilde{J}^g_{i,x-}\right) + \Sigma^g_{i,r}\tilde{\bar{\Phi}}^g_i = \tilde{\bar{S}}^g_i - \tilde{\bar{L}}^g_i, \tag{4.76}$$

where the group source term is again formally defined by eq. (4.64), using the appropriate flux variables. The doubly tilded symbols in the equation represent quantities that are integrally averaged over all transverse cross sections of the node along the x-axis. The last one, $\tilde{\bar{L}}^g_i$, is then the one-dimensional representation of the whole-node average of neutron leakage in the transverse direction, ${}^{\mathrm{C}}\bar{\bar{L}}^g_{i,y_t}$, that we are looking for.

The full-hexagonal balance relation may be rewritten from eq. (4.36) as

$$\begin{aligned}\frac{1}{h}\left({}^{\mathrm{C}}\bar{J}^g_{i,x+} - {}^{\mathrm{C}}\bar{J}^g_{i,x-}\right) + \Sigma^g_{i,r}\bar{\bar{\Phi}}^g_i = \\ = \bar{\bar{S}}^g_i - \left[-\frac{1}{3h}\left({}^{\mathrm{C}}\bar{J}^g_{i,x+} - {}^{\mathrm{C}}\bar{J}^g_{i,x-}\right) + \frac{2}{3h}\left({}^{\mathrm{C}}\bar{J}^g_{i,u+} - {}^{\mathrm{C}}\bar{J}^g_{i,u-}\right) + \frac{2}{3h}\left({}^{\mathrm{C}}\bar{J}^g_{i,v+} - {}^{\mathrm{C}}\bar{J}^g_{i,v-}\right)\right],\end{aligned} \tag{4.77}$$

or, in terms of face averaged leakages in given directions first mentioned in eq. (4.37), from eq. (4.55) as

$$\frac{1}{h}{}^{\mathrm{C}}\bar{L}^g_{i,x} + \Sigma^g_{i,r}\bar{\bar{\Phi}}^g_i = \bar{\bar{S}}^g_i - \left[\frac{2}{3h}({}^{\mathrm{C}}\bar{L}^g_{i,u} + {}^{\mathrm{C}}\bar{L}^g_{i,v}) - \frac{1}{3h}{}^{\mathrm{C}}\bar{L}^g_{i,x}.\right]. \tag{4.78}$$

Comparing it to the 1D balance relation (4.76) reveals the following agreement conditions that the approximation must ensure:

$$\tilde{J}^g_{i,x+} \equiv {}^{\mathrm{C}}\bar{J}^g_{i,x+}, \tag{4.80}$$

$$\tilde{\bar{\Phi}}^g_i \equiv \bar{\bar{\Phi}}^g_i, \tag{4.81}$$

$$\tilde{\bar{S}}^g_i \equiv \bar{\bar{S}}^g_i, \tag{4.82}$$

$${}^{\mathrm{C}}\bar{\bar{L}}^g_{i,y_t} = \tilde{\bar{L}}^g_i \equiv \frac{2}{3h}({}^{\mathrm{C}}\bar{L}^g_{i,u} + {}^{\mathrm{C}}\bar{L}^g_{i,v}) - \frac{1}{3h}{}^{\mathrm{C}}\bar{L}^g_{i,x}. \tag{4.83}$$

The first condition on currents consistency is satisfied since at $x = \pm h/2$, the transverse cross section of the node is actually the side $\Gamma_{i,x\pm}$ itself and hence both variables approximate the same integral average of neutron current. Consistency of average fluxes expressed by (4.81) is the actual approximating assumption whose consequence is then the sources consistency, (4.82), and hence also the expression for the approximate average transverse leakage, (4.83). By using this particular expression to estimate spatial variation of transverse leakage, $\tilde{L}^g_i(x)$, according to eq. (4.74), we assume that (4.81) truly holds. So when $\tilde{L}^g_i(x)$ is used in equation (4.72), any inconsistencies between $\tilde{\bar{\Phi}}^g_i$ and $\bar{\bar{\Phi}}^g_i$ will show up in the overall approximation error of its solution $\tilde{\Phi}^g_i(x)$.

Remark 4.4
Note that identity (4.80) *is essential for the presented nodal method as it allows to remove any discrepancy between transverse averaged current* $\tilde{J}^g_{i,x+}$*, obtained by applying* (4.75) *on the high-accurate solution of eq.* (4.76) *(see eq.* (4.98)*), and the coarse CMFD approximation* ${}^{\mathrm{C}}\bar{J}^g_{i,x+}$ *by setting them equal and appropriately adjusting the correction factor.*

Approximation of transverse leakage profile. Spatial variation of transverse leakage across the node along principal direction must be estimated in order to complete the approximation of the term and make numerical solution of eq. (4.72) possible. We stand at the problem of constructing a function $\tilde{L}^g_i = \tilde{L}^g_i(x)$ that resembles the true shape of average neutron leakage out of node $\mathcal{V}_i$ through $\pm y_{t,i}(x)$ as closely as possible. According to previous paragraph, we are furthermore constrained by eq. (4.74) in searching for such function in order not to break the consistency. Two choices have been compared in this thesis and will now be described.

Flat approximation. In this simple case, average transverse leakage is assumed to be a constant function over the node. The nodal average consistency constraint implies its form to be actually given by eq. (4.83):

$$\tilde{L}^g_i(x) = \frac{2}{3h}({}^{\mathrm{C}}\bar{L}^g_{i,u} + {}^{\mathrm{C}}\bar{L}^g_{i,v}) - \frac{1}{3h}{}^{\mathrm{C}}\bar{L}^g_{i,x}. \tag{4.84}$$

Although it is clearly a poor assumption, transverse leakage profile is still expected to be constant in some operating codes, though mainly for cores with rectangular nodes ([Mao00]).

Quadratic approximation. Most modern transverse-integrated nodal methods approximate the transverse leakage shape for node $\mathcal{V}_i$ by a second-order polynomial (besides Wagner, e.g. Turinsky et al. [T$^+$94] apply it in the hexagonal geometry case, and Fu and Cho, [FC02], in Cartesian geometry). I used the same form for the approximating function as Wagner,

$$\tilde{L}^g_i(x) = \frac{2}{3h}f(x)({}^{\mathrm{C}}\bar{L}^g_{i,u} + {}^{\mathrm{C}}\bar{L}^g_{i,v}) - \frac{1}{3h}{}^{\mathrm{C}}\bar{L}^g_{i,x}, \tag{4.85}$$

where

$$f(x) = s_0 + s_1 x + s_2 x^2. \tag{4.86}$$

In order to account for possibly different material composition of nodes $\mathcal{V}_{i\pm u}$ and $\mathcal{V}_{i\pm v}$ that would influence the transverse currents for the actual node, the polynomial is constructed so as to span three consecutive nodes $\mathcal{V}_{i-1}$, $\mathcal{V}_i$, $\mathcal{V}_{i+1}$ and preserve average transverse leakage

in each of them. According to consistency condition (4.74), this means that:

$$\begin{aligned}
\frac{1}{m_N}\int_{-3h/2}^{-h/2} 2y_{t,i-1}(x)\tilde{L}_i^g(x)\,\mathrm{d}x &= {}^{\mathrm{C}}\bar{\bar{L}}^g_{i-1,y_t},\\
\frac{1}{m_N}\int_{-h/2}^{h/2} 2y_{t,i}(x)\tilde{L}_i^g(x)\,\mathrm{d}x &= {}^{\mathrm{C}}\bar{\bar{L}}^g_{i,y_t},\\
\frac{1}{m_N}\int_{h/2}^{3h/2} 2y_{t,i+1}(x)\tilde{L}_i^g(x)\,\mathrm{d}x &= {}^{\mathrm{C}}\bar{\bar{L}}^g_{i+1,y_t},
\end{aligned} \tag{4.87}$$

where $y_{t,i\mp1}(x) = y_{t,i}(x \pm h)$. Inserting the chosen approximation expression of average transverse leakage (eq. (4.85)) into the left sides and the node averaged transverse leakage as defined by eq. (4.83) into the right sides of equations (4.87), we obtain after some obvious algebraic manipulations

$$\begin{aligned}
\int_{-3h/2}^{-h/2} 2y_{t,i-1}(x)f(x)\,\mathrm{d}x &= m_N\frac{{}^{\mathrm{C}}\bar{L}^g_{i-1,u}+{}^{\mathrm{C}}\bar{L}^g_{i-1,v}}{{}^{\mathrm{C}}\bar{L}^g_{i,u}+{}^{\mathrm{C}}\bar{L}^g_{i,v}},\\
\int_{-h/2}^{h/2} 2y_{t,i}(x)f(x)\,\mathrm{d}x &= m_N,\\
\int_{h/2}^{3h/2} 2y_{t,i+1}(x)f(x)\,\mathrm{d}x &= m_N\frac{{}^{\mathrm{C}}\bar{L}^g_{i+1,u}+{}^{\mathrm{C}}\bar{L}^g_{i+1,v}}{{}^{\mathrm{C}}\bar{L}^g_{i,u}+{}^{\mathrm{C}}\bar{L}^g_{i,v}}.
\end{aligned} \tag{4.88}$$

After expanding $f(x)$ and evaluating the integrals on left sides, one arrives at a set of algebraic equations for the unknown coefficients s_0, s_1, s_2 of polynomial $f(x)$. Since average transverse leakages on the right sides are in actual computation known from latest iteration of the global two-dimensional CMFD problem, this set may be readily solved to reconstruct the polynomial which is consequently used to obtain the transverse leakage term for the center node $\mathcal{V}_i$ via eq. (4.85).

4.4.2.2 Semi-analytic solution method

Semi-analytic method described in [FC02] has been used for solving the ODE arising from the transverse integration procedure. Unlike the full-analytic method (ANM) which truly approximates only the transverse leakage term in (4.72) and solves the equation analytically, the semi-analytic method introduces also an additional approximation of the group sources term. While this approximation is principially not necessary from the transverse

integration point of view, it helps the method avoid the algebraic complexity coming from exact treatment of this term.

Nodal balance equation (4.72) can be solved for both groups simultaneously by writing it in the following two-group matrix form:

$$-\frac{\mathrm{d}^2}{\mathrm{d}x^2}\tilde{\mathbf{\Phi}}(x) + \mathbf{R}\tilde{\mathbf{\Phi}}(x) = \mathbf{P}\tilde{\mathbf{\Phi}}(x) - \tilde{\mathbf{L}}(x), \tag{4.89}$$

where

$$\mathbf{R} = \mathbf{D}^{-1}\begin{bmatrix} \Sigma_{i,r}^1 & 0 \\ 0 & \Sigma_{i,r}^2 \end{bmatrix} \qquad (\textit{"group removal matrix"}),$$

$$\mathbf{P} = \mathbf{D}^{-1}\left(\begin{bmatrix} 0 & 0 \\ \Sigma_{i,s}^{1\to 2} & 0 \end{bmatrix} + \frac{1}{K_{\text{eff}}}\begin{bmatrix} \nu\Sigma_{i,f}^1 & \nu\Sigma_{i,f}^2 \\ 0 & 0 \end{bmatrix}\right) \qquad (\textit{"group production matrix"}),$$

$$\mathbf{D} = \begin{bmatrix} D_i^1 & 0 \\ 0 & D_i^2 \end{bmatrix}$$

are the matrices of group constants and

$$\tilde{\mathbf{\Phi}}(x) = \begin{bmatrix} \tilde{\Phi}_i^1(x) \\ \tilde{\Phi}_i^2(x) \end{bmatrix}, \quad \tilde{\mathbf{L}}(x) = \mathbf{D}^{-1}\begin{bmatrix} \tilde{L}_i^1(x) \\ \tilde{L}_i^2(x) \end{bmatrix}$$

are the vectors of group variables. To simplify the notation, node index i has been omitted from letters denoting the matrices.

The approximation undertaken by the semi-analytic method lies in the assumption that the group source term $\mathbf{P}\tilde{\mathbf{\Phi}}(x)$ and the transverse leakage term $\tilde{\mathbf{L}}(x)$ on the right-hand side of eq. (4.89) can be expanded into quadratic orthogonal polynomials (their exact form will be specified later in this section). The transverse averaged flux is then the analytic solution of the second-order ODE with such a polynomial right side. The solution can be written as a superposition of the particular solution, which will naturally also lie in the same space of second-order orthogonal polynomials:

$$\tilde{\mathbf{\Phi}}_p(x) = p_0(x)\mathbf{a}_0 + p_1(x)\mathbf{a}_1 + p_2(x)\mathbf{a}_2$$

and the homogeneous solution:

$$\tilde{\mathbf{\Phi}}_h(x) = \left(\sinh\sqrt{\mathbf{R}}x\right)\mathbf{a}_3 + \left(\cosh\sqrt{\mathbf{R}}x\right)\mathbf{a}_4.$$

Matrix functions are used in the homogeneous part and the transcendental nature of hyperbolic functions is supposed to ensure higher accuracy of the resulting solution than would be obtainable by purely polynomial methods like NEM ([FC02, p. 1019]).

Solving the auxiliary one-dimensional problem amounts to determination of the unknown constant vectors $\mathbf{a}_0, \ldots, \mathbf{a}_4$. For this to be possible, an appropriate polynomial set must be chosen to concretize the form of the particular solution. Fu and Cho developed the semi-analytic method for Cartesian geometry with the standard set of Legendre polynomials

on the interval $[-h/2, h/2]$. In order to fulfil the afforementioned consistency constraints, however, the hexagonal method must use a polynomial set which is orthogonal with respect to the following weighted inner product:

$$\big\langle g_0(x), g_1(x) \big\rangle = \int_{-h/2}^{h/2} y_{t,i}(x) g_0(x) g_1(x) \,\mathrm{d}x \,, \tag{4.90}$$

that is

$$\big\langle p_k(x), p_l(x) \big\rangle \begin{cases} = 0 & \text{if } k \neq l, \\ \neq 0 & \text{if } k = l. \end{cases}$$

Polynomials chosen by Wagner in [Wag89] may be used if suitably extended to interval $[-h/2, h/2]$:

$$p_0(x) = 1, \quad p_1(x) = x, \quad p_2(x) = x^2 - \frac{5}{72} h^2.$$

So we look for the solution of the transverse ODE (4.89) in the following form:

$$\tilde{\boldsymbol{\Phi}}(x) = \tilde{\boldsymbol{\Phi}}_p(x) + \tilde{\boldsymbol{\Phi}}_h(x) = \mathbf{a}_0 + x\mathbf{a}_1 + \left(x^2 - \frac{5}{72} h^2\right) \mathbf{a}_2 + \left(\sinh \sqrt{\mathbf{R}} x\right) \mathbf{a}_3 + \left(\cosh \sqrt{\mathbf{R}} x\right) \mathbf{a}_4. \tag{4.91}$$

The solution is required to fulfil the nodal average flux constraint (4.73):

$$\begin{aligned} \bar{\tilde{\boldsymbol{\Phi}}}_i &= \frac{1}{m_N} \int_{-h/2}^{h/2} 2 y_t(x) \tilde{\boldsymbol{\Phi}}(x) \,\mathrm{d}x \;= \\ &= \frac{2}{m_N} \left[\int_{-h/2}^{h/2} y_t(x) \mathbf{a}_0 \,\mathrm{d}x \;+ \int_{-h/2}^{h/2} y_t(x) x \mathbf{a}_1 \,\mathrm{d}x \;+ \int_{-h/2}^{h/2} y_t(x) \left(x^2 - \frac{5}{72} h^2\right) \mathbf{a}_2 \,\mathrm{d}x + \right. \\ &\qquad \left. + \int_{-h/2}^{h/2} y_t(x) \left(\sinh \sqrt{\mathbf{R}} x\right) \mathbf{a}_3 \,\mathrm{d}x \;+ \int_{-h/2}^{h/2} y_t(x) \left(\cosh \sqrt{\mathbf{R}} x\right) \mathbf{a}_4 \,\mathrm{d}x \right] = \\ &= \mathbf{a}_0 + \frac{2}{m_N} \int_{-h/2}^{h/2} y_t(x) \left(\cosh \sqrt{\mathbf{R}} x\right) \mathbf{a}_4 \,\mathrm{d}x \,, \end{aligned} \tag{4.92}$$

where the second and the third integral in square brackets vanishes by the orthogonality property of chosen polynomial basis and the fourth integral is a zero matrix[6] due to oddity of its integrand[7]. I retained the node index for $\bar{\tilde{\boldsymbol{\Phi}}}_i$ to distinguish this 2×1 column vector

[6] the integrals of matrices resulting from the matrix functions are taken entry-wise as usual

[7] product of an even and an odd function

consisting of average fluxes for the *local* node and the two groups from $\bar{\bar{\mathbf{\Phi}}}$ (eq. (4.44), sec. 4.3.4), which represented a $2N \times 1$ vector of average fluxes for *all* nodes and groups. It becomes apparent from this equation why orthogonality of the expansion polynomials with respect to weight function $y_t(x)$ must be required.

Additional relations necessary for obtaining the constant vectors are provided by applying the weighted residuals method with polynomials $p_k(x)$ as weight functions to eq. (4.89). Specifically, we require the solution given by eq. (4.91) to satisfy eq. (4.89) weakly in the sense of satisfying the zeroth, first and second order moment equations:

$$\mathbf{R}\mathbf{a}_0 - 2\mathbf{a}_2 = \mathbf{P}\bar{\bar{\mathbf{\Phi}}} - \mathbf{l}_0, \tag{4.93-0}$$

$$\mathbf{A}\mathbf{a}_1 = \mathbf{P}\mathbf{B}_1\mathbf{a}_3 - \mathbf{l}_1, \tag{4.93-1}$$

$$\mathbf{A}\mathbf{a}_2 = \mathbf{P}\mathbf{B}_2\mathbf{a}_4 - \mathbf{l}_2, \tag{4.93-2}$$

in which $\mathbf{A} = \mathbf{R} - \mathbf{P}$ and

$$\mathbf{B}_0 = \frac{1}{\langle 1, 1\rangle}\langle 1, \cosh\sqrt{\mathbf{R}}x\rangle, \tag{4.94-0}$$

$$\mathbf{B}_1 = \frac{1}{\langle x, x\rangle}\langle x, \sinh\sqrt{\mathbf{R}}x\rangle, \tag{4.94-1}$$

$$\mathbf{B}_2 = \frac{1}{\langle x^2 - \frac{5}{72}h^2, x^2 - \frac{5}{72}h^2\rangle}\langle x^2 - \tfrac{5}{72}h^2, \cosh\sqrt{\mathbf{R}}x\rangle. \tag{4.94-2}$$

(inner product $\langle \bullet, \bullet \rangle$ is defined by (4.90)). The g-th component of the k-th order expansion coefficient $\mathbf{l}_k$ of $\tilde{\mathbf{L}}(x)$ is given by

$$\frac{\langle \tilde{L}_i^g(x), p_k(x)\rangle}{\langle p_k(x), p_k(x)\rangle} \tag{4.95}$$

where the expression for $\tilde{L}_i^g(x)$ has been elaborated in previous section using eqs. (4.85–4.88)).

The nodal average constraint (4.92) can be rewritten using eq. (4.94-0) as:

$$\bar{\bar{\mathbf{\Phi}}}_i = \mathbf{a}_0 + \mathbf{B}_0\mathbf{a}_4. \tag{4.96}$$

Together with moment equations (4.93-0) and (4.93-2), it gives the following equation system which may be readily solved for the even constant vectors:

$$\begin{aligned} \mathbf{a}_0 &= \bar{\bar{\mathbf{\Phi}}}_i - \mathbf{B}_0\mathbf{a}_4, \\ \mathbf{a}_2 &= \frac{1}{2}(\mathbf{A}\bar{\bar{\mathbf{\Phi}}}_i + \mathbf{l}_0 - \mathbf{R}\mathbf{B}_0\mathbf{a}_4), \\ (\mathbf{A}\mathbf{R}\mathbf{B}_0 + 2\mathbf{P}\mathbf{B}_2)\mathbf{a}_4 &= \mathbf{A}(\mathbf{A}\bar{\bar{\mathbf{\Phi}}}_i + \mathbf{l}_0) + 2\mathbf{l}_2. \end{aligned}$$

The transverse average of flux at sides $\Gamma_{i,x\pm}$ is obtained by evaluating eq. (4.91) at $x = \pm h/2$:

$$\tilde{\mathbf{\Phi}}_{x\pm} = \pm\frac{h}{2}\mathbf{a}_1 \pm \left(\sinh\sqrt{\mathbf{R}}\frac{h}{2}\right)\mathbf{a}_3 + \mathbf{e}_\phi, \tag{4.97}$$

where $\mathbf{e}_\phi$ contains the resolved even[8] constant vectors:

$$\mathbf{e}_\phi = \mathbf{a}_0 + \frac{1}{6}h^2\mathbf{a}_2\left(\cosh\sqrt{\mathbf{R}}\frac{h}{2}\right)\mathbf{a}_4$$

Using the appropriate form of Fick's law (eq. (4.75)), approximation of the average net current at the interfaces may be obtained from (4.97):

$$\tilde{\mathbf{J}}_{x\pm} = -\mathbf{D}\left[\mathbf{a}_1 + \left(\sqrt{\mathbf{R}}\cosh\sqrt{\mathbf{R}}\frac{h}{2}\right)\mathbf{a}_3\right] \pm \mathbf{e}_J, \tag{4.98}$$

where

$$\mathbf{e}_J = -\mathbf{D}\left[h\mathbf{a}_2 + \left(\sqrt{\mathbf{R}}\sinh\sqrt{\mathbf{R}}\frac{h}{2}\right)\mathbf{a}_4\right].$$

Either $\mathbf{a}_1$ or $\mathbf{a}_3$ can be eliminated from eqs. (4.97) and (4.98) by reducing eq. (4.93-1) equivalently to

$$\mathbf{a}_1 = \mathbf{A}^{-1}(\mathbf{P}\mathbf{B}_1\mathbf{a}_3 - \mathbf{l}_1), \tag{4.99a}$$

or

$$\mathbf{a}_3 = (\mathbf{P}\mathbf{B}_1)^{-1}(\mathbf{A}\mathbf{a}_1 + \mathbf{l}_1). \tag{4.99b}$$

The criterion for selecting either of the two possible expressions is based on invertibility of the respective matrices and is described on p. 1019 of [FC02]: if matrix $\mathbf{A}$ is near singular, we use eq. (4.99b) to express $\mathbf{a}_3$ in terms of $\mathbf{a}_1$; on the contrary, if $\mathbf{P}\mathbf{B}_1$ can not be inverted, we express $\mathbf{a}_1$ in terms of $\mathbf{a}_3$ by using eq. (4.99a). If both matrices are well-conditioned, then eqs. (4.99a) and (4.99b) are equivalent.

At this moment, one of the constant vectors remains unknown in eqs. (4.97) and (4.98). Instead of trying to find a direct expression for it, Fu and Cho rather derived a relationship between the transverse flux and the net current on the same nodal face. By using coupling of the node with its neighbour through the continuity conditions for flux and net current on that face, this remaining degree of freedom can be removed. This approach is made possible by the iterative way of subdomains calculation since for a given node, the interface flux and current from its left neighbour will be known. On the outer boundaries of the reactor, the global boundary conditions may be used.

Relationship between flux and net current on the left and right face of the node may be written collectively as:

$$\tilde{\mathbf{\Phi}}_{x\pm} = \mp\mathbf{C}(\tilde{\mathbf{J}}_{x\pm} - \hat{\mathbf{J}}_{x\pm}) + \hat{\mathbf{\Phi}}_{x\pm}, \tag{4.100}$$

[8] hence the symbol, which has been however chosen primarily to agree with references [FC02] and [BK06] and must not be mistaken for a coordinate vector as defined in section 4.2.1

where

$$\begin{aligned}
\mathbf{C} &= \left(\frac{h}{2}\mathbf{A}^* + \sinh\sqrt{\mathbf{R}}\frac{h}{2}\right)\cdot\left(\mathbf{A}^* + \sqrt{\mathbf{R}}\cosh\sqrt{\mathbf{R}}\frac{h}{2}\right)^{-1}\cdot\mathbf{D}^{-1},\\
\hat{\mathbf{\Phi}}_{x\pm} &= \mp\frac{h}{2}\mathbf{l}_1^* + \mathbf{e}_\phi,\\
\hat{\mathbf{J}}_{x\pm} &= \mathbf{D}\mathbf{l}_1^* \pm \mathbf{e}_J;\\
\mathbf{A}^* &= \mathbf{A}^{-1}\mathbf{P}\mathbf{B}_1, \quad \mathbf{l}_1^* = \mathbf{A}^{-1}\mathbf{l}_1
\end{aligned} \tag{4.101a}$$

if eq. (4.99a) is used, or where

$$\begin{aligned}
\mathbf{C} &= \left[\frac{h}{2}\mathbf{I} + \left(\sinh\sqrt{\mathbf{R}}\frac{h}{2}\right)\mathbf{A}^{**}\right]\cdot\left[\mathbf{I} + \left(\sqrt{\mathbf{R}}\cosh\sqrt{\mathbf{R}}\frac{h}{2}\right)\mathbf{A}^{**}\right]^{-1}\cdot\mathbf{D}^{-1},\\
\hat{\mathbf{\Phi}}_{x\pm} &= \pm\left(\sinh\sqrt{\mathbf{R}}\frac{h}{2}\right)\mathbf{l}_1^{**} + \mathbf{e}_\phi,\\
\hat{\mathbf{J}}_{x\pm} &= -\mathbf{D}\left(\sqrt{\mathbf{R}}\cosh\sqrt{\mathbf{R}}\frac{h}{2}\right)\mathbf{l}_1^{**} \pm \mathbf{e}_J;\\
\mathbf{A}^{**} &= (\mathbf{P}\mathbf{B}_1)^{-1}\mathbf{A}, \quad \mathbf{l}_1^{**} = (\mathbf{P}\mathbf{B}_1)^{-1}\mathbf{l}_1
\end{aligned} \tag{4.101b}$$

when eq. (4.99b) is used. In the second set of equations, $\mathbf{I}$ denotes the 2×2 identity matrix.

Two-node interface current. In the actual iteration of the two-node solution process, denoted by index i (such that $\mathcal{V}_i$ is not a boundary node), the considered subdomain will comprise the left node $\mathcal{V}_{i-1}$ and its right neighbour $\mathcal{V}_i$. The two-node coupling is given by the following continuity conditions on the right face of the left node and the left face of the right node:

$$\mathbf{F}_{i-1,x+}\tilde{\mathbf{\Phi}}_{i-1,x+} = \mathbf{F}_{i,x-}\tilde{\mathbf{\Phi}}_{i,x-}, \tag{4.102a}$$

$$\tilde{\mathbf{J}}_{i-1,x+} = \tilde{\mathbf{J}}_{i,x-}, \tag{4.102b}$$

where flux is actually assumed to be discontinuous (compare with (3.36), p. 31) by factors given on the diagonal of the 2×2 matrices $\mathbf{F}$. This condition is neccessary to account for material differences between the two neighbouring nodes and the discontinuity factors in matrix $\mathbf{F}$ can be precisely determined from the homogenization procedure ([SA96, p. 149]). As this thesis already assumes homogenized nodes, the discontinuity factors are not computed and for simplicity are completely neglected. Hence $\mathbf{F}_{x+} = \mathbf{F}_{x-} = \mathbf{I}$ is set for each node.

Using eq. (4.100), the interface fluxes may be eliminated from the coupling relations to yield the 2×2 system for the transverse averaged current at the interface between the left and the right node:

$$(\mathbf{F}_{i,x-}\mathbf{C}_i + \mathbf{F}_{i-1,x+}\mathbf{C}_{i-1})\tilde{\mathbf{J}}_{i-1,x+} = \mathbf{F}_{i,x-}(\mathbf{C}_i\hat{\mathbf{J}}_{i,x-} - \hat{\mathbf{\Phi}}_{i,x-}) + \mathbf{F}_{i-1,x+}(\mathbf{C}_{i-1}\hat{\mathbf{J}}_{i-1,x+} + \hat{\mathbf{\Phi}}_{i-1,x+}). \tag{4.103}$$

System (4.103) is constructed by computing $\mathbf{C}_i$, $\hat{\mathbf{J}}_{i,x-}$ and $\hat{\mathbf{\Phi}}_{i,x-}$ from either (4.101a) or (4.101b) and using $\mathbf{C}_{i-1}$, $\hat{\mathbf{J}}_{i-1,x+}$ and $\hat{\mathbf{\Phi}}_{i-1,x+}$ from previous iteration. Its solution is the high order representation of the average current of neutrons migrating from the left node into the actual computational node through their common interface. Hence we also set $\tilde{\mathbf{J}}_{i,x-} := \tilde{\mathbf{J}}_{i-1,x+}$ after the system is solved (cond. (4.102b)).

Current across the left core boundary. At the left boundary of the reactor, the two node problem reduces to a "left-boundary right-node" problem, so the required boundary condition for the actual node will be given by the global albedo condition on the negative x-side of the reactor. The condition may be stated for the current node (the right one in the current subdomain) as:

$$\tilde{\mathbf{J}}_{i,x-} = -\mathbf{G}\tilde{\mathbf{\Phi}}_{i,x-},$$

where $\mathbf{G} = \mathrm{diag}\,(\gamma^1, \gamma^2)$. By using eq. (4.100), we eventually obtain the two-group system for the unknown left-face current:

$$\begin{aligned} \tilde{\mathbf{J}}_{i,x-} &= -\mathbf{G}(\mathbf{C}_i\tilde{\mathbf{J}}_{i,x-} + \mathbf{C}_i\hat{\mathbf{J}}_{i,x-} - \hat{\mathbf{\Phi}}_{i,x-}), \\ \left(\mathbf{G}^{-1} + \mathbf{C}_i\right)\tilde{\mathbf{J}}_{i,x-} &= \mathbf{C}_i\hat{\mathbf{J}}_{i,x-} - \hat{\mathbf{\Phi}}_{i,x-}. \end{aligned} \tag{4.104}$$

Current across the right core boundary. The last subdomain in each row of nodes will present a "left-node right-boundary" problem and the following system can be obtained from the right boundary condition $\tilde{\mathbf{J}}_{i,x+} = \mathbf{G}\tilde{\mathbf{\Phi}}_{i,x+}$ and eq. (4.100) for the right face of current node:

$$\left(\mathbf{G}^{-1} + \mathbf{C}_i\right)\tilde{\mathbf{J}}_{i,x+} = \mathbf{C}_i\hat{\mathbf{J}}_{i,x+} + \hat{\mathbf{\Phi}}_{i,x+}. \tag{4.105}$$

Determination of the correction factors. The solution vector of systems (4.103), resp. (4.104) or (4.105), contains the transverse averaged neutron currents at given face for the two groups: $\tilde{\mathbf{J}}_{i,x\pm} = \left[\tilde{J}^1_{i,x\pm}, \tilde{J}^2_{i,x\pm}\right]^T$. By identity (4.80), these are the high order representations of the corrected approximations of face averaged currents. When they are used in eqs. (4.52), resp. (4.54), in place of the CMFD approximations ${}^{\mathrm{C}}\bar{J}^g_{i,x\pm}$ with the latest values of average fluxes (those that have also been used in the nodal-average flux constraint for the actual problem), the correction factors may be calculated from the equations so as to force the original CMFD currents match the more accurate ones:

- correction of currents across the interface between two interior nodes

$${}^{\mathrm{C}}D^g_{i-1,x+} = \frac{1}{\bar{\tilde{\Phi}}^g_{i-1} + \bar{\tilde{\Phi}}^g_i}\left[\tilde{J}^g_{i-1,x+} + D^g_{i-1,\xi+}\left(\frac{\bar{\tilde{\Phi}}^g_i - \bar{\tilde{\Phi}}^g_{i-1}}{h}\right)\right], \tag{4.106a}$$

- correction of current across the left core boundary

$${}^{\mathrm{C}}D^g_{i,x-} = \frac{\tilde{J}^g_{i,x-}}{\bar{\tilde{\Phi}}^g_i} + \frac{2D^g_i\gamma^g}{h\gamma^g + 2D^g_i}, \tag{4.106b}$$

- correction of current across the right core boundary

$$ {}^{\mathrm{C}}D^g_{i,x+} = \frac{\tilde{J}^g_{i,x+}}{\bar{\bar{\Phi}}^g_i} - \frac{2D^g_i\gamma^g}{h\gamma^g + 2D^g_i}. \tag{4.106c} $$

Note that the form of eqs. (4.103) and current continuity condition (4.102b) imply ${}^{\mathrm{C}}D^g_{i,x-} \equiv {}^{\mathrm{C}}D^g_{i-1,x+}$.

4.4.3 Numerical properties

By adding correction factors to the FV matrix $\mathbf{M}$, the resulting matrix ${}^{\mathrm{C}}\mathbf{M}$ may generally not possess the properties listed in section 4.3.4 and convergence may not be rigorously guaranteed. However, if the balance relations used in local problems adequately represent the original continuous nodal balance (modelled by the FV matrix in the infinitely-fine mesh limit) and if an adequate method is used for solving these nodal subproblems in the context of the whole reactor, then the corrections obtained by such solution bring the CMFD solution closer to the exact continuous one. The continuous problem is guaranteed to converge (see section 3.3.1.1, eventually section 4.3.3) and so the same is expected for the corrected approximated problem.

Also if the word "adequate" above is replaced by "exact", the correction factors will vanish upon convergence. However, the nodal method employed for their determination is only approximate, although with higher order of approximation than the original CMFD method. It can thus correct the errors of the CMFD discretization only to some extent, which manifests in stabilization of the correction factors at some non-zero value. This means that the correction method can no longer provide better results than the CMFD method used with the latest version of matrix ${}^{\mathrm{C}}\mathbf{M}$. This allows for an alternative stopping condition for the corrected scheme, given at the end of the following algorithm.

4.4.4 Solution procedure

1. *Initialization*

$$K_{\text{eff}}^{(0)} := {}^{0}K_{\text{eff}}, \quad \bar{\bar{\mathbf{\Phi}}}^{(0)} := {}^{0}\bar{\bar{\mathbf{\Phi}}}, \quad {}^{\text{C}}\mathbf{D}^{(0)} := \mathbf{0}, \quad {}^{\text{C}}\mathbf{M}^{(0)} := \mathbf{M};$$

${}^{0}K_{\text{eff}}$ and ${}^{0}\bar{\bar{\mathbf{\Phi}}}$ are guesses of initial criticality and flux distribution

2. *CMFD iterations*

for $s = 1, 2, \ldots, m$

(a) *Eigenvalue iterations (power method)*

- *Initialization*

$$\lambda^{(0)} := K_{\text{eff}}^{(s-1)}, \quad \mathbf{\Psi}^{(0)} := \bar{\bar{\mathbf{\Phi}}}^{(s-1)}$$

- **for** $p = 1, 2, \ldots, l$

i. *flux update* (by a suitable iterative method as in (4.48))

$$\mathbf{\Psi}^{(p)} := \frac{1}{\lambda^{(p-1)}} \left({}^{\text{C}}\mathbf{M}^{(s-1)}\right)^{-1} \mathbf{S}_{\text{f}} \mathbf{\Psi}^{(p-1)},$$

ii. *eigenvalue update*
(choice of the weighting factor $\mathbf{w}$ has been discussed in remark 4.3)

$$\lambda^{(p)} := \lambda^{(p-1)} \frac{\mathbf{w}^T \mathbf{S}_{\text{f}} \mathbf{\Psi}^{(p)}}{\mathbf{w}^T \mathbf{S}_{\text{f}} \mathbf{\Psi}^{(p-1)}},$$

iii. *power method stopping condition*
terminate if for an appropriately small convergence criterion ε

$$\left| \frac{\lambda^{(p)} - \lambda^{(p-1)}}{\lambda^{(p)}} \right| < \varepsilon,$$

- *CMFD solution variables update*

$$K_{\text{eff}}^{(s)} := \lambda^{(p)}, \quad \bar{\bar{\mathbf{\Phi}}}^{(s)} := \mathbf{\Psi}^{(p)}$$

(b) *CMFD stopping condition (eigenvalue difference variant)*

terminate if for an appropriately small convergence criterion ε'

$$\left| \frac{K_{\text{eff}}^{(s)} - K_{\text{eff}}^{(s-1)}}{K_{\text{eff}}^{(s)}} \right| < \varepsilon',$$

(c) *Internode leakage update*

use the latest flux solution vector to obtain the vector of average leakages in all three principal directions for all nodes:

$$ {}^{\mathrm{C}}\mathbf{l}^g := {}^{\mathrm{C}}\mathbf{L}^g \bar{\bar{\mathbf{\Phi}}}^{(s)} $$

(d) *Two-node subdomains sweep*

for each principal hex-direction $\xi = x, u, v$
for each row $j = 1, \ldots, M_\xi$ in given direction,
for each node $\mathcal{V}_i$ $(i = 1, \ldots, N_j)$ in row j

- *Problem construction*
  i. use $K_{\mathrm{eff}}^{(s)}$ and given physical constants to define the local 1D balance eq. (4.89) for the transverse averaged flux in ξ-direction
  ii. use elements ${}^{\mathrm{C}}\bar{L}^g_{i-1,u}$, ${}^{\mathrm{C}}\bar{L}^g_{i-1,v}$, ${}^{\mathrm{C}}\bar{L}^g_{i,x}$, ${}^{\mathrm{C}}\bar{L}^g_{i,u}$, ${}^{\mathrm{C}}\bar{L}^g_{i,v}$, ${}^{\mathrm{C}}\bar{L}^g_{i+1,u}$, ${}^{\mathrm{C}}\bar{L}^g_{i+1,v}$ from vector ${}^{\mathrm{C}}\mathbf{l}^g$ to compute the expansion coefficients $\mathbf{l}_0$, $\mathbf{l}_1$, $\mathbf{l}_3$ for the transverse leakage term according to eq. (4.95) (let ${}^{\mathrm{C}}\bar{L}^g_{i-1,\xi} = {}^{\mathrm{C}}\bar{L}^g_{N_j+1,\xi} = 0$)
  iii. use elements $\bar{\bar{\Phi}}^{1,(s)}_i$ and $\bar{\bar{\Phi}}^{2,(s)}_i$ from vector $\bar{\bar{\mathbf{\Phi}}}^{(s)}$ to construct the 2×1 vector $\bar{\bar{\mathbf{\Phi}}}_i$ for local computation and use it to obtain the nodal average flux constraint (4.96)
  iv. use the expansion coefficients of transverse leakage to obtain the moment conditions (4.93)
- *Solution*
  i. resolve the even constant vectors
  ii. check for singularity of matrix $\mathbf{A}$ and select an appropriate set of equations from (4.101) for calculating the nodal variables
  iii. compute $\mathbf{C}_i$, $\hat{\mathbf{J}}_{i,\xi-}$, $\hat{\mathbf{\Phi}}_{i,\xi-}$ for actual node $\mathcal{V}_i$ and $\hat{\mathbf{J}}_{i,\xi+}$, $\hat{\mathbf{\Phi}}_{i,\xi+}$ to be used in next iteration step
  iv. **if** $i = 1$,
    – compute the left-boundary current $\tilde{\mathbf{J}}_{1,\xi-}$ according to eq. (4.104), using $\mathbf{C}_i$, $\hat{\mathbf{J}}_{i,\xi-}$ and $\hat{\mathbf{\Phi}}_{i,\xi-}$,
    – use its components in (4.106b) with most recent flux averages $\bar{\bar{\Phi}}^{g,(s)}_i$ $(g = 1, 2)$ to obtain left-boundary corrections ${}^{\mathrm{C}}D^g_{i,\xi-}$ for both groups;
  else if $i = 2, \ldots, N_j$,
    – compute current $\tilde{\mathbf{J}}_{i-1,\xi+}$ according to (4.103), using $\mathbf{C}_i$, $\hat{\mathbf{J}}_{i,\xi-}$, $\hat{\mathbf{\Phi}}_{i,\xi-}$ and $\mathbf{C}_{i-1}$, $\hat{\mathbf{J}}_{i-1,\xi+}$, $\hat{\mathbf{\Phi}}_{i-1,\xi+}$,
    – use its components in (4.106a) with most recent flux averages $\bar{\bar{\Phi}}^{g,(s)}_{i-1}$ and $\bar{\bar{\Phi}}^{g,(s)}_i$ $(g = 1, 2)$ to obtain corrections ${}^{\mathrm{C}}D^g_{i-1,\xi+} \equiv {}^{\mathrm{C}}D^g_{i,\xi-}$ for both groups;

else if $i = N_j$,

– compute the right-boundary current $\tilde{\mathbf{J}}_{i,\xi+}$, according to (4.105), using $\mathbf{C}_i$, $\hat{\mathbf{J}}_{i,\xi+}$, $\hat{\mathbf{\Phi}}_{i,\xi+}$

– use its components in (4.106c) with most recent flux averages $\bar{\bar{\Phi}}^{g,(s)}_{N_j}$ ($g = 1, 2$) to obtain right-boundary corrections ${}^{\mathrm{C}}D^{g}_{N_j,\xi+}$ for both groups;

(e) *CMFD matrix update*

i. populate matrix ${}^{\mathrm{C}}\mathbf{D}^{(s)}$ with correction factors ${}^{\mathrm{C}}D^{g}_{i,\xi\pm}$

ii. build new global iteration matrix: ${}^{\mathrm{C}}\mathbf{M}^{(s)} := \mathbf{M} + {}^{\mathrm{C}}\mathbf{D}^{(s)}$

(f) *CMFD stopping condition (correction factors difference variant)*

for suitably small ε'', terminate if

$$\left\| {}^{\mathrm{C}}\mathbf{D}^{(s)} - {}^{\mathrm{C}}\mathbf{D}^{(s-1)} \right\|_{\infty} < \varepsilon''$$

Remark 4.5

The sequence described above is only illustrative and can be enhanced in several ways for practical computation. For instance, since real cores are often loaded in symmetrical fashion, the number of iterations required for the subdomains sweep can be greatly reduced.

Chapter 5

Numerical results

5.1 Model problem

Nodal method suggested in previous chapter has been used to calculate criticality and power production capability of an example loading configuration of a VVER-1000 type reactor, described in the article by Chao and Shatilla [CS95]. The particular configuration defines material composition of the core as shown in figure 5.1. Values of physical constants corresponding to each material type are given in table 5.2. The model planar core consists of $N = 163$ assemblies, distributed in a hexagonal lattice with $M_\xi = 15$ rows in each principal direction. Number of nodes in each row is the same for each direction and is shown together with their linear indexing in the x-direction in fig. 4.2. Width (also called *pitch*) of each assembly is $h = 23.6\,\mathrm{cm}$. Surroundings of the core have been modelled by a single albedo value for both energy groups. Two cases have been considered, the vacuum-surrounded core with $\alpha^g = 0$ ($\gamma^g = 0.5$) and that with a reflector region around, $\alpha^g = 0.6$ ($\gamma^g = 0.125$).

5.2 Solution procedure

One sixth core cyclic symmetry of the problem can be spotted from the loading map figure 5.1. It allows an optimization of the iterative solution procedure outlined in section 4.4.4. Specifically, the subdomains sweep (step 2-(d)) could be performed only in the $\xi = x$ direction, to one half of the core (i.e. in rows $j = 1, \ldots, 8$, terminating in the last row after resolving node $\mathcal{V}_{83}$). In this way, surface currents and correction factors will be obtained for nodes in three sixths of the core and two sixths of each node (at both faces $\Gamma_{i,x+}$ and $\Gamma_{i,x-}$ by continuity conditions). Totally, one sixth of the unknowns will be calculated, utilizing the core symmetry to obtain the rest[1].

In the experiments performed, stopping condition on eigenvalue difference (step 2-(b)) (or correction factors norm difference, step 2-(f)) has been replaced with a fixed maximum

[1] Alternatively, this one sixth of unknowns could have been obtained by performing complete three sweeps in all principal directions in one sixth of the core.

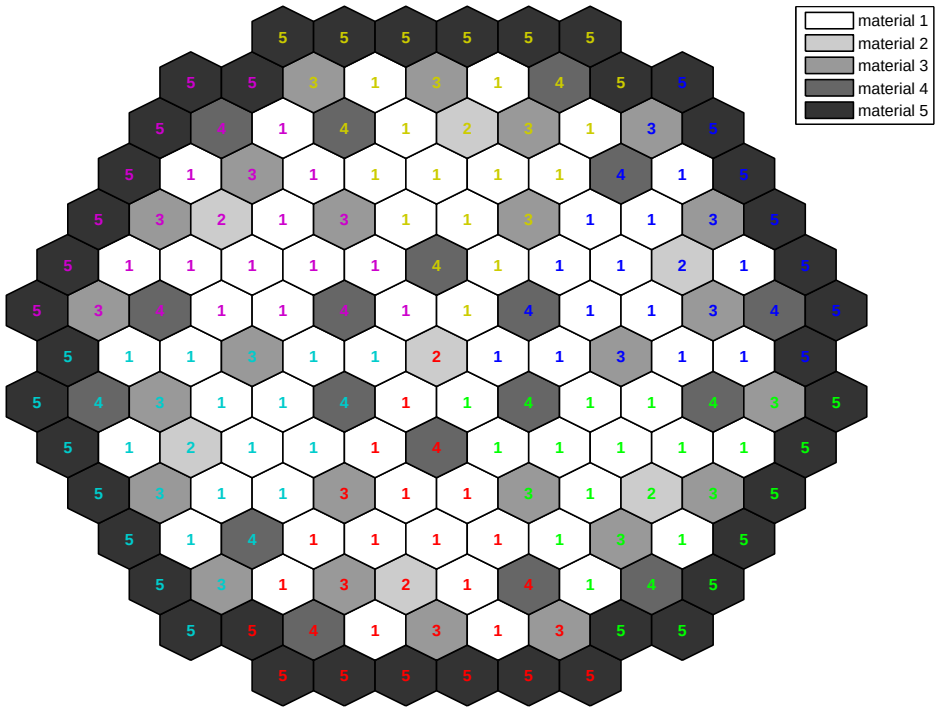

Figure 5.1: Reactor loading map

Group Constants for the VVER-1000 Problem

Material	1	2	3	4	5
D_1	1.3832	1.38299	1.39522	1.39446	1.39506
D_2	0.386277	0.389403	0.386225	0.387723	0.384492
$\Sigma_{a1} + \Sigma_{12}$	2.48836E−2[a]	2.62865E−2	2.45662E−2	2.60117E−2	2.46141E−2
Σ_{a2}	6.73049E−2	8.10328E−2	8.44801E−2	9.89671E−2	8.93878E−2
Σ_{12}	1.64977E−2	1.47315E−2	1.56219E−2	1.40185E−2	1.54981E−2
Σ_{f1}	1.86139E−3	1.81560E−3	2.36371E−3	2.31026E−3	2.50773E−3
Σ_{f2}	3.48111E−2	3.50622E−2	4.91322E−2	4.95721E−2	5.31856E−2
$\nu\Sigma_{f1}$	4.81619E−3	4.66953E−3	6.04889E−3	5.91507E−3	6.40256E−3
$\nu\Sigma_{f2}$	8.46154E−2	8.52264E−2	1.19428E−2	1.20497E−2	1.29281E−2

[a]Read as 2.48836×10^{-2}.

Figure 5.2: Table of material constants (from ref. [Wag89])

number of CMFD (correction) iterations: $m = 20$. At each CMFD iteration, $l = 5$ power method iterations have been carried out to advance the eigenvalue and average flux solution. Put in another way, the CMFD system represented by matrix ${}^{C}\mathbf{M}$ have been used in five power method iterations until being improved by solving the local dual node problems. Initial flux distribution has been set to a unity vector, since only its relative

shape is of interest[2], and also the critical eigenvalue has been set to unity at the beginning.

Matlab routine `lu` for direct solution of the CMFD system has been used in step 2-(a)-i The solution consisted of two single-group problems with block heptadiagonal CMFD sub-matrices with non-adjacent diagonals as given by eqs. (4.62). The solver could take advantage of sparsity of each sub-matrix, since it contains less than 4% nonzero elements (see figure 5.3).

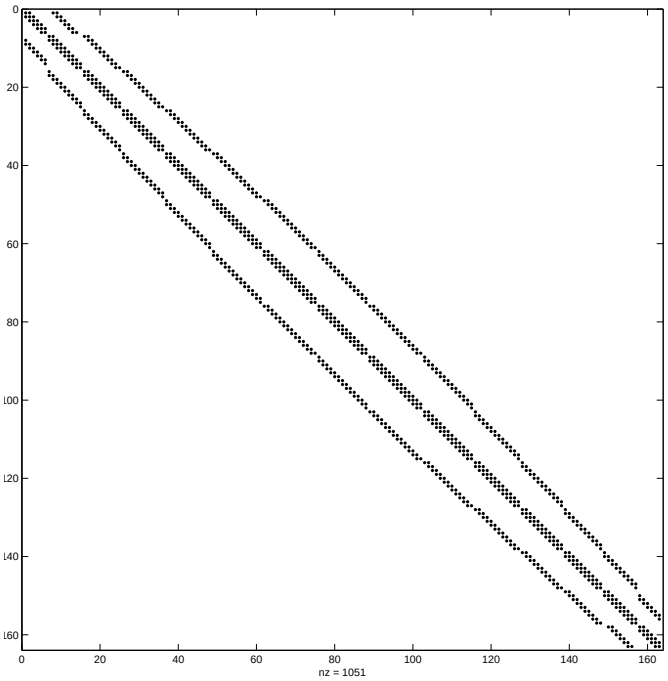

Figure 5.3: Nonzero pattern of matrix $\mathbf{L}^1 + {}^{\mathrm{C}}\mathbf{D}^1 + \mathbf{\Sigma}_r^1$ (nz denotes number of non-zero entries)

After completing the solution process, converged vector of flux averages can be used to determine the average power production in each node:

$$\bar{\bar{P}}_i := \nu\Sigma_{i,f}^1 \bar{\bar{\Phi}}_i^1 + \nu\Sigma_{i,f}^2 \bar{\bar{\Phi}}_i^2.$$

As in Chao and Shatilla's article, resulting power densities were normalized to the whole core average power:

$$\bar{\bar{P}}_i := \frac{\bar{\bar{P}}_i}{\frac{1}{N}\sum_{i=1}^{N} \bar{\bar{P}}_i}.$$

Quality of the tested method has been assessed by computing relative differences between the calculated normalized power distribution within a reference hexant and the correspond-

[2]Recall from sec. 3.3.1.1 that being an eigenvector, the flux is determined uniquely only up to a scalar multiple – steady operation of the reactor can be achieved with given material configuration at different power levels

ing results obtained by Chao and Shatilla:

$$\bar{\bar{P}}_i \text{ error } = \frac{\bar{\bar{P}}_i - \bar{\bar{P}}_i^{\text{Ch-Sh}}}{\bar{\bar{P}}_i^{\text{Ch-Sh}}} \cdot 100\%.$$

Error in the calculated criticality coefficient served as a second measure:

$$K_{\text{eff}} \text{ error } = \frac{K_{\text{eff}} - K_{\text{eff}}^{\text{Ch-Sh}}}{K_{\text{eff}}^{\text{Ch-Sh}}} \cdot 10^5 \text{ pcm},$$

represented in units of *pcm* (percent-milli, i.e. 10^{-5}).

5.3 Results

This section presents results of tests performed on the two problems differing in the used albedo values as described above. Implementation of Fu and Cho's semi-analytic method ([FC02]) in the hexagonal geometry setting based on Wagner's modification of transverse integration procedure ([Wag89]) has been compared to the conformal-mapping based code ANC-HM by Chao and Shatilla ([CS95]). Both flat and quadratic transverse leakage term approximations have been considered. The expected superiority of the latter is confirmed by the results, exposing of an order better agreement of the calculated criticality coefficient and a more closer fit to the reference power/flux profile. Larger errors in first few nodes (mainly for the unreflected core) could be attributed to the simplified treatment of boundary conditions (see section 4.4.1), although the primary limitation of the method lies in the transverse integration procedure (as noted in all three references mentioned above).

For each result set, also the convergence behaviour of the two fundamental solution parts of the described method – namely the power method iteration and the two-node subdomains iteration – is shown. To better display convergence of the former, two initial iterations are omitted from the graph. For the latter, the correction factor with a maximum absolute value is plotted for each iteration instead of the norm of the whole correction matrix ${}^{\text{C}}\mathbf{D}$ since it produces a more informative (although principially equivalent) graph.

In the power densities maps, each hexagon represents one assembly in the hexant marked by red assembly numbers in figure 5.1. Information the hexagon provides is schematized in figure 5.4

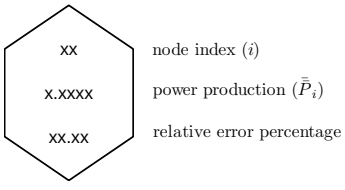

Figure 5.4: Legend for power densities maps

5.3.1 $\gamma = 0.5$, flat leakage approximation

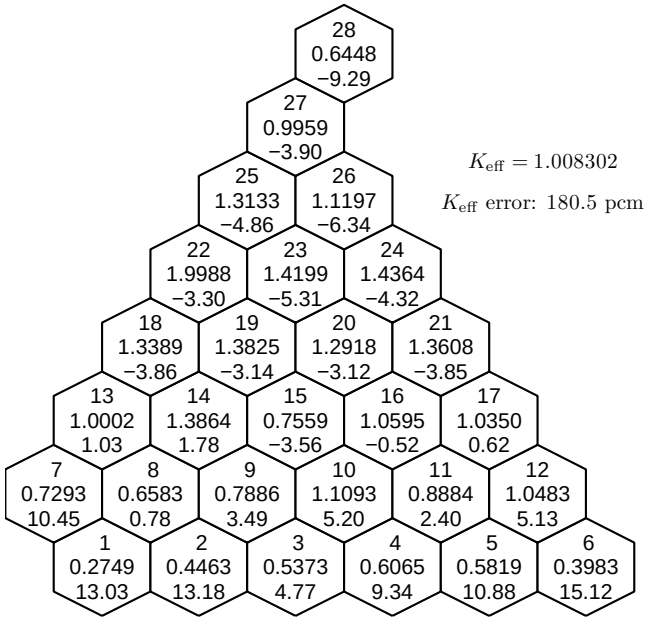

Figure 5.5: Normalized power densities and relative errors ($\gamma = 0.5$, flat leakage)

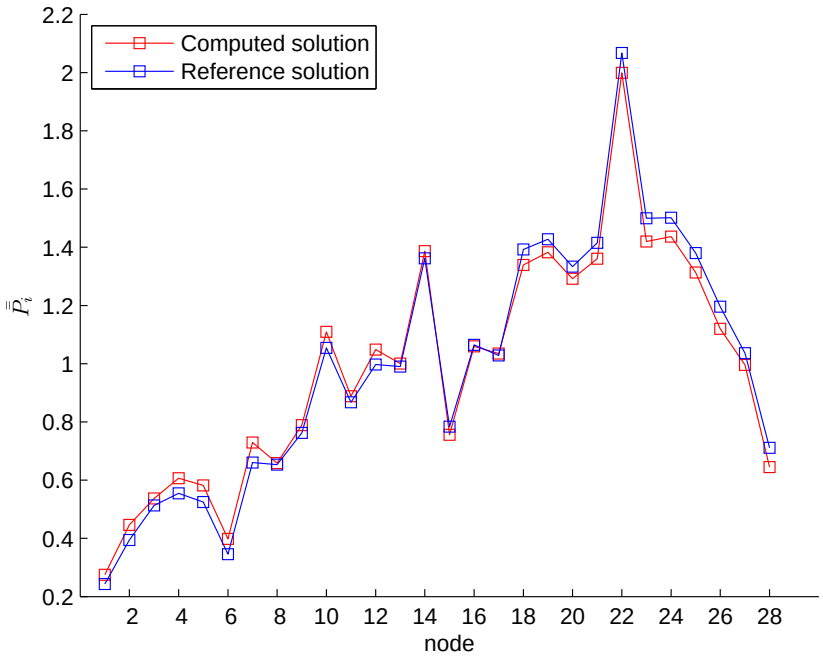

Figure 5.6: Node-wise power distribution profile ($\gamma = 0.5$, flat leakage)

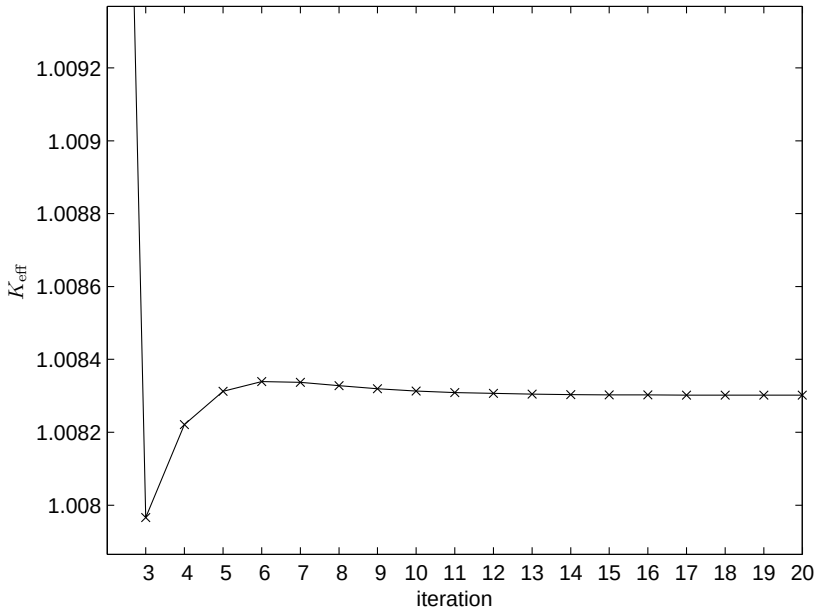

Figure 5.7: Eigenvalue convergence ($\gamma = 0.5$, flat leakage)

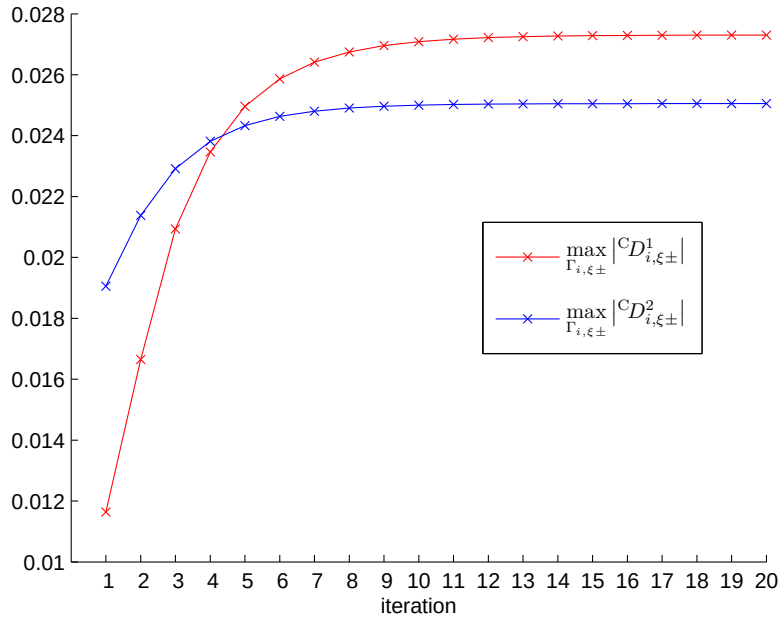

Figure 5.8: Convergence of correction factors ($\gamma = 0.5$, flat leakage)

5.3.2 $\gamma = 0.5$, quadratic leakage approximation

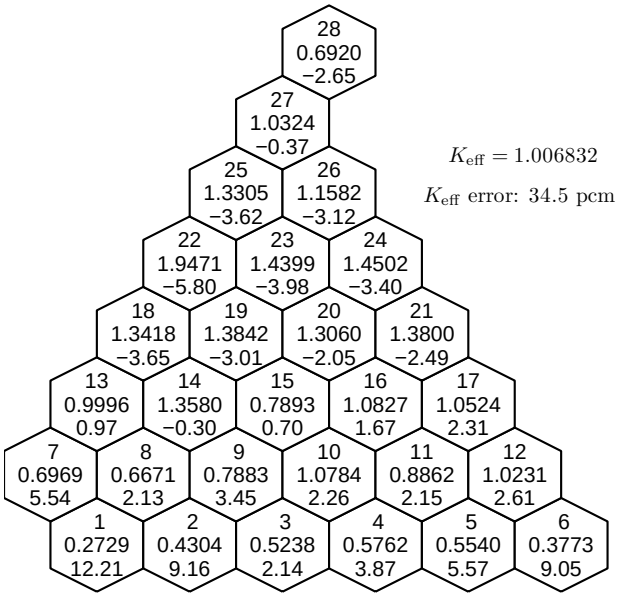

Figure 5.9: Normalized power densities and relative errors ($\gamma = 0.5$, quadratic leakage)

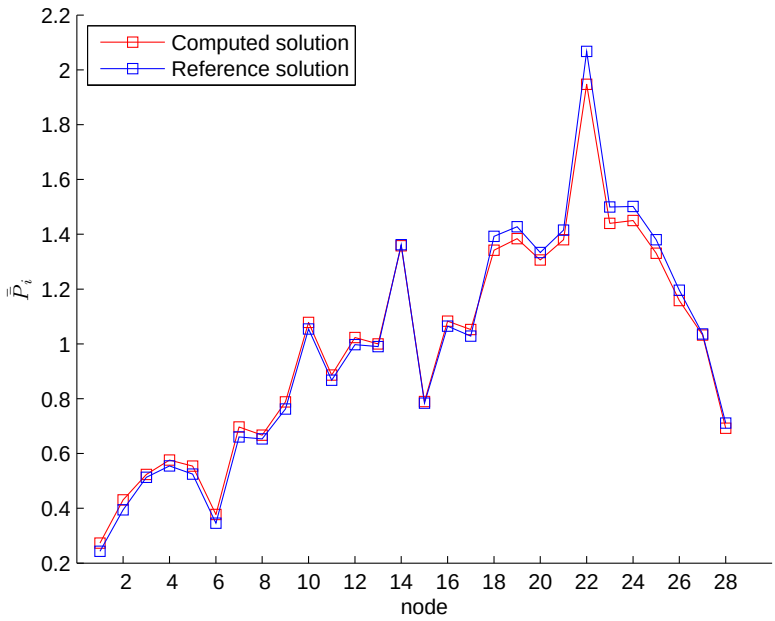

Figure 5.10: Node-wise power distribution profile ($\gamma = 0.5$, quadratic leakage)

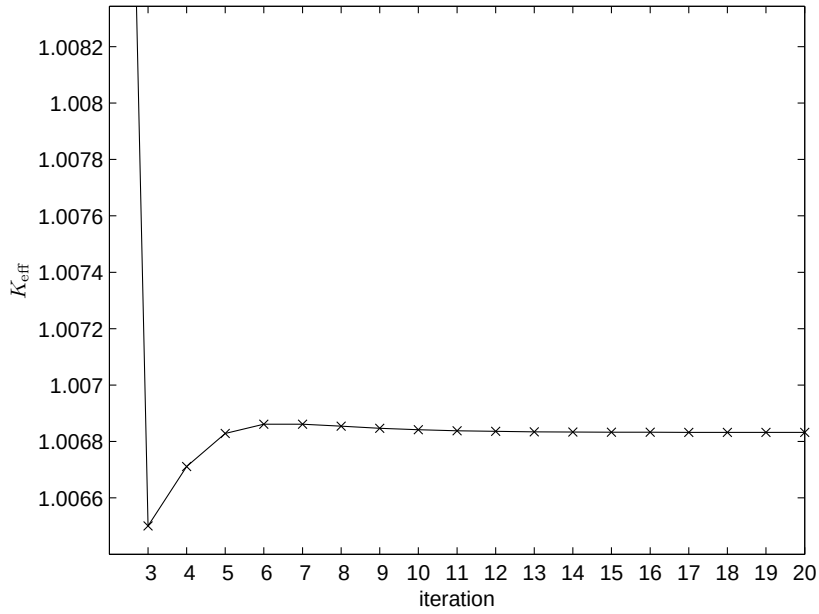

Figure 5.11: Eigenvalue convergence ($\gamma = 0.5$, quadratic leakage)

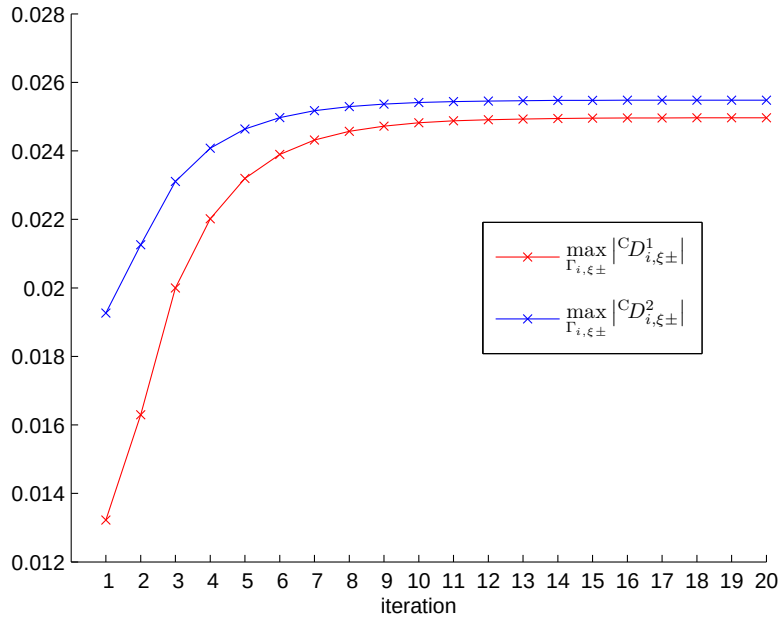

Figure 5.12: Convergence of correction factors ($\gamma = 0.5$, quadratic leakage)

5.3.3 $\gamma = 0.125$, flat leakage approximation

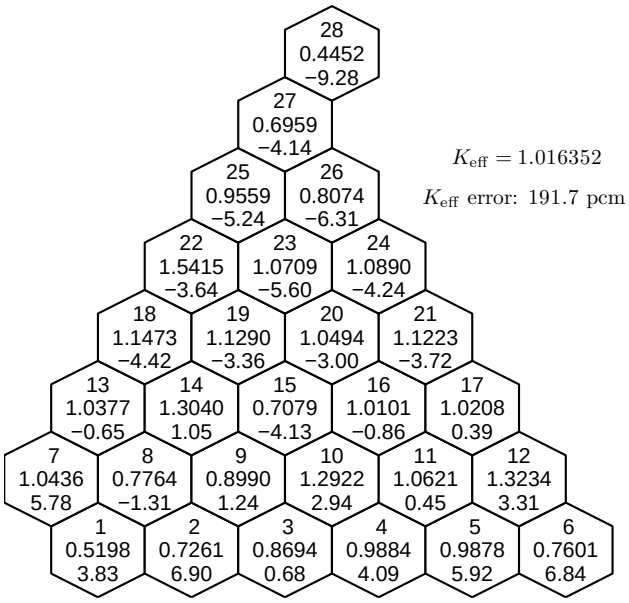

Figure 5.13: Normalized power densities and relative errors ($\gamma = 0.125$, flat leakage)

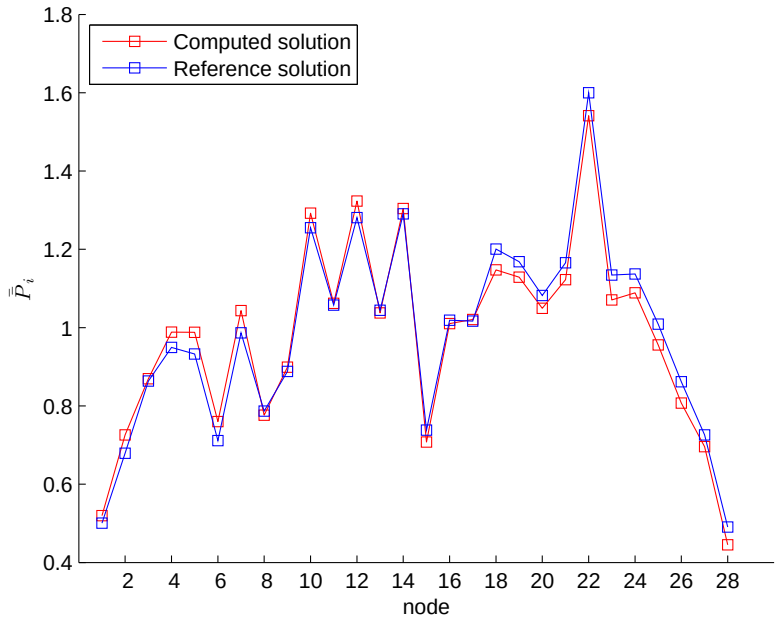

Figure 5.14: Node-wise power distribution profile ($\gamma = 0.125$, flat leakage)

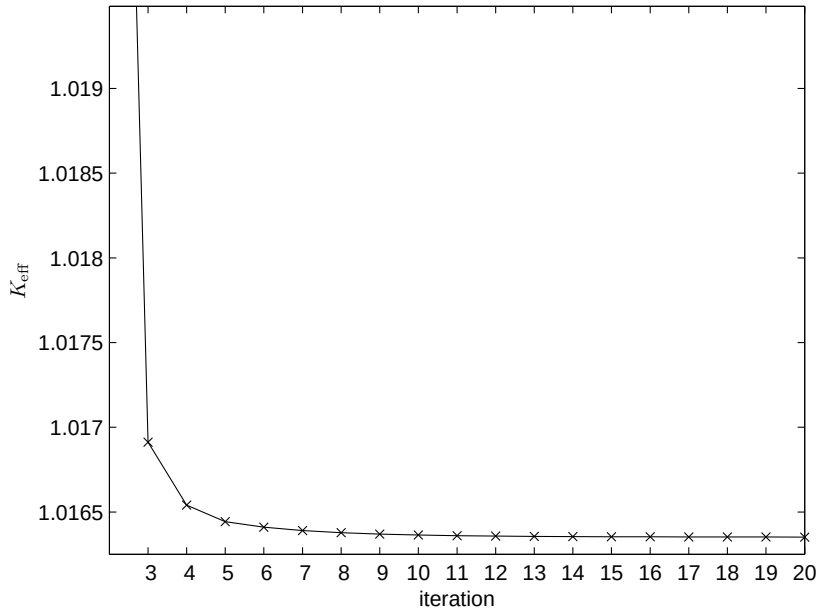

Figure 5.15: Eigenvalue convergence ($\gamma = 0.125$, flat leakage)

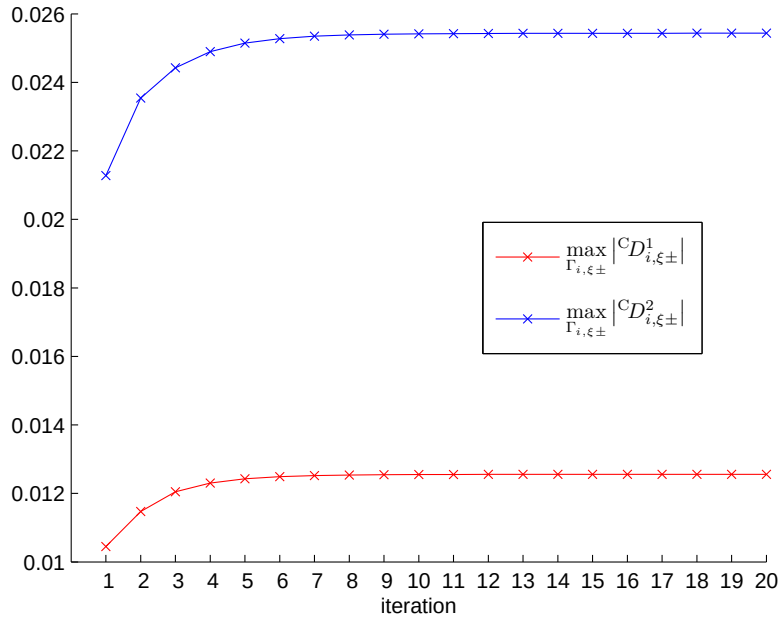

Figure 5.16: Convergence of correction factors ($\gamma = 0.125$, flat leakage)

5.3.4 $\gamma = 0.125$, quadratic leakage approximation

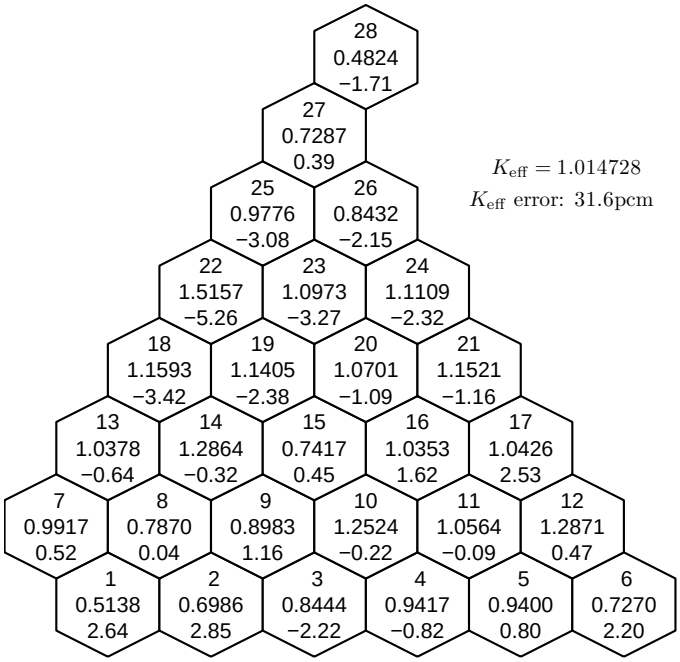

Figure 5.17: Normalized power densities and relative errors ($\gamma = 0.125$, quad. leakage)

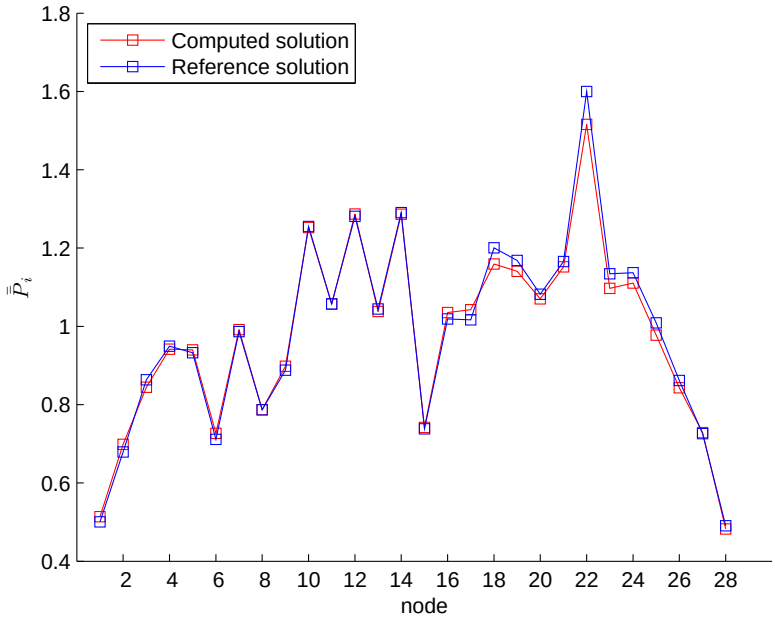

Figure 5.18: Node-wise power distribution profile ($\gamma = 0.125$, quadratic leakage)

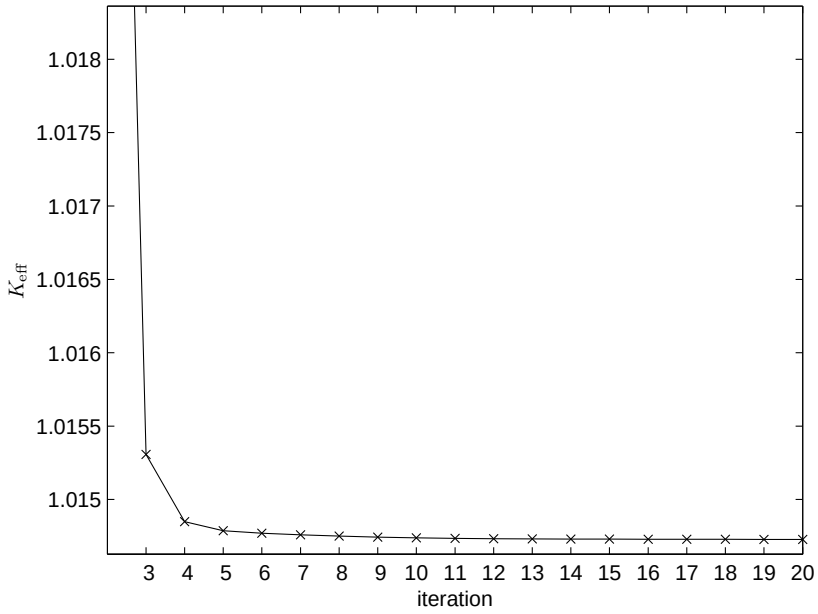

Figure 5.19: Eigenvalue convergence ($\gamma = 0.125$, quadratic leakage)

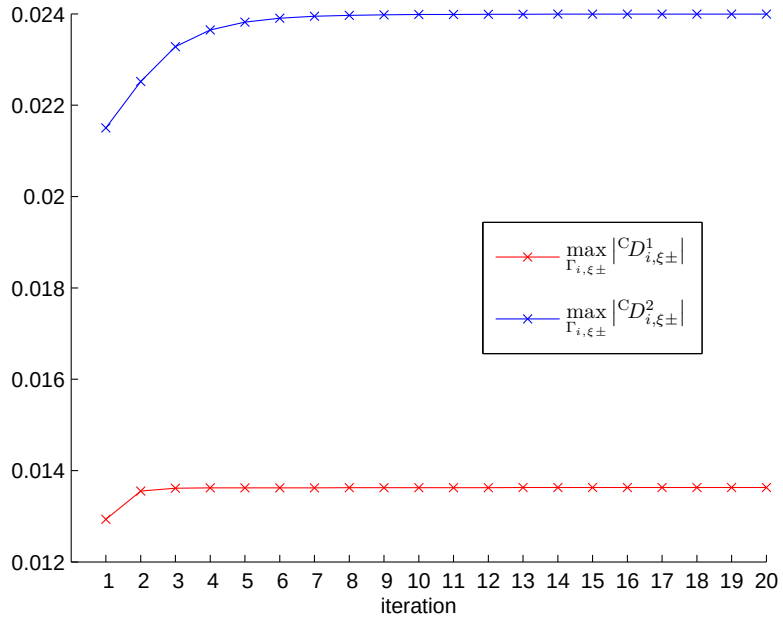

Figure 5.20: Convergence of correction factors ($\gamma = 0.125$, quadratic leakage)

Chapter 6

Conclusion

6.1 Summary

The purpose of this thesis has been to research, design and implement an efficient numerical method for solving the neutron transport problem. Knowing a precise distribution of neutrons within a reactor is of utmost importance to reactor analyses since it determines its overall power generation performance as well as its long-term effectivity and durability. Solution of neutron transport problem provides this information for a given reactor core composition and can hence help with its proper adjustment. The primary application domain of the developed method for neutron transport solution is precisely this core configuration optimization. To be usable in practice, the method must find neutron distribution for a testing composition quickly so that lots of possible configurations may be assessed in short time.

Chapter two has provided a theoretical overview of reactor physics. Various quantities needed for the precise description of the reactor and processes occuring within have been identified and their natural origins have been explained. The notion of reactor criticality has been introduced at the end of the chapter with its relation to the optimization problem under consideration.

The presented physical quantities have then been used at the beginning of chapter 3 to derive an accurate mathematical model for the reactor. Based on the general balance principle, the derivation resulted in a complicated integro-differential equation known as the neutron transport equation.

Recognizing that this model is overly involved for practical use, the third chapter has next proceeded with its simplification in various directions. Dependence of the governing equation on time could be removed since the configuration optimization problem requires only a steady-state solution from the method. The concept of criticality has then been evolved into a means of measuring the optimality of given material composition by using the solution of the stationary equation. Further on, the angular dependency of the equation has been removed to produce the diffusion approximation, consisting of a standard set of an elliptic-type PDR and a constitutive relation known as Fick's law. Finally, ener-

getic dependence has been discretized into so called energy groups, yielding the system of multigroup neutron diffusion equations prepared for numerical treatment. Calculation of reactor criticality manifests itself as an eigenvalue problem for these equations.

Numerical method for solving the two-group diffusion equations in a two-dimensional core has been presented in chapter 4. It is based on the standard finite volume discretization scheme for elliptic boundary value problems which has been described first. The approximation of numerical flux variables (represented here by integral averages of neutron currents) on the surfaces of control volumes (called nodes) by the primary unknown quantities (integral averages of neutron flux) plays a crucial role in such scheme.

The method of transverse integration has been used as a cornerstone for this task, giving rise to the so-called nodal method. It results in coupled one-dimensional representations of the original diffusion equation, for which sufficiently accurate solution techniques may be developed. One such technique, known as semi-analytic method, has been described later on in the fourth chapter. It is based on decomposing the whole-core problem into local two-node subproblems and solving the equations arising from transverse integration in these local subdomains analytically, with only one approximation neccessary due to the transverse integration procedure and one additional inexact assumption to keep the solution algebraically simple.

When constructing the nodal scheme, a special care must have been taken due to the hexagonal computational mesh required by the real core design. Specifically, a suitable approximation of transverse leakage terms in the one-dimensional equations must have been found so that consistency of integral averages in the local 1D problems and the global 2D problem could have been preserved, which proved more elaborate than in the Cartesian case.

Efficiency of the nodal method when used for determining the whole-core flux distribution has been ensured by employing a non-linear refining scheme known as the CMFD acceleration method. In it, the solutions of the coarse grained whole-core problem obtained by a low-order finite-difference like method are used to define the local subproblems, whose higher-order solutions are used in turn to correct the low accurate coarse mesh solutions. The corrected global flux solutions are then used in the power method iteration for computing the critical reactor eigenvalue and new estimates of global average fluxes.

Finally, results of numerical experiments performed on an example configuration of a VVER-1000 type reactor have been presented in chapter 5. Two actual implementations of the developed nodal method have been compared, differing in the approach to the transverse leakage approximation. The resulsts have been validated against verified solutions obtained by other authors.

6.2 Further research

The numerical method developed within this thesis can only be considered basic and its implementation a mere prototype rather than an operational code. Improvements are possible in both the whole-core eigenvalue updating part of the solution process and the local subproblems part.

A more appropriate treatment of boundary conditions should be considered in the phase of construction of the CMFD system. Solving then the system by a direct method like LU-factorization is clearly not the best technique to obtain the core-wise neutron flux distribution. Iterative Krylov subspace methods have recently been shown to perform well ([Pal97], [Sch97]) and will be more adequate. Performance of the global solution may further be enhanced by choosing a more advanced method for eigenvalue calculation. For instance, the Wielandt's shifting technique is a popular approach in this area (e.g. [Mao00]).

Major difficulties of solving the local two-node problems arise from transverse integration in hexagonal node geometry. As acknowledged in many references, main limitation of the procedure lies in the transverse leakage approximation. Although the quadratic fit is generally considered adequate, there are cases which render it insufficient ([FC02]). A better estimation of leakage shape can thus be pursued in order to attain better results.

Since the transverse integration procedure is much easier to formulate in rectangular domains, finding a proper way of transforming the hexagonal problem into a rectangular one without affecting its final solution seems to be a promising research direction. Indeed, significant accuracy improvements have been reported by Chao and Shatilla ([CS95]) who utilized conformal mapping for this purpose. Another way of avoiding the hexagonal geometry problems could be to suitably subdivide the hexagons (e.g. into parallelograms, [BK06]) to obtain a mesh with more convenient properties.

For solving real world problems, taking inhomogeneity of the reactor as well as intranodal burnup gradients into account may be neccessary. A proper selection of the homogenization method and incorporation of spatially varying cross sections into the model should hence be investigated to achieve these goals. Also the transient calculations and extension to third dimension may be performed.

In order to achieve best possible accuracy, the exact transport equations should be used instead of their diffusion approximations. This would of course demand more computational resources but this problem will likely be diminishing with the continuing progress in computing technology. An example of a method solely based on transport theory can be found in the thesis by Scott W. Mosher, [Mos04].

Bibliography

[AC02] G. Allaire and C. Castro. Optimization of nuclear fuel reloading by the homogenization method. *Struct. Multidisc. Optim.*, 24:1–22, 2002.

[Axe96] Owe Axelsson. *Iterative Solution Methods*. Cambridge University Press, 1996.

[BK06] Marek Brandner and Roman Kužel. Nodální metody pro difúzní dvougrupový model reaktoru. Technical report, Západočeská univerzita v Plzni, January 2006.

[Cap99] Yves Capdebosq. *Homogeneisation des modeles de diffusion en neutronique*. PhD thesis, Centre d'Etudes de Saclay, Direction des Réacteurs Nucléaires, Département de Mécanique et de Technologie, September 1999. Available from: `http://www-ist.cea.fr/publicea/exl-doc/00000037296.pdf`.

[ČEZ] ČEZ, a.s. Technologie a zabezpečení JE Temelín. Available from: `http://www.cez.cz/presentation/cze/instance_list.jsp?folder_id=1426` [cited 18-03-2007].

[CS95] Y. A. Chao and Y. A. Shatilla. Conformal Mapping and Hexagonal Nodal Methods – II: Implementation in the ANC-H Code. *Nucl. Sci. Eng.*, 121:210–225, 1995.

[EGH03] Robert Eymard, Thierry Gallouët, and Raphaèle Herbin. Finite Volume Methods. Update of the preprint n0 97-19 du LATP, UMR 6632, Marseille, September 1997, which appeared in Handbook of Numerical Analysis, P. G. Ciarlet, J. L. Lions, vol. 7, pp. 713-1020, January 2003.

[FC02] Xue Dong Fu and Nam Zin Cho. Nonlinear analytic and semi-analytic nodal methods for multigroup neutron diffusion calculations. *J. Nucl. Sci. Technol. (Tokyo, Jpn.)*, 39(10):1015–1025, October 2002.

[Gar05] William J. Garland. Reactor physics: Point kinetics, July 2005. Part of lecture notes for the course Engineering Physics 4D3/6D3 - Nuclear Reactor Analysis taught at McMaster University, Hamilton, Ontario, Canada. Available from: `http://www.nuceng.ca/ep4d3/text/10-kinetics-r1.pdf` [cited 04-02-2007].

[Geh92] Jess C. Gehin. *A Quasi-Static Polynomial Nodal Method for Nuclear Reactor Analysis*. PhD thesis, Massachusetts Institute of Technology, September 1992.

[GHV00] Thierry Gallouët, Raphaèle Herbin, and Marie Hélène Vignal. Error estimates on the approximate finite volume solution of convection diffusion equations with general boundary conditions. *SIAM J. Numer. Anal.*, 37(6):1935–1972, 2000.

[Heř81] Bedřich Heřmanský. *Jaderné reaktory*. SNTL, Praha, 1981.

[JJD98] Han Gyu Joo, Guobing Jiang, and Thomas J. Downar. Stabilization techniques for the nonlinear analytic nodal method. *Nucl. Sci. Eng.*, 130(1), 1998. Available from: `citeseer.ist.psu.edu/355997.html`.

[Kor] Korea Atomic Energy Research Institute. Online Plotter for MCNP and ENDF Cross Section Data. Pointwise ENDF-VI Library. Available from: `http://atom.kaeri.re.kr/cgi-bin/endfplot.pl` [cited 03-04-2007].

[Mao00] Jinchao Mao. Implementation of the analytic nodal method in the NDF code and applications to CANDU reactors. Master's thesis, École Polytechnique de Montréal, 2000.

[MK93] Stanislav Míka and Alois Kufner. *Parciální diferenciální rovnice eliptického typu*. Vydavatelství Západočeské univerzity v Plzni, 1993.

[Mos04] Scott W. Mosher. *A Variational Transport Theory Method for Two-Dimensional Reactor Core Calculations*. PhD thesis, School of Mechanical Engineering, Georgia Institute of Technology, June 2004.

[Mou96] David J. Moulton. *Nodal Methods: Analysis, Performance and Fast Iterative Solvers*. PhD thesis, University of British Columbia, Institute of Applied Mathematics, November 1996. Available from: `http://www.iam.ubc.ca/theses/moulton/moulton.ps.Z` [cited 01-19-2007].

[Pal97] Scott P. Palmtag. *Advanced Nodal Methods for MOX Fuel Analysis*. PhD thesis, Massachusetts Institute of Technology, August 1997.

[SA96] T.M Sutton and B.N. Aviles. Diffusion theory methods for spatial kinetics calculations. *Progr. Nucl. En.*, 30(2):119–182, 1996.

[Sch97] Robert Scheichl. Parallel Solution of the Transient Multigroup Neutron Diffusion Equations with Multi-grid and Preconditioned Krylov-subspace Methods. Master's thesis, Johannes Kepler Universität Linz, September 1997. Available from: `http://www.maths.bath.ac.uk/~masrs/diplom.ps.gz` [cited 30-01-07].

[Sta01] Weston M. Stacey. *Nuclear Reactor Physics*. John Wiley & Sons, Inc., New York, 2001.

[T+94] Paul J. Turinsky et al. NESTLE few-group neutron diffusion equation solver utilizing the nodal expansion method for eigenvalue, adjoint, fixed-source steady-state and transient problems. Technical report, Electric Power Research Center, North Carolina State University, Raleigh, NC 27695-7909, June 1994.

[Wag89] M. R. Wagner. Three-Dimensional Nodal Diffusion and Transport Theory Methods for Hexagonal-z Geometry. *Nuc. Sci. Eng.*, 103:377–391, May 1989.

[Wil71] M. M. R. Williams. *Mathematical Methods in Particle Transport Theory.* Butterworths, London, 1971.

[Y+06] W.-M. Yao et al. Review of particle physics. *J. Phys. G: Nucl. Part. Phys.*, 33(1), 2006. Available from: `http://pdg.lbl.gov` [cited 02-01-2007].